ABSTRACT

NUCKOLS, RICHARD WINSTON. Effects of Elastic Ankle Exoskeleton Stiffness and Walking Speed on Human Locomotor Performance from Whole-Body Energetics to Individual Muscle Neuromechanics. (Under the direction of Gregory S. Sawicki).

Robotic assistive devices show promise for improving gait outcomes in both healthy and impaired populations. For individuals with spinal cord injuries or post-stroke, commercial devices are now available as assistive aids and therapeutic tools for rehabilitation (e.g. EksoGT, Indego). For healthy individuals, clever assistive devices have been shown capable of enhancing performance. However, the complex mechanisms by which the assistive devices can lead to positive (or negative) neuromechanical outcomes are not yet fully understood. A human-centric approach to designing wearable devices is crucial for optimizing efficacy of wearable robotic systems. The goal of this work was to (1) determine beneficial exoskeleton assistive strategies for providing ankle assistive torque and (2) identify why certain assistance strategies are or are not effective with a core focus on the physiological response of the user.

In Chapter 1, I constructed and validated a laboratory-based robotic exoskeleton emulator capable of applying plantarflexion torques to the human ankle during locomotion. We developed a series of bio-inspired control algorithms based on an ankle stiffness ('exo-tendon'), a neuromuscular-based model, and adaptive-proportional electromyography. In unimpaired human walking, we have shown that the exoskeleton emulator provided high-fidelity impedance (stiffness) control with minimum torque error and low net power generation. This hardware and control system allows us to rapidly and systematically test a variety of exoskeleton torque assistance strategies.

In Chapter 2, we used this system to evaluate the coupled effects of speed and ankle exoskeleton rotational stiffness on human locomotor performance. In taking a human-centric approach, we evaluated the effect of exoskeleton assistance on the user from whole-body metabolic cost, joint dynamics, neural activation, down to individual muscle length and velocity dynamics. First, we hypothesized that we could find an optimal exoskeleton stiffness at each of the three speeds (1.25, 1.5, and 1.75 m s^{-1}) where metabolic demand of walking would be minimized. Our results showed that the optimal

stiffness of 50 Nm rad^{-1} reduced metabolic demand by 4.2 and 4.7% at 1.25 and 1.75 m s^{-1} respectively. However, no stiffness condition provided metabolic improvement at 1.5 m s^{-1}. Evaluation of joint dynamics and muscle activation demonstrated decreased biological ankle moment and decreased soleus activation concomitant with increased exoskeleton stiffness and torque. Similar trends in joint and activation dynamics were seen across all three speeds.

In Chapter 3, I used B-mode ultrasound imaging to look "under the skin" at soleus muscle fascicles during human walking with the exoskeleton assistance. We hypothesized that exoskeleton rotational stiffness would disrupt fascicle dynamics, resulting in longer fascicles and suboptimal metabolic improvements. Results showed that the stiffest assistance, compared to no assistance, resulted in a significant 11.8% increase in fascicle length at peak dorsiflexion. At the metabolically optimal stiffness (50 N m rad^{-1}), the fascicle length was slightly shorter (-0.6%). We found a significant positive linear relationship between metabolic demand and fascicle length. Increased fascicle lengths in walking appear to result in increased muscle economy (force per activation) in early stance, but decreased economy in late stance trends with increased fascicle velocity.

In Chapter 4, I performed a preliminary study to demonstrate the application of elastic-ankle exoskeletons to alter the biological structure in older adults and restore performance. Because older adults have lower Achilles tendon stiffness, we hypothesized that by adding parallel stiffness via an elastic-ankle exoskeleton, we would improve the muscle economy and whole-body efficiency of the older user. Data showed that exoskeleton assistance on older adults results in increased fascicle lengths, reduced muscle activation, and improved walking efficiency up to 5%.

Effects of Elastic Ankle Exoskeleton Stiffness and Walking Speed on Human Locomotor Performance from Whole-Body Energetics to Individual Muscle Neuromechanics

by
Richard Winston Nuckols

A dissertation submitted to the Graduate Faculty of
North Carolina State University
in partial fulfillment of the
requirements for the degree of
Doctor of Philosophy

Biomedical Engineering

Raleigh, North Carolina

2017

APPROVED BY:

Gregory Sawicki Committee Chair	Helen Huang
Katherine Saul	Michael Lewek Inter-Institutional Member
Michael Goldfarb External Member	

DEDICATION

To Kristin, this wouldn't have been possible without your love and support. Thanks for reminding me that it's worth it.

To Brooke and Hudson, may you have the opportunity to pursue what you love.

BIOGRAPHY

I received my Bachelors of Science in Mechanical Engineering with a minor in Chemistry from Virginia Tech in 2006 graduating Summa Cum Laude. After graduation, I worked as an engineer for Dominion Energy and then as an asset specialist for Dominion Energy Marketing. I returned to school in 2011 to pursue a Masters in Biomedical Engineering from Virginia Commonwealth University investigating the mechanisms by which blind and sighted humans localize dynamic spatial auditory targets in their physical environment. Upon graduating in 2013 with a MS in Biomedical Engineering, I pursued a Ph.D. in the Joint Department of Biomedical Engineering at North Carolina State University and University of North Carolina at Chapel Hill. For my dissertation, I studied the effects of wearable ankle exoskeletons on humans during locomotion under the direction of Dr. Gregory Sawicki.

ACKNOWLEDGMENTS

First, I must thank my family for their love, support, and for putting concerns into perspective. Kristin, I couldn't have done it without you. You are also the reason I started graduate school with zero children and I'm leaving with two. Brooke and Hudson, it wasn't easy but you mean everything to me. Finally, thank you to Mom and Dad and my brothers, Michael and William, for your constant support and love.

To the friends that I've made over the past four years, Kristin and I are eternally grateful for you.

I was fortunate during my time to have the guidance, advice, and friendship of three excellent post-doctoral fellows. Kota Takahashi, Tracy Giest, and Taylor Dick, I would not have been successful without you. You taught me an incredible amount about biomechanics, muscle physiology, human data collections, and how to conduct research.

Thank you to the many individuals who provided advice, guidance, and support. Thank you to all the past and present members of the PoWeR lab. To my committee members, thank you for your time and contribution to my dissertation.

Finally, thank you Greg Sawicki. Your passion for science and knowledge is incredible and has been an inspiration to me. You taught me to be a scientist and made me a better engineer. Thank you for your mentorship, advice, and friendship.

TABLE OF CONTENTS

LIST OF TABLES

LIST OF FIGURES

Chapter 1 - Development and Validation of a Laboratory-based Robotic Exoskeleton Emulator.

Introduction

The coordination between a wearable robotic assistive device and the human user is crucial for effective mechanical assistance. Assistive devices have shown promising results in aiding human users by decreasing metabolic power or increasing joint power in both healthy and diseased populations [1-3]. However, adequately evaluating the multi-dimensional parameter space that includes control design, control parameters, and gait condition has high cost in terms of both time and expense. Parameters in one-off prototype devices are often static or are limited in parameter settings. Additionally, the construction of prototypes to test theoretical designs and parameters require significant investment of time and cost. In the past, when studies have insufficiently considered the important role of device design variables (e.g. rotational stiffness, actuation timing) in the coordination between user and device, outcomes have been ineffective in improving patient outcomes [4]. However, when the importance of control parameters was addressed and assessed systematically, effective assistance in powered [5] (power actuation timing) and passive devices [6] (rotational stiffness) was achievable. Of note in both studies was that only one locomotor condition out of five was found to have a significant metabolic improvement in comparison to no exoskeleton condition. The optimal actuation timing result agrees with model predictions [7], but the ideal exoskeleton stiffness parameter was a small percentage of estimated biological ankle quasi-stiffness [8]. Therefore, a means for a systematic and rapid experimental system to examine the space of different controllers, parameters, and devices was required [9].

The goal of this work was to develop a co-robot exoskeleton testbed, capable of physiological levels of torque and with high bandwidth, with which to systematically and rapidly evaluate control parameters and strategies within a single experiment. To allow us

to expand the work from our previous studies [6], we demonstrated that we can effectively emulate an elastic element for providing rotational stiffness plantarflexion assistance to bilateral ankle exoskeletons.

Methods

The exoskeleton testbed was a research tool capable of providing bilateral mechanical plantarflexion assistance to the user. A similar device has been demonstrated in previous work [10-12]. We developed the device in our lab to efficiently and systematically test exoskeleton torque assistive strategies including impedance, proportional electromyography (EMG) control, and force feedback neuromuscular model-based control. The testbed consists of three primary components: (1) bilateral ankle exoskeleton end effectors, (2) benchtop motors and transmission, and (3) control system (Fig 1).

Hardware: The exoskeleton end effector was a lightweight carbon fiber ankle foot orthosis (AFO) capable of applying plantarflexor torque to the ankle. To allow for flexible testing across subjects, we designed the end effector to be modular such that we can accommodate anthropometric variation in subjects' foot, ankle and shank with four effectors (Short/Small, Short/Large, Tall/Small, Tall/Large). Ankle position was accommodated by moving the joint forward and backward on the end effector. Mass of the end effector without attachment hardware was 415g. A free body diagram showing force balance is shown in figure 1.

Two offboard powerful 1.61 kW bench top motors (Baldor Electric Co, Fort Smith, AR) motors delivered plantarflexion torque to the bilateral ankle exoskeletons by applying a pulling force to the end of the exoskeleton moment arm through a flexible Bowden-cable transmission. The motor was coupled to the pulley through a 10:1 gearbox (Baldor). At the motor, we attached the Bowden cable to the motor platform by a compressive

clamp and the internal cable was connected to the pulley in line with a breakaway cable as a safety mechanism. The external Bowden cable was 58" long (5/16", LEXCO CABLE MFG, Norridge IL) and the internal cable was low stretch Vectran rope (V-12 Vectran Single Braid, 3mm, 1900 lb, West Marine, USA). Linear motion in the cable was delivered from rotational motion of the motor. The motors were positioned behind the subject at approximate shoulder height (54" with respect to treadmill). Through pilot testing evaluation, this height and position provided the best combination of subject ROM, exoskeleton controllability, and limited the interference with camera line of sight.

At the other end of the Bowden cable we connected the Bowden cable to the proximal posterior aspect of the end effector with an aluminum compressive clamp. The internal cable attached to the moment arm of the exoskeleton (~10 cm) through an inline tensile load cell (DCE-2500N, LCM Systems, UK) and series elastic element.

Software and Control: The exoskeleton control consisted of a high-level controller which calculates a desired torque and low-level controller providing torque tracking. The system was implemented through a real-time control package (DS1103, dSpace Inc, Germany) where analog sensor data was sampled at 5kHz and motor command signals are generated at 500 Hz. Motor commands were implemented through a motor driver (ABB, Cary, NC) operating in velocity control mode.

The real-time control system was hierarchical with a low level and high level control (Fig 2). The low-level control was a modified PD controller where torque error was driven to zero using proportional torque error and motor velocity damping feedback in combination with inter-stride learning of torque-error [11]. An inline load cell measured exoskeleton torque (250Hz LP Filter, LCM Systems Ltd, UK) and an optical encoder (E5 Optical Encoder, US Digital, Vancouver, WA) measured motor pulley velocity (250Hz LP Filter).

Desired exoskeleton torque was determined through a high-level controller. As part of the development, we generated three high level control algorithms within our

system. The primary focus of the thesis work was on the impedance control for emulating elastic elements. We also showed development and feasibility of two other control strategies to demonstrate adaptability of the system.

1. Impedance Control (Fig 2): Models an 'exo-tendon' that provided rotational stiffness at the joint in parallel with the biological muscle-tendon unit. Total stiffness of the ankle was the summation of exoskeleton and biological stiffness ($k_{total} = k_{exo} + k_{bio}$). The 'exo-tendon' stiffness can be controlled in software to provide a range of assistance levels.
2. Adaptive Proportional Electromyography (EMG) (Fig 3): Timing and magnitude of the soleus EMG signal determines the magnitude of torque assistance. System adapts to the user's walking speed and attenuation of EMG magnitude.
3. Neuromuscular model based (NMM) (Fig 4): Model which incorporates Hill-type muscle dynamics (force-length, force-velocity) and neural force feedback and activation dynamics.

Impedance Control: A high-level impedance controller determined the desired exoskeleton torque. The impedance controller was designed to emulate a physical passive elastic element capable of providing plantarflexion torque (rotational stiffness) to the ankle akin to other studies [6]. As such, we set the velocity term, b, to zero. We calculated desired torque based off a predefined rotational stiffness and the real-time ankle angle (Eq 1.1)

$$\tau_{exo} = k_{exo} \times \left(\theta_0 - \theta_{ankle} \right) \quad (1.1)$$

where k_{exo} is rotational stiffness of the exoskeleton, θ_0 is the onset angle, and θ_{ankle} is the real-time ankle angle. A goniometer (5 kHz, 250Hz Biometrics, UK) between the exoskeleton foot and shank segment measured real-time sagittal plane ankle angle, and onset angle (θ_0) is set at contact of the foot with the treadmill. We determined gait state and heal strike by sampling vertical ground reaction force from the instrumented treadmill (Bertec, Columbus, OH).

Feasibility of other control strategies: The impedance controller designed to emulate elastic assistance was the primary control strategy of interest. The other goal of the work was to demonstrate capability of implementing different control strategies. Therefore, we also validated development and feasibility of the proportional EMG and NMM controllers. The adaptive proportional EMG control was developed as an extension from previous work using proportional EMG with pneumatic actuators (Fig 3) [1, 13, 14]. We recorded muscle activation levels from the soleus muscle and used the processed EMG envelope to control the timing and amplitude of the exoskeleton torque demand (Eq 1.2).

$$\tau_{exo} = G_{speed} \times G_{adp} \times (EMG) \quad (1.2)$$

EMG was the rectified EMG envelop signal from the soleus muscle (10 Hz HP, rectify, 20Hz LP), G_{speed} was the speed adaptive gain, and G_{adp} was the adaptive EMG gain. The adaptive EMG gain was calculated from a moving average of the peak EMG signal from five previous steps. This ensured that the EMG signal remained saturated. Peak desired torque was speed dependent and calculated based on biological torque profiles in walking over a range of speeds.

The neuromuscular model (Fig. 4) was a reflex-based feedback controller similar to Eilenberg *et al* [15]. The emulated plantarflexor muscle tendon unit (MTU) was based on a Hill-type muscle model that consisted of a contractile element (CE), possessing both active and passive components in parallel, in series with a series elastic element (SEE). The internal states of the muscle-tendon model (Fig.4B) were calculated in the high-level control. Length of the MTU was a function of modeled musculoskeletal geometry and ankle angle (Fig.4A) (1.3). SEE length was calculated by subtracting CE length from MTU length (1.4). The force developed in the MTU (F_{MTU}) was a function of the modeled non-linear stiffness of the SEE and the calculated strain in the SEE (1.5). CE velocity was calculated from muscle force-length, force-velocity, and activation relationships derived from a Hill Model (1.6). The CE velocity was then integrated to calculate the length of the

CE in the next time step $\left(L_{i+1}\right)$ (1.7). In the reflex pathway, the MTU force (Fig.4C) was normalized to F_{max}, multiplied by a feedback gain, and delayed to emulate a neural positive force feedback neural signal (Stim) (Fig. 4D). The feedback loop was closed by modeling the activation dynamics (ACT) of the CE (1.8). The desired exoskeleton assistance was calculated as a percentage of estimated biological moment (1.9) (Fig 4E) where ψ represented a percentage of the estimated biological torque.

$$L_{MTU,i} = f\left(\theta_{ank}, r_{ank}\right) \quad (1.3)$$

$$L_{SEE,i} = L_{MTU,i} - L_{CE,i} \quad (1.4)$$

$$F_{MTU,i} = f\left(L_{SEE,i}, k_{SEE,i}\right) \quad (1.5)$$

$$\dot{\mathrm{L}}_{CE,i} = f\left(\mathrm{F-L}, \mathrm{F-V}, a_i\right) \quad (1.6)$$

$$L_{CE,i+1} = \int \dot{L}_{CE} dt \quad (1.7)$$

$$a_{i+1} = \int \dot{a}_i dt \quad (1.8)$$

$$\tau_{exo} = F_{MTU} \times r_{ankle} \times \psi \quad (1.9)$$

System performance: Primary outcome measures for the performance of the exoskeleton testbed were calculated based on the impedance controller. Due to our desire to use the system for emulating a physical spring, the impedance control required accurate torque tracking with minimal hysteresis. Tracking error was calculated at both peak moment and as RMS error during stance. Hysteresis was evaluated as the integral of the exoskeleton power during stance.

Results

The exoskeleton testbed using the impedance controller could generate a range of rotational stiffness profiles across a range of walking speeds. Torque error and work loops are presented in Figure 5. Maximum torque tracking error was 2.8% and RMS error was 1.8 ± 1.7 N m kg^{-1}. Net work performed by the system was -0.02 W kg^{-1} in the least stiff

condition and +0.02 W kg^{-1} in the stiffest condition. Relative to metabolic demand, net work removed/added to system was 0.1% of whole body metabolic rate.

We generated torque profiles for the adaptive proportional EMG control and neuromuscular based model controller (Fig 6 and 7). The proportional EMG system responded to speed changes with increased torque and maintained saturated activation profiles. The NMM system generated muscle-tendon and ankle joint work profiles like those generated by biological ankle joints [16].

Discussion

We could achieve good performance from the exoskeleton testbed operating in impedance control mode. Torque tracking error was similar to error reported from other groups using the similar exoskeleton testbed [11]. Work loop hysteresis was minimized such that the system removed/added little energy from/to the system and was minor compared to the whole-body work.

Our intention was to tightly control stiffness so that we could measure its effect on the user. The system behaved like an ideal spring rather than a physical elastic element where energy is always dissipated. In this sense, the exoskeleton testbed 'exo-tendon' was different from biological elastic tendon which dissipates 15% energy [17] and from the portable elastic system previously tested in our lab which dissipates energy [6]. Damping could be added in future designs to control for energy dissipation if desired.

Controlling stiffness through feedback also allowed us to compensate for uncontrolled stiffness (unintended deflection) in the exoskeleton end effector. Again, comparing the testbed to the portable system, the measured stiffness of the portable system was less than that of the rated spring stiffness due to deformation within the end effector. This unknown deformation can make future device development more difficult because the stiffness of the end effector must be accounted for. With the testbed, we compensate for deformation by imposing a torque angle relationship where we

constantly track and control applied torque. This potentially makes adoption of the stiffness results by future studies easier as the reported stiffness is invariant of end effector characteristics. There was still the potential for compliance in the interface between the shank and exoskeleton that was not accounted for.

Although the assessment of the testbed with other control systems was minimal, we have shown that the exoskeleton testbed developed here provided assistive torque profiles using three different control schemes. The versatility of the system was an important characteristic and will allow for the rapid evaluation and assessment of exoskeleton designs in future studies. We only tested this system with ankle end effectors, but the transmission could easily be connected to exoskeletons at the hip or knee. Finally, the system can be used to quickly assess the effects of exoskeletons in a variety of populations including healthy, ageing, and with stroke survivors.

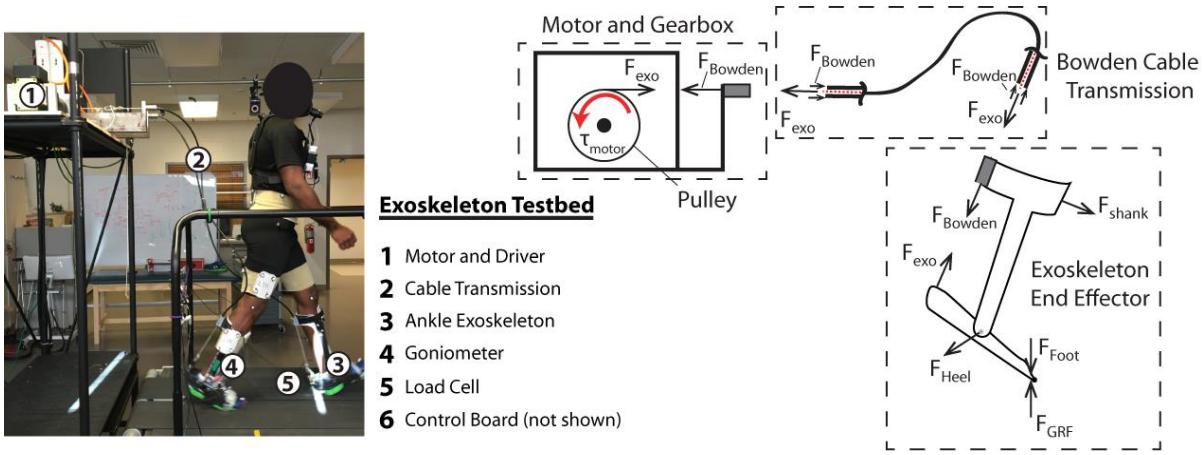

Figure 1.1: Ankle exoskeleton testbed and free-body diagram. a, Representative setup of the exoskeleton testing platform for evaluating ankle plantarflexion assistance. The exoskeleton provided plantarflexion torque to the bilateral ankle exoskeletons through off-board motors. **b,** Free body diagram showing force balance on end effector, Bowden cable transmission, and motor. Force was transmitted from the motor, through the cable transmission, to the moment arm of the exoskeleton.

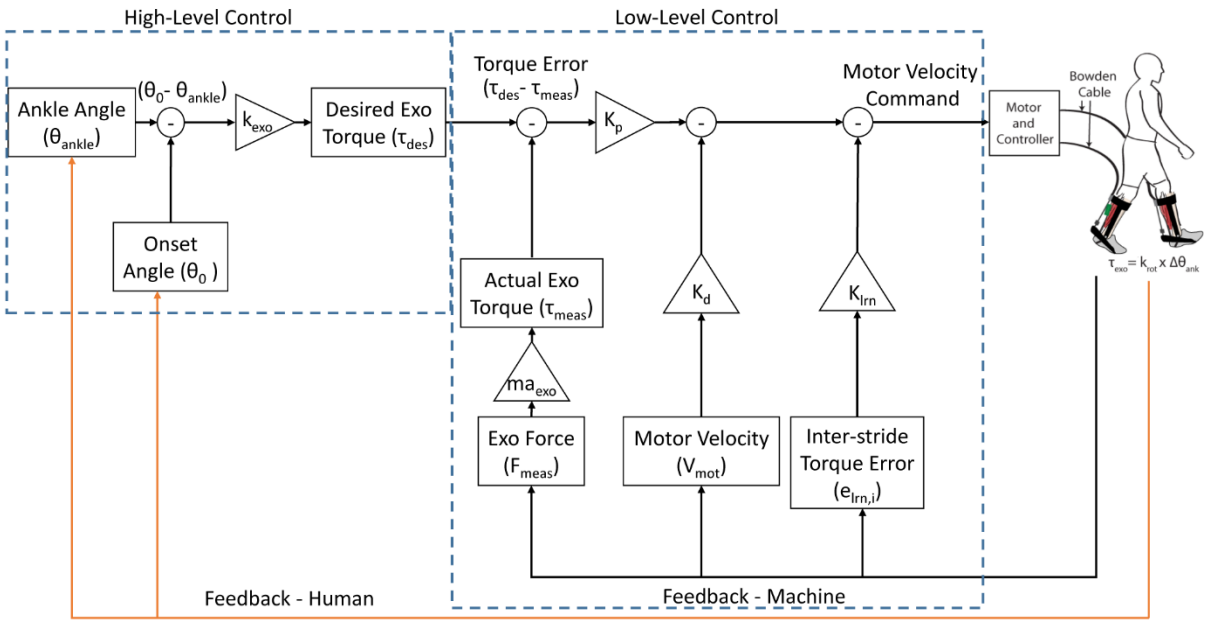

Figure 1.2: Block diagram of control framework for exoskeleton stiffness control. Exoskeleton torque was prescribed through a hierarchical high-level and low-level control system. Desired torque was calculated in the high-level loop (impedance/stiffness shown), and low-level PD feedback loop calculated desired motor velocity to minimize torque error. Inter-stride error represents the error from the previous stride and was particularly important for early stance (low torque/error) and push-off (high velocity).

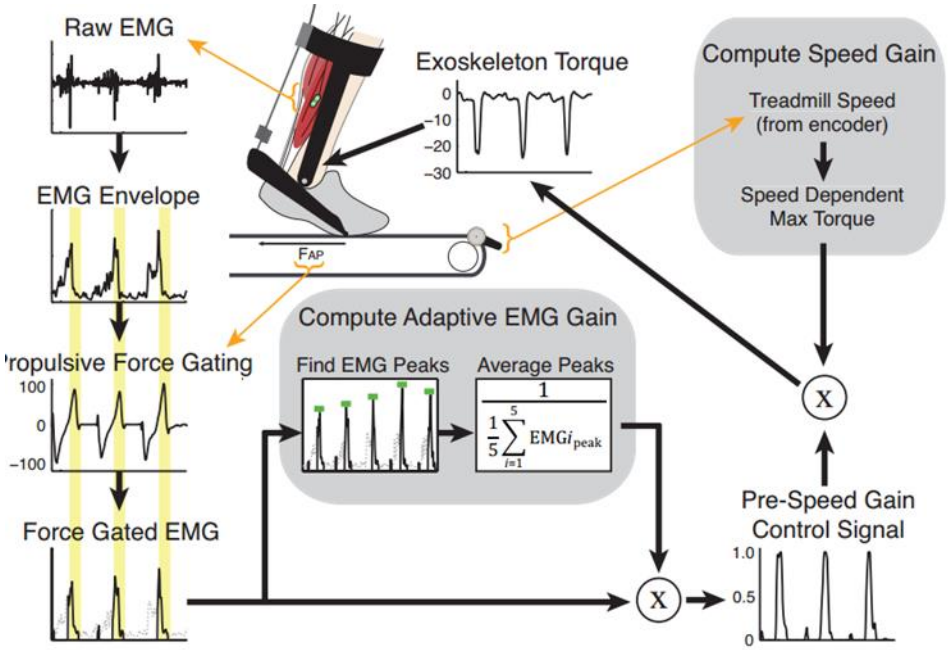

Figure 1.3: Control structure for speed adaptive proportional EMG controller. The exoskeleton torque was in proportion to the user's soleus EMG envelope. Gains (gray blocks) were applied based on the speed of walking and to ensure saturation of the EMG envelope [18].

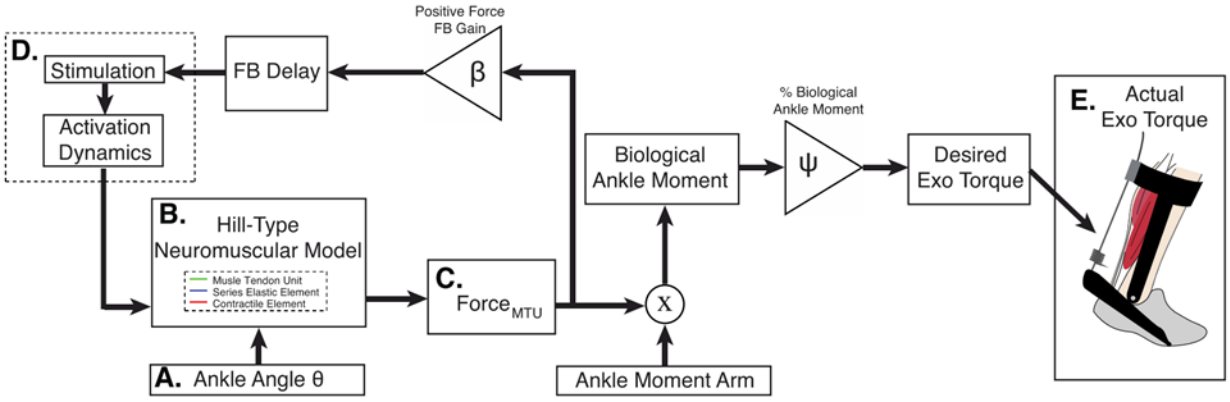

Figure 1.4: Control structure for neuromuscular model (NMM) based controller. The desired exoskeleton torque was applied based of a percentage of modeled biological torque. Activation of the muscle model was based off a force feedback loop that incorporated a FB gain and delay [19].

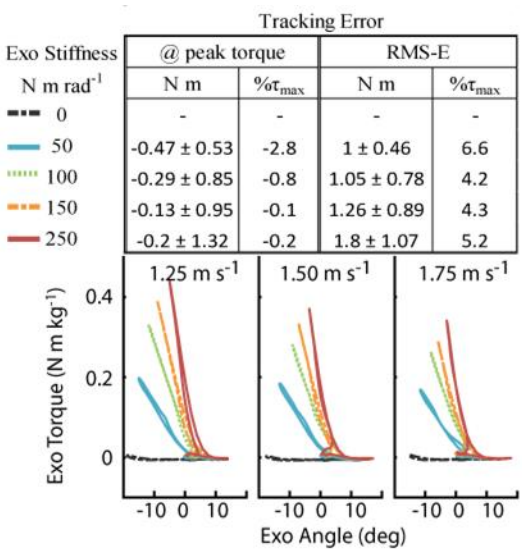

Figure 1.5: Exoskeleton torque tracking error and work loops for three walking speeds. Torque error was minimized through PD feedback and inter-stride learning. The slope of the work loop represents stiffness and the area within the work loop represented energy added/dissipated. Maximum net work was 0.02 W kg^{-1} representing 0.1% of metabolic power.

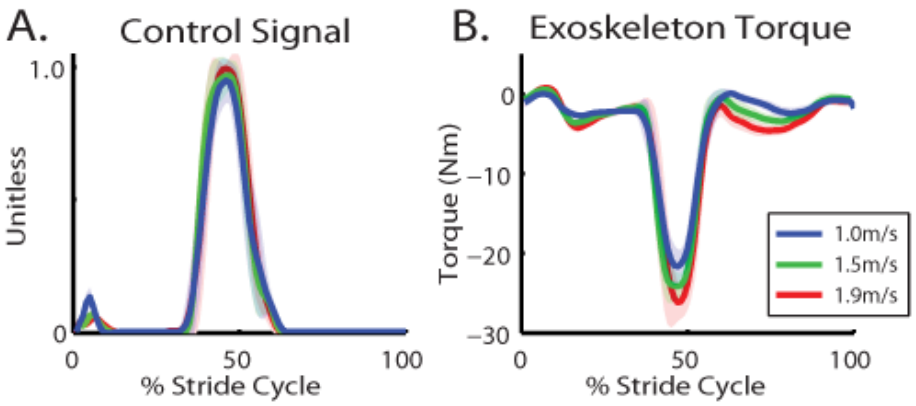

Figure 1.6: Exoskeleton proportional EMG control signal and torque for three walking speeds. Control signal remained saturated at 1 for the three walking speeds. Applied exoskeleton torque also adapted to faster walking speeds with increased peak torque [18].

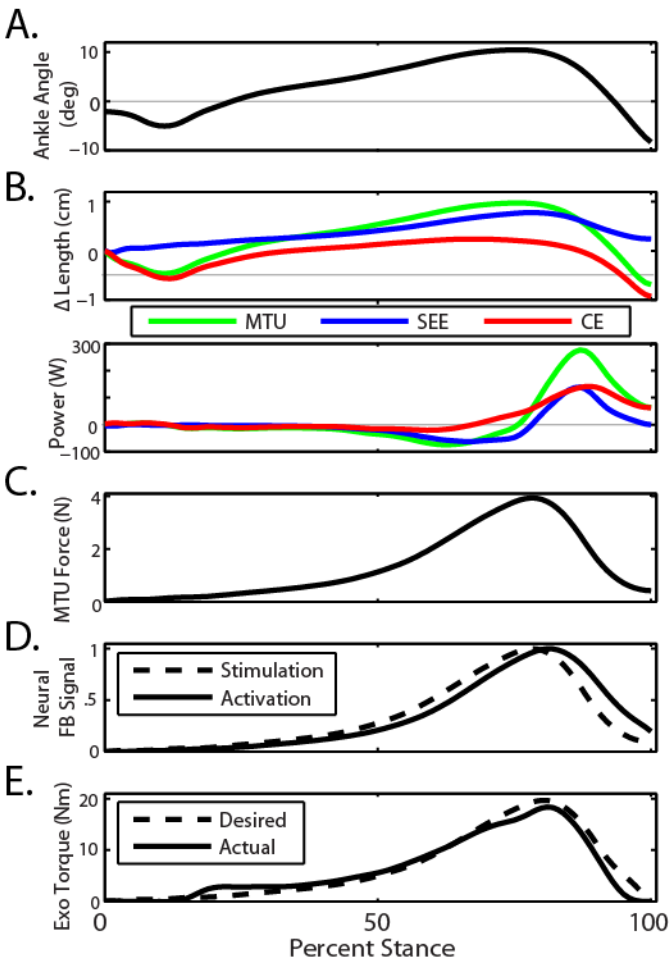

Figure 1.7: Exoskeleton NMM states and exoskeleton torque for walking at 1.25 m s^{-1}. The behavior of the internal muscle states are similar to those observed in walking humans [16]. The contractile element is isometric in early/mid stance followed by shortening in late stance (B). Increase in MTU force (C) results in increased NF FB signal (D) and increased exoskeleton torque (E) [19].

Chapter 2 - The Goldilocks Zone: Interplay of Elastic Ankle Exoskeleton Assistance and Walking Speed on the Mechanics and Energetics of Human Walking

In preparation for submission to Science Robotics

Introduction

The field of wearable robotic devices for improving walking performance is a quickly expanding. In fact, it has been less than five years since the first tethered ankle exoskeleton broke the metabolic barrier milestone [5]. Since this first study, the results have only improved. More recently, a portable powered ankle exoskeleton have shown improvements up to 8% [2] and soft exo-suits powering both the ankle and hip have shown reduced metabolic demands up to 22% [20]. These and other lower limb powered wearable systems accomplish the goal of reducing metabolic demand by transferring net energy to the user and reducing mechanical power required from skeletal muscle. Our lab has shown that a passive elastic system can reduce metabolic demand while delivering no net work [6]. Although the means of delivering the assistance to the user varies across devices, one similarity among most of these systems was the gait conditions tested for evaluation. Most exoskeleton devices have been tested on level ground at one single speed. Although the level-ground, single speed condition has proven an important benchmark for across study comparisons, if the devices are to be used in the real-world, further work in evaluation of exoskeleton assistance in variable gait conditions is needed. Our world is dynamic - we walk, run, change speeds, walk uphill and downhill. Only a few exoskeleton devices have been tested in non-baseline conditions such as load carriage [2], incline walking [21, 22], and intermediate speed walking [2]. To our knowledge, no study has evaluated the effect of multiple walking speeds on the exoskeleton and human response within a single study. Our approach allows us to benchmark the performance against previous work and evaluate exoskeleton performance across gait speed.

The goal of this work was to evaluate the coupling between walking speed and ankle exoskeleton rotational stiffness. Our previous research indicates that bilateral elastic ankle exoskeletons with intermediate stiffness springs placed in parallel with the human triceps surae and Achilles' tendon reduces the metabolic demand during level walking at 1.25 m s^{-1} by up to 7% [6]. Whether this same parallel stiffness is optimal at other walking speeds has yet to be determined. As a starting point for developing hypotheses for how ankle exoskeleton stiffness will change with speed, we use the biological response as inspiration. Specifically, we can measure how the human plantarflexors quasi-stiffness changes with speed and use that knowledge to predict how exoskeleton stiffness responds to speed.

The ankle is an important contributor to positive joint power in both walking and running over a range of gait speeds. In normal gait, the muscle tendon unit (MTU) of the ankle joint efficiently provides approximately half of the mechanical positive power [23]. In late stance, the ankle provides almost the entirety of positive power for redirecting the center of mass [24]. In providing efficient and powerful ankle plantarflexion torque, the muscle and tendon work in concert as series elements. In early stance, as the MTU lengthens, the Achilles tendon stretches and stores elastic energy against the clutch-like isometric triceps surae muscles [25]. This is followed by a rapid period of muscle contraction and tendon recoil where the tendon provides nearly half the positive power [16].

The combined effect of tendon stretch and muscle contraction, in addition to other possible neural and co-contraction effects during specific phases of walking gait can be estimated by the ankle joints quasi-stiffness. The literature detailing how biological joint quasi-stiffness changes with gait frequency is unclear. In a forward-dynamic walking model, ankle AFO optimal stiffness (meant to simulate a passive ankle) remains mostly constant over gait speeds. However, in this study the simulated walking speeds were much slower than preferred walking speed in able-bodied adults [26]. In humans, the biological ankle quasi-stiffness appears to increase with increasing gait speed. However,

the relative increase in stiffness depends on the phase of stance (*i.e.* early, mid, late stance) [8].

We hypothesize that we will find an optimal exoskeleton rotational stiffness at each speed where the metabolic minimum is achieved. In accordance with expected biological response to walking speed, we also hypothesize that the optimal stiffness for the greatest metabolic reduction will increase with increased walking speed. This hypothesis extends our previous work in passive elastic devices [6] and provides additional insight into device development and human response to assistive exoskeletons.

Methods

Participants: Eleven healthy adults (n = 11, 7 male 4 female, mass: 76.8 ± 8.2 kg, age: 27.7 ± 3.3 years, height: 1.75 ± 0.07 m) participated in the study. All participants gave written consent prior to participation in the study which was approved by the Institutional Review Board at University of North Carolina at Chapel Hill.

Exoskeleton testbed: The exoskeleton testbed was a research tool capable of providing bilateral mechanical plantarflexion assistance to the user. A similar device has been demonstrated in previous work [10, 12]. We developed the device in our lab to efficiently and systematically test exoskeleton assistance strategies, and, in this study, we used the system to apply rotational stiffness to bilateral ankle exoskeletons. The device consisted of three primary components: (1) bilateral ankle exoskeleton end effectors, (2) benchtop motors and transmission, and (3) control system (Fig 1).

The exoskeleton end effector was a lightweight carbon fiber ankle foot orthosis (AFO) that applies plantarflexor torque to the ankle. To allow for flexible testing across subjects, we designed the end effector to be modular such that we can accommodate anthropometric variation in subjects' foot, ankle and shank with four effectors (Short/Small, Short/Large, Tall/Small, Tall/Large). Ankle position was accommodated by

moving the joint forward and backward on the end effector. Mass of the end effector without attachment hardware was (415g).

Two offboard 1.61 kW benchtop motors (Baldor Electric Co, Fort Smith, AR) delivered plantarflexion torque to the bilateral ankle exoskeletons by applying a pulling force to the end of the exoskeleton moment arm through a flexible Bowden-cable transmission. At the end effector, we terminated the internal cable to an inline tensile load cell (DCE-2500N, LCM Systems, UK) and attached to the end effector moment arm (~10 cm) through a series elastic element. The motors were positioned behind the subject at approximate shoulder height (54" with respect to treadmill). Through pilot testing evaluation, this height and position provided the best combination of subject ROM, exoskeleton controllability, and limited the interference with camera line of sight.

The exoskeleton control consisted of a high-level controller which calculated a desired torque and low-level controller providing torque tracking. The system was implemented through a real-time control package (DS1103 dSpace Inc, Germany) where analog sensor data was sampled at 5kHz and motor command signals were generated at 500 Hz. A high-level impedance controller determined the desired exoskeleton torque. The impedance controller was designed to emulate a physical passive elastic element capable of providing plantarflexion torque (rotational stiffness) to the ankle akin to our previous device [6]. As such, we set the velocity term, b, to zero. We calculate desired torque based off a predefined rotational stiffness and the real-time ankle angle (Eq 2.1)

$$\tau_{exo} = k_{exo} \times \left(\theta_0 - \theta_{ankle}\right) \quad (2.1)$$

where k_{exo} was rotational stiffness of the exoskeleton, θ_0 was the onset angle, and θ_{ankle} was the real-time ankle angle. A goniometer (5 kHz, 250Hz Biometrics, UK) between the foot and shank segment measures real-time sagittal plane ankle angle, and onset angle (θ_0) was set at contact of the foot with the treadmill. We determined gait state and heel strike by sampling vertical ground reaction force from the instrumented treadmill (Bertec, Columbus, OH).

The low-level controller was a modified PD controller where torque error was driven to zero using proportional torque error and motor velocity damping feedback in combination with inter-stride learning of torque-error [11]. An inline load cell measured exoskeleton torque (250Hz LP Filter, LCM Systems Ltd, UK) and an optical encoder (E5 Optical Encoder, US Digital, Vancouver, WA) measured motor pulley velocity (250Hz LP Filter). An analog velocity command was calculated and sent to the motor controller operating in velocity mode.

Walking Trials: Participants completed testing over a four-session period in which they walked at three speeds (1.25, 1.5, and 1.75 m s^{-1}) at five ankle exoskeleton rotational stiffness conditions (k_{exo} = 0, 50, 100, 150, 250 Nm rad^{-1}) and one no exoskeleton condition (NE). The order of the four testing sessions was (1) exoskeleton training, (2) gait mechanics, (3) steady state metabolic demand, (4) instantaneous metabolic demand. The imposed waiting period between testing session was 2-7 days to allow for learning and retention [27].

1. **Training:** Previous work has demonstrated the importance of training on the acceptance of mechanical assistance in exoskeletons [13, 28, 29]. Each participant walked in the exoskeleton at 1.25 m s^{-1} for a total of 95 minutes over 5 trials. The participants walked at each of intermediate stiffness conditions (k_{exo} = 50, 100 150 Nm rad^{-1}) for 25 minute trials and at the min and max condition (k_{exo} = 0, 250 Nm rad^{-1}) for 10 minutes. Indirect calorimetry data was collected for each of the trials.
2. **Gait Mechanics:** The participant walked for 2 minutes for each of the 18 trials (6 conditions x 3 speeds). The order of the trials was pseudo-randomized where the order of the walking speed was randomized and within each speed the order of the stiffness was additionally randomized. The NE condition was performed at either the beginning or end of the study. The participant was instrumented with EMG on the left shank and lower limb motion capture markers.

3. **Steady State Metabolic Demand:** The order of the steady state metabolic cost was counterbalanced with the instantaneous metabolic cost testing day and was either performed on session 3 or session 4. To allow participants metabolic rate to reach steady state, each walking trial lasted 5 minutes. Similar to the gait mechanics session, the subjects walked for each of the 18 trials and order was pseudo-randomized. The testing order was not maintained between the gait mechanics session and steady state metabolic demand session. Indirect calorimetry data was collected for each of the trials.
4. **Instantaneous Metabolic Demand:** With the participant walking continuously at 1.25 m s^{-1}, we performed two stepwise sweeps of the rotational stiffness parameter through the full range (k_{exo} = 0-250 Nm rad^{-1}) over 25 minutes. The sweep began at either the lowest/highest stiffness (randomized), and, following a five-minute acclimation at the first condition, a 25 Nm rad^{-1} step increase/decrease in stiffness was applied every two minutes. The stiffness sweep in the opposite direction was then applied following a 10-minute break. Indirect calorimetry data was collected for each of the trials.

Biomechanics measurements: Lower limb kinematics was measured using reflective marker motion capture system (120 Hz, Vicon, Oxford, UK) and the subject was instrumented with 44 reflective markers to capture 6-DOF motion of the foot, shank, thigh, and pelvis. Joint angles were calculated from marker data and joint velocity was calculated as the first derivative of angle (Visual 3D, C-Motion Germantown, MD). Force ergometry was captured with a split-belt instrumented treadmill (960 Hz, Bertec). We performed inverse dynamic analysis to calculate the joint moment of the ankle, knee, and hip (Visual 3D). Analog data was filtered at 25Hz and marker positions were filtered at 6Hz. The biological contribution to ankle moment was calculated by subtracting the directly measured exoskeleton torque from the total ankle moment. Joint angles and moments

were reported for the sagittal plane. 6-DOF joint power with a rigid foot was calculated using techniques similar to Zelik *et al* [30].

For a given subject, time-domain measurements for each of the 18 conditions were calculated by time normalizing each stride between heel-strike and heel-strike of the subsequent stride. Multiple strides (15.5 ± 1.1) were then averaged together to obtain a single normalized stride for the condition. Integrated and peak values were calculated prior to intra-stride averaging. Average stride joint moment and power were calculated by integrating the time-domain moment/power and dividing by stride time. Average data for particular phases was the time-integral over that phase divided by the time of the gait phase. Peak values for a given measurement and condition are the average of the peaks for each stride within that condition.

EMG measurements: Muscle activity of the ankle plantarflexors (medial and lateral gastrocnemius, soleus) and ankle dorsiflexor (tibialis anterior) were measured with electromyography on the left leg (SX230, Biometrics, UK). To obtain EMG envelope, the raw EMG data was high-pass filtered at 20 Hz, rectified, and low-pass filtered at 10 Hz. Integrated EMG (iEMG) is the time-integral of the EMG envelope averaged across each stride for a condition. The amplitude of the EMG envelope and the integrated EMG for each muscle was normalized to the peak amplitude for the muscle across all conditions and speeds for each subject.

Energetic measurements: We calculated metabolic power (W kg^{-1}) using a portable indirect calorimetry system (OxyCon Mobile, Carefusion, USA) and applying standard calorimetry equations [31]. To obtain net metabolic power for each condition, we subtracted metabolic power collected during the pre/post standing trials from metabolic power for the walking conditions. For steady-state metabolic demand, we averaged the breath-by-breath data for the last minute of each five-minute trial.

Instantaneous metabolic demand: Instantaneous metabolic demand has been demonstrated in previous work applied to identifying optimal walking speed and exoskeleton assistance[32-34]. We modeled the relationship between steady-state metabolic demand and instantaneous metabolic demand as a first-order relationship. We calculated the model time constant prior to the stiffness sweep by having the participant walk on the treadmill and applying a step change in metabolic demand. This was done by having the participant walk for 5 minutes with no assistance at 1.25 m s^{-1} followed by a step change in speed to 1.75 m s^{-1} for 5 minutes. The time constant and first-order relationship was applied to breath-by-breath data collected during the stiffness sweep conditions to calculate the instantaneous metabolic cost at each condition. In post-processing we applied the algorithm developed by Koller *et al.*[34] to calculate the polynomial relationship between metabolic demand and exoskeleton stiffness.

Statistics: Statistical analysis was only performed on exoskeleton conditions to isolate the role of stiffness rather than the effect of the weight and other structural impacts of the device. For joint dynamics, EMG, and net metabolic demand, we reported the means and standard error calculated across subjects. Metabolic demand was the primary outcome measure for this study. Based on our previous work, we expected second-order relationship between metabolic cost and exoskeleton stiffness. We therefore performed a three-factor mixed-model ANOVA for each speed (random effect: subject; main effect: k_{exo} k^2_{exo}) to test the effect of exoskeleton assistance ($\alpha = 0.05$; JMP Pro, SAS). For the speeds where we found a main effect, we ran post-hoc pairwise t-tests at each speed to compare the condition that yielded the largest reduction in metabolic cost against the no assistance condition ($p < 0.05$). For each speed, we performed two-factor ANOVA (random: subject, main effect: k_{exo}) to test the relationship between user's biomechanics and EMG response and exoskeleton stiffness. Finally, we performed a 2-factor ANOVA to test the effect of speed on the users' response (random: subject, main effect: walking speed, k_{exo}). A Shapiro-Wilk W test confirmed normality for affected tests.

Results

Steady State Metabolic Demand: Exoskeleton rotational stiffness reduced metabolic cost of walking at 1.25 m s^{-1} and 1.75 m s^{-1}. At 1.5 m s^{-1}, exoskeleton assistance resulted in increased metabolic demand for all conditions (Fig 2). A three-factor mixed-model ANOVA indicated a significant relationship between net metabolic demand and stiffness squared at both 1.25 m s^{-1} (n=11, k^2_{exo} p = 0.022) and 1.75 m s^{-1} (k^2_{exo} p = 0.009). There was little relationship at the intermediate speed (k^2_{exo} p = 0.71). The reduction in net metabolic cost between the no assistance condition and the optimal condition was also significant at the slowest speed (k_{exo} = 50 Nm rad^{-1}; -4.2% CI<0.4%, 7.8%>; two tailed paired t-test p = 0.032) and fastest speed (k_{exo} = 50 Nm rad^{-1}; -4.7% CI<1.4%, 7.1%>; two tailed paired t-test p =0.009). The optimal stiffness calculated as the minimum of the model was 69 Nm rad^{-1} and 78 Nm rad^{-1} for slow and fast walking. No optimal stiffness was determined for the intermediate speed. For simplicity, the 50 Nm rad^{-1} condition is referred to as the optimal condition for slow and fast walking for the remainder of the paper. Metabolic results for individual subjects is reported in Table 2.1.

Gait mechanics at 1.25 m s^{-1}: With increasing exoskeleton stiffness, we observed an overall increase in exoskeleton torque and a decrease in biological moment at the ankle for all conditions ($p < 0.0001$) (Fig 3a). At the time of peak moment, the total torque remained constant as exoskeleton torque increased causing biological moment to decrease ($p < 0.0001$). Compared to the no assistance condition, the optimal stiffness resulted in a 0.05 Nm kg^{-1} (13%) reduction in average biological moment and a 0.19 Nm kg^{-1} (12%) reduction in peak biological moment. Application of the highest stiffness resulted in a 0.09 Nm kg^{-1} (22%) reduction in average biological moment and a 0.46 Nm kg^{-1} (29%) reduction in peak biological moment with respect to no assistance. Conversely, in early stance (0-40%), biological moment decreased only slightly ($p < 0.005$) and increased exoskeleton assistance

resulted in amplification of total ankle torque ($p < 0.0001$). Average positive power of the ankle declined with increasing stiffness ($p < 0.0001$) with a maximum reduction of 30% at maximum stiffness (0.21 W kg^{-1}) compared to no assistance (0.30 W kg^{-1}) (Fig 3b). Negative power also declined and net power increased slightly ($p < 0.005$). Exoskeleton average power increased with initial increase in stiffness (0.04 W kg^{-1} at 50 Nm rad^{-1}) but was the same for the 100 Nm rad^{-1} through 250 Nm rad^{-1} conditions (0.06 W kg^{-1}).

With increasing exoskeleton stiffness, stance average soleus muscle activation decreased ($p < 0.0001$) by 10% for optimal condition and 24% at the stiffest condition (Fig 3c). When exoskeleton assistance was applied, peak dorsiflexion decreased ($p < 0.0001$) by 3.0 degrees (17%) at the optimal condition and 10.4 degrees (59%) at the highest stiffness. For the other muscles about the ankle (lateral and medial gastrocnemius and TA), we measured an increase in average stance activation although the only significant increase was for the TA ($p < 0.0001$) (Fig. 2.7). At more proximal joints, increasing exoskeleton stiffness resulted in a shift from knee extension to knee flexion (Fig. 2.8). Average extension moment decreased ($p < 0.0001$) from 0.19 to 0.09 Nm kg^{-1} and average flexion increased from 0.17 to 0.41 Nm kg^{-1} across the range of exoskeleton stiffness. Knee average negative and net power increased as stiffness increased ($p <0 .0001$). Hip extension ($p < 0.005$) and flexion ($p < 0.05$) increased and average positive and net power increased ($p < 0.05$) with increasing stiffness (Fig. 2.9).

Gait mechanics at 1.50 m s^{-1} and 1.75 m s^{-1}: In terms of gait mechanics, similar results were observed for intermediate (1.5 m s^{-1}) (Fig 4) and fast walking speeds (1.75 m s^{-1}) (Fig 5). Compared to the no assistance condition, at 1.5 and 1.75 m s^{-1} the optimal stiffness resulted in a 9% and 7% reduction in average moment and a 9% and 10% reduction in peak moment (Fig 4a and 5a). Application of the highest stiffness resulted in a 17% and 14% reduction in average moment and a peak moment reduction of 24% and 23% at respective mid and high walking speeds. Like the slower speed, average positive power of the ankle declined with increasing stiffness with a maximum reduction of 20% at maximum stiffness (0.29 and 0.35

W kg^{-1}) compared to no assistance (0.36 and 0.44 W kg^{-1}) (Fig 4b and 5b). Exoskeleton average positive power was constant at the faster speeds and higher stiffness values (0.06 W kg^{-1}).

With increasing exoskeleton stiffness, soleus muscle activation decreased for 1.5 and 1.75 m s^{-1} walking speeds ($p < 0.001$) by 9% and 9% respectively for optimal condition and 15% and 11% at the stiffest condition (Fig 4c and 5c). Finally, when exoskeleton assistance was applied, peak dorsiflexion decreased ($p < 0.0001$) by 17% and 22% at the optimal condition and 65% and 73% at the highest stiffness for 1.5 and 1.75 m s^{-1} walking respectively (Fig 4d and 5d). For the other muscles about the ankle (lateral and medial gastrocnemius and TA), we observed an increase in average activation (Fig. 2.7). At 1.5 m s^{-1}, there was a significant relationship between stiffness and the activation for all three muscles ($p < 0.05$). The 1.75 m s^{-1} walking speed was the only speed where we didn't see a significant increase in TA activity. At more proximal joints, increasing exoskeleton stiffness resulted in a shift from knee extension to knee flexion for both speeds ($p < 0.0001$) and shift to more negative joint power ($p < 0.0001$) (Fig. 2.8). At the hip, there was a slight increase in flexion moment in 1.5 m s^{-1} walking ($p < 0.05$) (Fig. 2.9).

Comparison Across Speeds: We measured a decrease in relative exoskeleton contribution as walking speed increased. From the slowest (1.25 ms^{-1}) to the fastest (1.75 ms^{-1}) walking speed, peak exoskeleton torque decreased ($p < 0.01$) by 23% at the highest stiffness (250 N m rad^{-1}) despite a 12% increase in peak total ankle torque ($p < 0.0001$) and 26 % increase in biological peak moment ($p < 0.0001$) (Fig. 2.6). In the highest stiffness conditions, total positive power at the ankle increased ($p < 0.0001$) by 64% from 1.25 m s^{-1} to 1.75 m s^{-1} despite exoskeleton positive power not increasing (0.5%). Only in the lowest stiffness condition did we measure an increase in exoskeleton positive power (16%) with increased speed. From slow to fast walking, the ankle peak dorsiflexion angle decreased ($p < 0.01$) for all conditions with an average decrease in ankle angle of 25%. Peak plantarflexion increased

($p < 0.0001$). In the no assistance condition the angle declined by 11% (2 degrees) and the decrease at the highest stiffness was 43% (3.1 degrees).

Training: Results from the training day indicate that participants adapted in a metabolically beneficial manner only in the 50 Nm rad^{-1} stiffness condition (Fig. 2.10). Over the training period, for 50 Nm rad^{-1} subjects on averaged reduced metabolic demand by 5.6%. Two testing sessions later, the metabolic rate during the steady state testing day was on average 3% lower than the rate at the end of training day. Conversely, we measured an increase in metabolic rate over the testing period of 1.7% for the three stiffest conditions. The steady state metabolic sessions on average were 7.8% lower for the three high stiffness conditions than training day rates.

Instantaneous Metabolic Demand: Both the steady state and instantaneous metabolic demand approaches found an average metabolic minimum at low rotational stiffness values (Fig. 2.11). Using the steady state approach, the metabolic minimum was found at 50 Nm rad^{-1} (3.00 ± 0.13 W kg^{-1}). Using the instantaneous approach, the metabolic minimum was found at 25 Nm rad^{-1} (3.05±0.1). When comparing like conditions, the minimum for the instantaneous approach was 50 Nm rad^{-1} (3.06 ± 0.1 W kg^{-1}). Time constant for the first order model was 58 ± 19 seconds averaged across subjects.

Discussion

Our data suggests that passive elastic ankle exoskeletons improved metabolic demand at multiple walking speeds. The lowest tested rotational stiffness condition (50 Nm rad^{-1}) resulted in a metabolic reduction of -4.2% at slow (1.25 m s^{-1}) and -4.7% at fast (1.75 m s^{-1}) walking speeds. Surprisingly, no stiffness condition resulted in an average decrease in metabolic demand at the intermediate speed (1.5 m s^{-1}). Several subjects had a slight decrease in metabolic rate at the intermediate speed (Table 2.1).

The results from this study for walking at 1.25 m s^{-1} support findings in a previous study from our lab where rotational stiffness was applied using physical springs rather than the emulated elastic system we present here [6]. We found a second order relationship (k^2_{exo}) between stiffness and metabolic demand where a balance between low and high stiffness is necessary for metabolic improvement. Whole body metabolic demand for walking with the exoskeleton can in part be attributed to the energetic demand of the muscles (i.e. use of ATP for cycling cross-bridges). Application of exoskeleton assistance beneficially resulted in reduction in biological ankle moment and power, and a decrease in soleus muscle activity. Conversely, exoskeleton assistance resulted in an increase in gastrocnemius and tibialis activity and a shift from knee extension to knee flexion moment. Although not reported here, we expect that other knee flexor muscles (*e.g.* biceps femoris longhead) EMG would be higher to account for increased flexion moment. These trends are consistent across speeds. The balance between beneficial reductions and compensations gives justification for the bowl shape in metabolic demand with application of exoskeleton stiffness.

We believe that much of the metabolic improvement from the elastic device was provided by reducing ankle moment and therefore muscle force. Recent work in muscle energetics suggests that muscle energy use is driven by force production rather than work [35]. These results showed that a muscle stretch-shorten cycle requires similar amounts of energy to that of an isometric contraction. In an exoskeleton hopping study, metabolic demand was reduced when muscle force was reduced but muscle work remained constant [36]. This would suggest that applying more assistance and thereby reducing biological load should be the simple solution. To an extent this appears correct as we achieved a reduction in metabolic at low stiffness values when muscle force was reduced. However, our data suggest that more assistance is not better, and that a sweet spot in metabolic benefit is found by balancing force assistance with neural, muscle-tendon dynamics, and limb kinetic chain side effects that may be present.

As assistance is increased, the participants were unable to maximize the benefit of the assistance. In fact, we see diminishing returns where at the high stiffness values, although the stiffness is increased by 67%, peak exoskeleton torque increases by only 13%. We've noted that subjects compensate by decreasing dorsiflexion, but the mechanism for this compensation is unclear. One potential explanation is that the user is unable to 'turn down' their muscle activation in proportion to the level of assistance provided. Research has shown that joints (and limbs) maintain constant stiffness during a given locomotion condition [37]. It is believed that this is accomplished through a combination of stretch reflexes (spindle organs) and force transducers (Golgi tendon organs) that are responsible for maintaining a nearly constant ratio of force to length [37, 38]. We observed a decrease in ankle moment from which we can predict a decrease in plantarflexor force. Studies suggests that muscle fascicle lengths become longer with increasing assistance [39], so a sensory feedback Golgi tendon / muscle spindle mismatch could be a possibility. Much of walking is automatic and unconsciously controlled though spinal level central pattern generator, reflexes, cerebellar regulation, and the brainstem [40]. For this reason, users of the exoskeleton may not be able to turn off their plantarflexors as would be required to obtain maximal benefit or coordination with the exoskeleton. Further work in humans and animals into the role of feedforward/feedback mechanisms and the effect of disrupted dynamics in walking would be insightful.

Another potential side effect of applying exoskeleton assistance was that the normally efficient muscle-tendon dynamics become 'detuned'. Muscles dynamics are governed by intrinsic muscle properties where force production and economy are dependent upon the length of the muscle and the contraction velocity [41, 42]. When exoskeleton assistance was applied, biological moment and thus MTU force decreased and strain on the tendon decreased. Modeling data and hopping studies suggest that muscle lengths are in fact longer and undergo increased excursion with increased assistance which may limit force production capacity and economy [39, 43]. The biological system may be resistant to increased muscle strain as expected from

exoskeleton assistance and compensation may arise to limit range of motion [44-46]. Further work assessing in vivo analysis of muscle dynamics with exoskeleton assistance was addressed in Chapter 3.

In early stance, the application of exoskeleton torque did not reduce the biological moment but rather enhanced the amount of total ankle moment. In late stance, the exoskeleton reduced biological moment and peak ankle moment remained fairly constant. Literature suggests that subjects try to maintain constant joint torques [47] so why was torque enhanced at the beginning of stance? One possible explanation was that the biarticulated gastrocnemius muscles are active to prevent hyperextension of the knee. Due to the kinetic chain of the lower limb, the plantarflexion torque of the exoskeleton also generates an extension moment at the knee through dynamic coupling [48]. As a likely compensation for the extension moment with increasing stiffness, gastrocnemius activity was higher and the knee moment was pushed towards flexion as the knee angle becomes more extended. The effect exists for the entire stride but may be more pronounced in early stance when the center of pressure (COP) vector is in front of the knee. Gastrocnemius moment arm was also larger at the knee at more extended postures [49]. The additional flexion moment on the knee was generated by knee flexors (*e.g.* gastrocnemius, biceps femorus longhead). Alternatively, a biarticulated knee/ankle exoskeleton could be designed where the knee component acted in a similar manner to the gastrocnemius and compensates for additional load on knee flexors. An exoskeleton with non-linear or piecewise stiffness profiles where stiffness was low until the COP passes behind the knee could also be a potential solution. Unfortunately, delaying the onset angle for the spring or limiting stiffness also has the effect of limiting the amount of energy that can be stored in the spring.

We did not find that optimal exoskeleton stiffness increased with walking speed when comparing all three speeds. When only comparing the slowest and fastest walking speeds, the optimal stiffness from the regression curve was slightly higher (78 Nm rad^{-1}) at fast walking than slow walking (69 Nm rad^{-1}). The 13% increase in optimal exoskeleton

stiffness was proportional to a 10% increase in ankle quasi-stiffness during dorsiflexion calculated from regression models of humans walking [8]. However, the exoskeleton stiffness increase was not in proportion to the speed dependent increase in ankle quasi-stiffness during plantarflexion (21%) and dual-flexion (*i.e.* late dorsiflexion) (46%). During late dorsi-flexion (dual-flexion) and plantarflexion the contraction of the soleus muscle likely increased the quasi-stiffness of the joint while adding work to the system. As walking speed increased, muscle activity was higher, plantarflexion began earlier, and quasi-stiffness in late stance was higher. Having no 'muscle', the exoskeleton could not maintain low stiffness in early stance while increasing stiffness in late stance for increased walking speeds. Considering that the soleus muscle was likely isometric during dorsiflexion [25], the Achilles tendon was responsible for large percentage of rotational stiffness and energy storage during dorsiflexion [16]. It was not surprising therefore that the user should beneficially respond to the stiffness of the exoskeleton (acting like an exo-tendon) at faster walking speeds in a similar manner to that of the biological tendon. That is, the optimal increase in stiffness of the exoskeleton should be similar to the increase in stiffness of the biological tendon during dorsiflexion.

Contrary to the dynamics of the biological ankle where moment and power increase with increasing walking speed [23, 50], the exoskeleton torque decreased as walking speeds increased. These results are perhaps not surprising considering exoskeleton torque was proportional to dorsiflexion angle and ankle peak dorsiflexion decreases with speed [51]. Our results indicate that dorsiflexion decreased by 11% in unassisted conditions and as much as 43% in the stiffest condition. We observed very little increase in exoskeleton power with speed and exoskeleton power increase is small compared to the biological increase calculated from previous work (45%) [23] and measured from our data when no assistance is provided (44.7%).

The question for why metabolic improvement was not obtained at intermediate speeds was not easily resolved by assessing joint mechanics and muscle activations alone. We did observe an increase in gastrocnemius and TA activity for the 1.5 m s^{-1} walking

speed, and TA activity during stance decreased for 1.75 m s^{-1}. However, joint mechanics and muscle activation patterns are similar for all three speeds and any changes observed in terms of phasing or amplitude are further magnified at the highest speed. For example, the decrease in soleus activation for the 50 Nm rad^{-1} condition was smaller for the intermediate speed (9.1%) than the slow speed (10.5%) but smaller still for the fastest walking speed (8.9%). Exoskeleton torque was further reduced and the biological contribution increases at the fastest walking speeds. This suggest to us that perhaps the difference we observed at the intermediate speed was due to muscle-tendon dynamics that were not evident in joint and activation data. Previous literature suggests that preferred walking speed in adults is close to 1.42 m s^{-1} which also aligns closely with the metabolically optimal walking speed [52]. Humans also select step-frequencies that reduce energetic demand of walking [53, 54]. The structure of the ankle is important for maximizing muscle efficiency [55, 56] (i.e. minimize metabolic demand) and models of walking have suggested that walking efficiency was maximized when step length and frequency and matched to ankle stiffness [57]. Therefore, ankle plantarflexors are likely tuned preferentially to the subjects preferred walking speed. Preferred walking speed collected from the subjects using a 10m over ground test was 1.39 ± 0.04 m s^{-1} and average cost of transport with no assistance at 1.25, 1.50, and 1.75 m s^{-1} were 2.5 ± 0.11, 2.67 ± 0.13, and 3.22 ± 0.15 J m^{-1} respectively. We suspect that the muscle-level detuning associated with the exoskeleton assistance may be more pronounced at the 1.5 m s^{-1} walking speed due to proximity to preferred speed and was further addressed in Chapter 3.

Upon initial inspection, one notable difference between these study results and our previous work in passive exoskeletons, was that the optimal stiffness reported in this study (50 Nm rad^{-1}) was substantially lower than the reported optimal stiffness from the previous work (180 Nm rad^{-1}). However, the stiffness values previously reported were the stiffness of spring elements rather than the stiffness of the exoskeleton system. Conversely, our exoskeleton testbed imposed a torque/angle relationship rather than

relying on physical components to provide stiffness and was less sensitive to structural stiffness and deformation. If deformation in the previous system was accounted for by measuring stiffness from the exoskeleton torque/angle relationship, the optimal stiffness in previous work was approximately 80 Nm rad. This value is close to the minimum found from the regression at slow speed (69 Nm rad^{-1}). There may still be some movement between the human and device that was not accounted for in our system, but we believe that our recent study gave a more accurate portrayal of the applied rotational stiffness.

We found similar values for optimal exoskeleton stiffness using the instantaneous metabolic calculation (25 N m rad^{-1}) and steady state calculation (50 N m rad^{-1}). Part of the reason for the slight discrepancy could be due to the high variability in metabolic data with respect to the slight reduction in metabolic demand using the passive device (low signal to noise ratio). Other experiments that use powered exoskeletons have better signal to noise ratios [34]. For post-experiment analysis of preferred parameters, the time required using the instantaneous approach is not substantially reduced. The time required for the two sweeps (50 min) was only slightly less than the time it would take us to sweep the same conditions using five-minute steady state trials (60 min). However, the power of the instantaneous technique appears to be in online optimization of multiple parameters using techniques such as gradient decent methods or genetic algorithms that showed large improvements in metabolic demand [58].

We acknowledge that there are limitations with our study. The exoskeleton emulator behaved more like an ideal spring rather than a physical spring which dissipates energy. Nor was it like a biological 'exo-tendon' where Achilles tendon hysteresis can be approximately 15% [17] though the true value may be smaller and still debated [59]. Our intention was to tightly control stiffness so that we could measure its effect on the user. Small amounts of work were generated/dissipated but relative to total metabolic power the percent is estimated at less than 0.1%. Future work could consider damping as an additional term to control if energy dissipation or generation is desired. We assessed the performance calculations with respect to the no assistance condition. Increase in

metabolic demand due to added mass of the system is on average 19%. However, we knew from previous work that systems can reduce metabolic demand below added mass effects [6]. We were interested in a system to rapidly and robustly test the effects across exoskeleton control designs and parameter and weight was not a primary concern. Although we have attempted to sample the range of walking speeds, the variation in speed was still narrow. Humans walk at a range of walking speeds and we have only sampled three. We also did not correct for body height which has a factor on preferred walking speed and did not account for strength which affects Achilles tendon stiffness [60].

Conclusion

The metabolic improvement of 4.2% was modest compared to powered devices capable of reductions approaching 22% [20]. The successful active exoskeletons reduce metabolic demand by adding net work to the system. However, results from this study and our previous study indicated that we can reduce metabolic demand by offloading force from the muscles rather than performing work. In fact, the passive systems operated by overcoming an inefficiency in biological muscle – the requirement of consuming energy for isometric contractions. Despite a limited metabolic benefit, passive assistive devices are advantageous given their minimal weight and simplified design in comparison to active systems. Our results suggested that a single compliant exoskeleton spring can achieve metabolic reductions across a range of walking speeds. The findings simplify the design of an elastic device where only one stiffness is required. Furthermore, elastic systems, like the one tested here, may simplify prescription of devices intended to restore structural stiffness to joints in specific populations such as older adults that experience a decrease in Achilles tendon stiffness [61] contributing to reduced push-off capability [62]. A framework for this approach was addressed in Chapter 4.

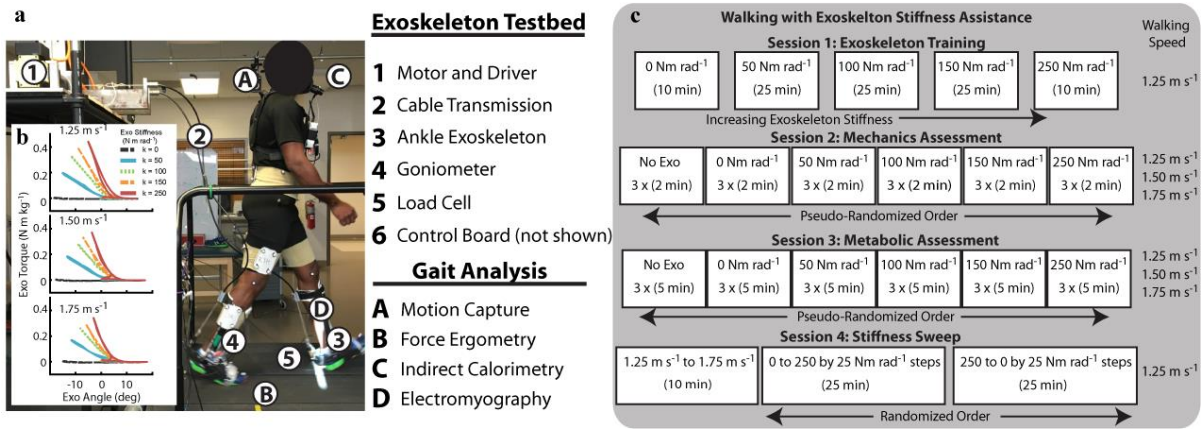

Figure 2.1: Exoskeleton testbed and test protocol. a, Representative setup of the exoskeleton testing platform for evaluating rotational stiffness plantarflexion assistance. The exoskeleton provided plantarflexion torque to the bilateral ankle exoskeletons through off-board motors. The controller emulated elastic rotational stiffness by imposing a torque angle relationship control law ($t_{exo} = k_{exo} * \Delta\theta_{ankle}$) where ankle angle was measured with a goniometer. Torque tracking was accomplished by feedback of applied force. **b,** Work loops for three walking speeds. The slope of the work loop represents stiffness and the area within the work loop represents energy added/dissipated. **c,** Protocol for the four testing sessions.

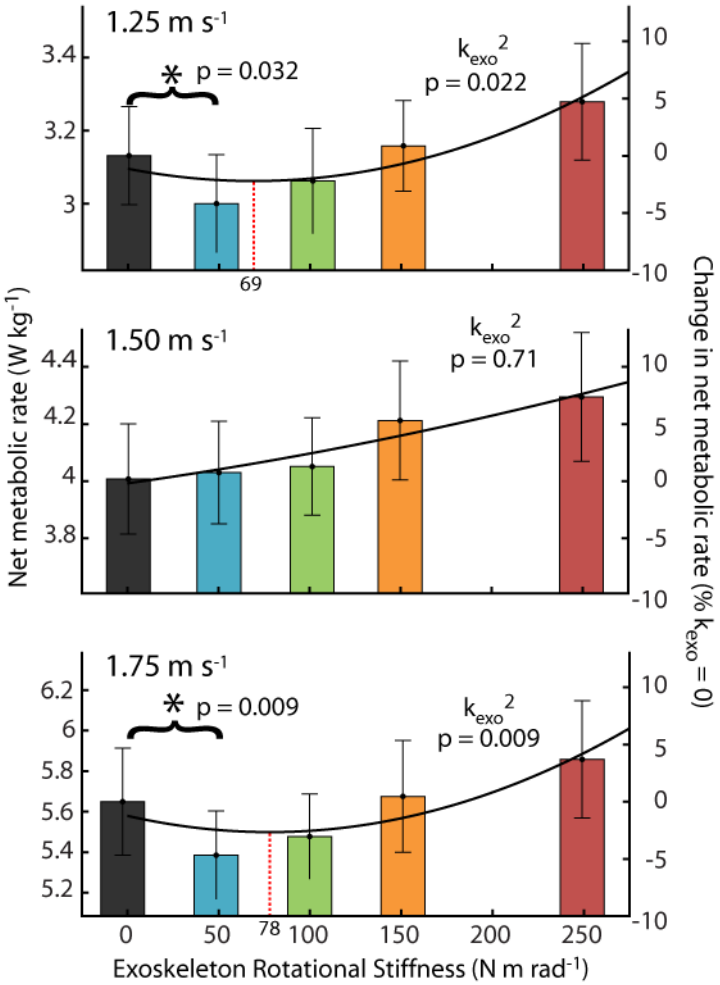

Figure 2.2: Net metabolic rate across speed and stiffness. Steady state metabolic demand for five exoskeleton stiffness conditions (k_{exo} = 0, 50, 100, 150, 250 N m rad^{-1}) and three walking speeds (1.25, 1,50, 1.75 m s^{-1}). A significant relationship was found between rotational stiffness and metabolic rate at slow and fast walking speed (n= 11; mixed model ANOVA with second order term k^2_{exo}; 1.25 m s^{-1} $p_{stifffness}{}^2$ =0.022;1.75 m s^{-1} $p_{stifffness}{}^2$ =0.009). No significant relationship was observed for the intermediate speed. The lowest stiffness (50 N m rad-1) resulted in a 4.2 ± 1.7% (mean ± s.e.m) at 1.25 m s^{-1} and 4.7 ± 1.3% at 1.75 m s^{-1} (paired t-test). The dashed line is a quadratic best where the stiffness at the minima is indicated by the vertical dashed line.

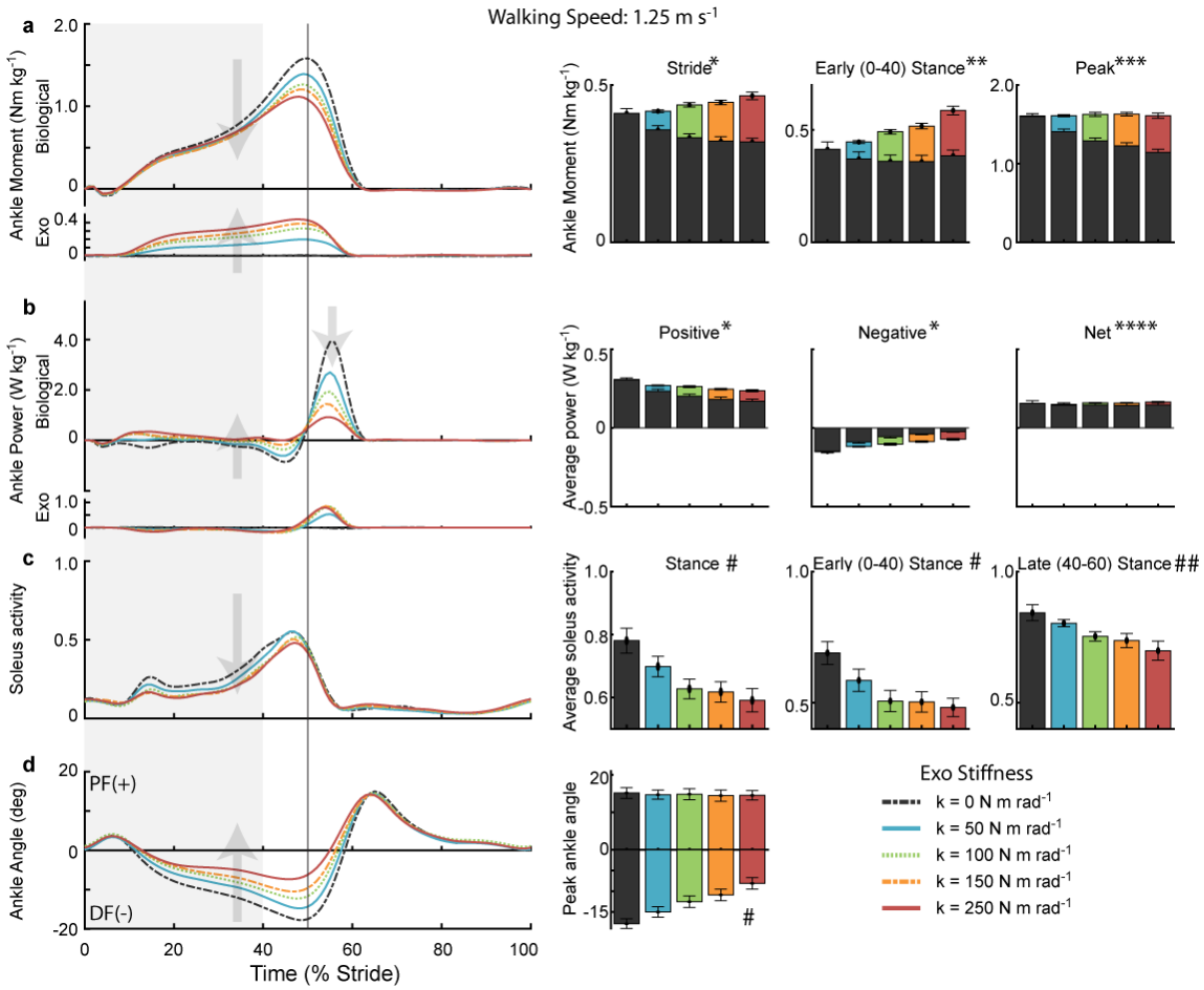

Figure 2.3: Ankle mechanics and muscle activity during walking at 1.25 m s^{-1}. a, Increasing exoskeleton stiffness resulted in increased exoskeleton torque and decreased biological moment. Total ankle torque increased at early stance but peak torque remained nearly constant. Mass normalized biological moment and exoskeleton torque for each stiffness averaged over participants. Stacked bar charts represent the average biological (black-lower) and exoskeleton (colors-upper) contribution to total ankle moment for phases of the gait cycle. **b**, Exoskeleton power remained fairly constant at high stiffnesses and biological power decreased with increased stiffness. Time series of 6DOF biological power and exoskeleton torque for each stiffness. Stacked charts represent biological and exoskeleton contribution to ankle power. Biological net power was net positive for all conditions and exoskeleton net power was negligible. **c**, Muscle activation decreased with increasing stiffness. Time series of soleus muscle activation where amplitude is normalized to the peak activation across all conditions (speed and stiffness) for each subject. **d**, Peak ankle dorsiflexion increased with increased stiffness. Time series of ankle joint plantarflexion (PF) and dorsiflexion (DF) angle. [main effect: stiffness * p<0.0001 (BIO, EXO, and ANK); ** p<0.0001 (ANK, EXO) p<.005 (BIO); *** p<0.0001 (BIO, EXO); **** p<0.0001 EXO only; # p<0.0001; ## p<.005]

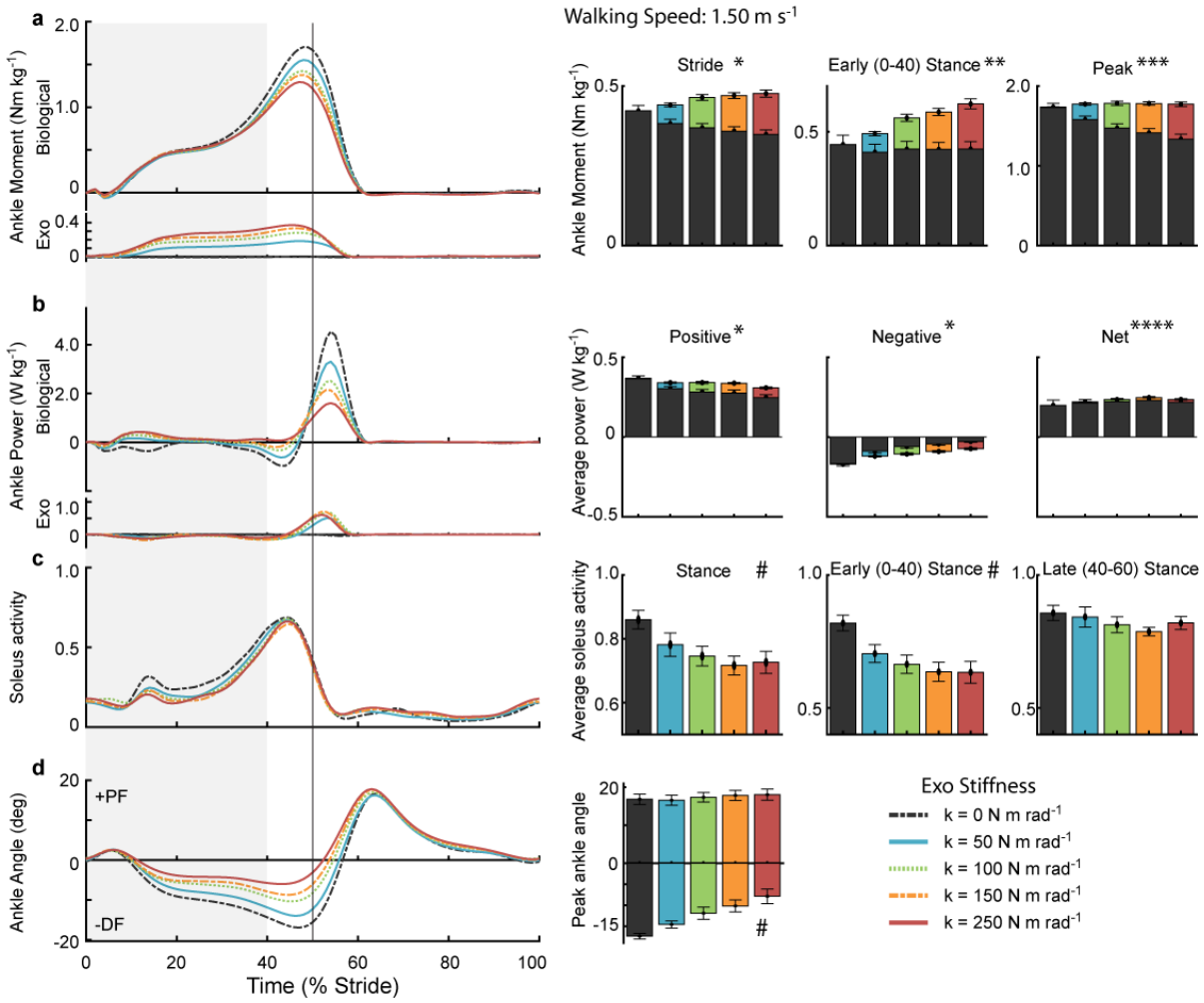

Figure 2.4: Ankle mechanics and muscle activity during walking at 1.50 m s^{-1}. a, Increasing exoskeleton stiffness resulted in increased exoskeleton torque and decreased biological moment. Total ankle torque increased at early stance but peak torque remained nearly constant. Mass normalized biological moment and exoskeleton torque for each stiffness averaged over participants. Stacked bar charts represent the average biological (black-lower) and exoskeleton (colors-upper) contribution to total ankle moment for phases of the gait cycle. **b**, Exoskeleton power remained fairly constant at high stiffnesses and biological power decreased with increased stiffness. Time series of 6DOF biological power and exoskeleton torque for each stiffness. Stacked charts represent biological and exoskeleton contribution to ankle power. Biological net power was net positive for all conditions and exoskeleton net power was negligible. **c**, Muscle activation decreased with increasing stiffness. Time series of soleus muscle activation where amplitude is normalized to the peak activation across all conditions (speed and stiffness) for each subject. **d**, Ankle peak dorsiflexion angle increased with increased stiffness. Time series of ankle joint plantarflexion (PF) and dorsiflexion (DF) angle. [main effect: stiffness * p<0.0001 (BIO, EXO, and ANK); ** p<0.0001 (ANK, EXO); *** p<0.0001 (BIO, EXO); **** p<0.005 (ANK) p<0.0001 (EXO); # p<0.0001]

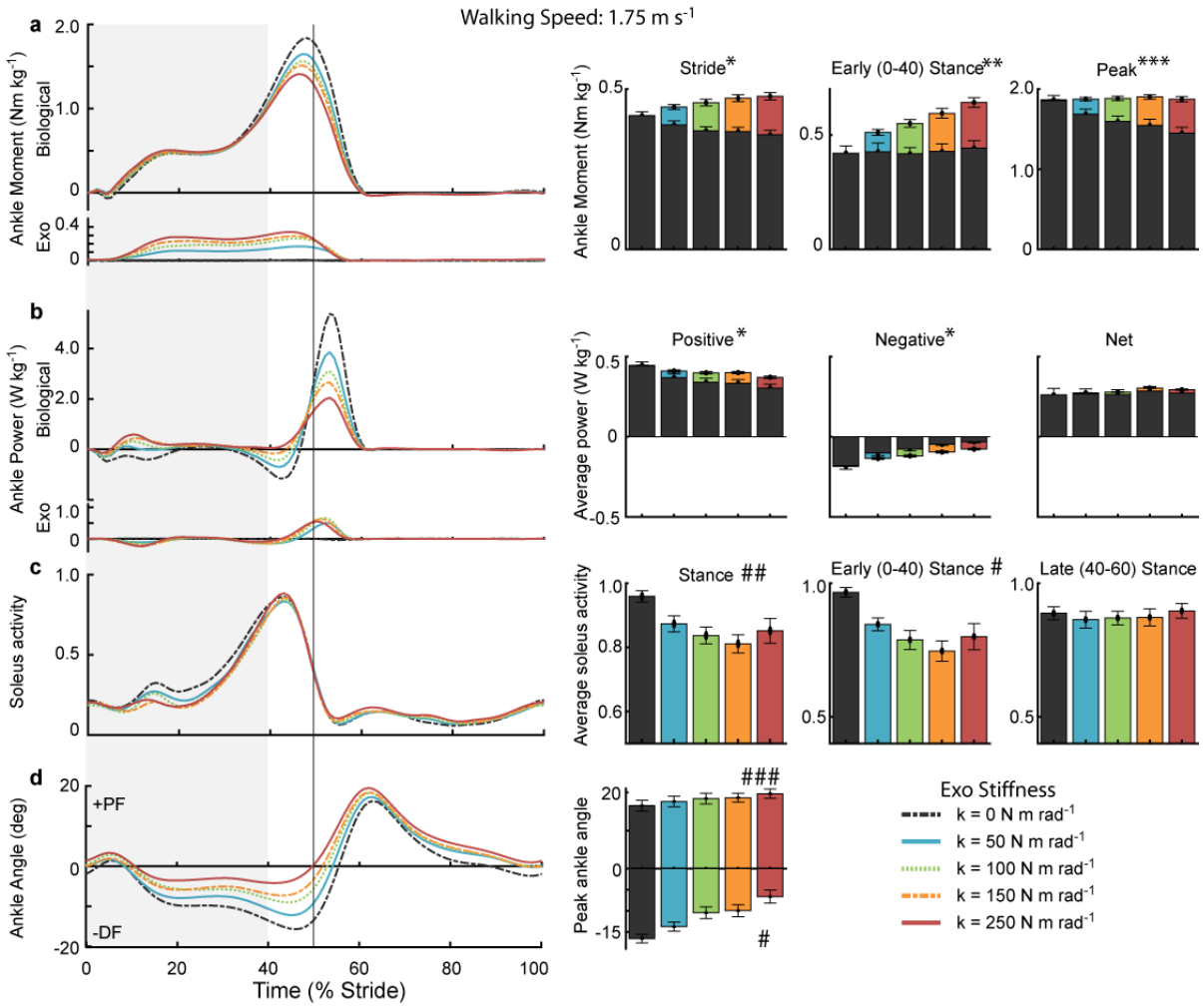

Figure 2.5: Ankle mechanics and muscle activity during walking at 1.75 m s^{-1}. a, Increasing exoskeleton stiffness resulted in increased exoskeleton torque and decreased biological moment. Total ankle torque increased at early stance but peak torque remained nearly constant. Mass normalized biological moment and exoskeleton torque for each stiffness averaged over participants. Stacked bar charts represent the average biological (black-lower) and exoskeleton (colors-upper) contribution to total ankle moment for phases of the gait cycle. **b**, Exoskeleton power remained fairly constant at high stiffnesses and biological power decreased with increased stiffness. Time series of 6DOF biological power and exoskeleton torque for each stiffness. Stacked charts represent biological and exoskeleton contribution to ankle power. Biological net power was net positive for all conditions and exoskeleton net power was negligible. **c**, Muscle activation decreased with increasing stiffness. Time series of soleus muscle activation where amplitude is normalized to the peak activation across all conditions (speed and stiffness) for each subject. **d**, Time series of ankle joint plantarflexion (PF) and dorsiflexion (DF) angle. Ankle peak dorsiflexion angle increased with increased stiffness. [main effect: stiffness * p<0.0001 (BIO, EXO, and ANK);** p<0.0001 (ANK, EXO) p<.005 (BIO); *** p<0.0001 (BIO, EXO); **** p<.05 (BIO) p<0.0001 (EXO); # p<0.0001; ## p<.001; ### p < .05]

Table 2.1: Steady-state metabolic rate for each subject, condition, and speed. Highlighted cells represent conditions where the subject's metabolic rate was less than the no assistance condition. The metabolic rate for the no exoskeleton (NE) assistance was less for all conditions. Fewer conditions were metabolically beneficial in the 1.5 m s^{-1} walking speed.

	1.25 m / s						1.50 m / s						1.75 m / s					
	Rotational Stiffness (Nm / rad)						Rotational Stiffness (Nm / rad)						Rotational Stiffness (Nm / rad)					
Subject	**0**	**50**	**100**	**150**	**250**	**NE**	**0**	**50**	**100**	**150**	**250**	**NE**	**0**	**50**	**100**	**150**	**250**	**NE**
2	2.36	**2.23**	**2.24**	2.68	2.60	**1.95**	3.14	**3.11**	**3.08**	3.18	**3.08**	**2.37**	4.06	4.10	4.30	4.14	4.40	**3.50**
3	3.03	**2.99**	**2.83**	3.22	3.10	**2.71**	3.99	4.33	4.03	4.39	4.52	**3.77**	5.38	**5.08**	5.42	5.64	5.45	**4.91**
4	2.99	3.02	**2.90**	**2.81**	**2.88**	**2.22**	3.32	3.51	3.80	3.79	**3.30**	**2.74**	5.31	**4.91**	**4.84**	**4.82**	**5.10**	**4.05**
5	2.68	**2.39**	**2.46**	**2.52**	**2.63**	**2.25**	3.42	**3.37**	**3.38**	3.45	3.62	**3.16**	5.08	**4.95**	**4.76**	**4.86**	**4.94**	**4.59**
6	4.04	**3.91**	**3.96**	**3.98**	4.25	**3.29**	5.23	5.28	5.20	5.52	5.62	**4.35**	7.32	**6.75**	**6.62**	**7.02**	**7.06**	**5.61**
7	3.63	**3.19**	**3.54**	**3.59**	4.07	**2.89**	4.58	**4.40**	**4.57**	5.17	5.14	**3.76**	5.97	**5.46**	6.02	6.55	6.84	**5.24**
8	3.28	**3.21**	**3.08**	**3.19**	**3.13**	**2.87**	4.05	4.08	4.19	**4.02**	4.29	**2.82**	6.24	6.28	**6.23**	6.63	7.35	**5.06**
9	3.01	3.25	3.26	3.10	3.55	**2.62**	3.92	4.07	4.22	4.08	4.45	**3.44**	5.63	**5.39**	**5.33**	**5.47**	5.66	**4.85**
10	3.28	**3.06**	**3.11**	**3.25**	3.46	**2.88**	4.75	**4.41**	**4.05**	**4.53**	**4.58**	**3.70**	6.67	**5.92**	**6.04**	**6.56**	**6.59**	**5.18**
11	3.08	**2.87**	**2.95**	**3.06**	3.25	**2.63**	3.99	**3.96**	**3.78**	**3.90**	4.13	**3.37**	5.23	**5.05**	5.29	**5.19**	5.36	**4.82**
12	3.05	**2.87**	3.34	3.34	3.14	**2.83**	3.68	3.82	4.26	4.32	4.50	**3.39**	5.26	5.34	5.39	5.56	5.69	**4.51**
Average	**3.13**	**3.00**	**3.06**	**3.16**	**3.28**	**2.65**	**4.01**	**4.03**	**4.05**	**4.21**	**4.29**	**3.35**	**5.65**	**5.38**	**5.48**	**5.68**	**5.86**	**4.76**
s.e.m	0.040	0.040	0.043	0.037	0.048	0.034	0.058	0.054	0.051	0.063	0.068	0.051	0.079	0.066	0.063	0.083	0.087	0.053

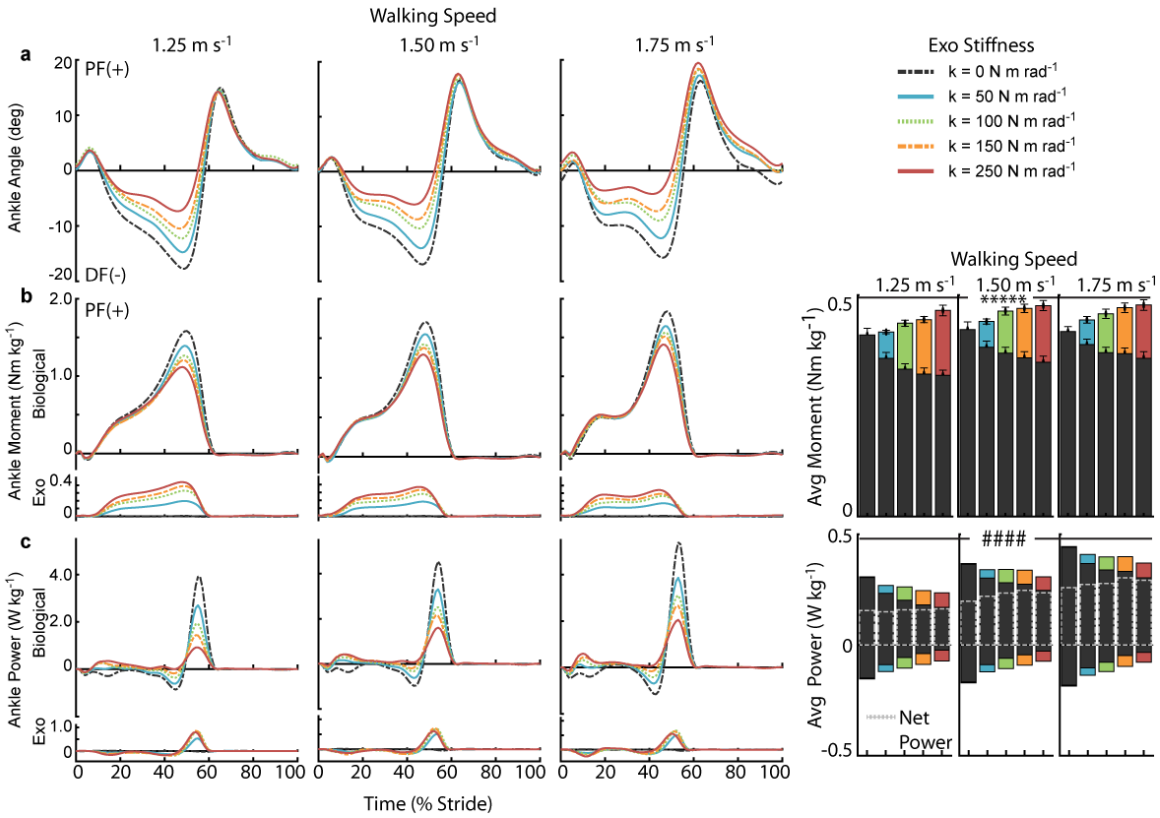

Figure 2.6: Ankle joint mechanics across speeds. a, Ankle angle became less dorsiflexed ($p < 0.01$) and more plantarflexed ($p< 0.0001$) with increased stiffness and speed. Time series of ankle joint plantarflexion (PF) and dorsiflexion (DF) angle for each stiffness and speed averaged across participants. **b**, Exoskeleton peak torque decreased with increasing speed ($p<0.01$) while ankle and biological moment increased with speed ($p<0.0001$). Mass normalized biological moment and exoskeleton torque for each stiffness and speed. Stacked bar charts represent the average biological (black-lower) and exoskeleton (colors-upper) contribution to total ankle moment for each speed over the stride. **c**, Peak ankle and biological power increased with speed ($p<0.0001$). Positive and net power increased with increasing speed. Time series of 6DOF biological power and exoskeleton torque for each stiffness and speed. Stacked charts represent biological and exoskeleton contribution to ankle power and net total power is the dashed insert. [main effect: speed *****$p<0.0001$ (BIO) $p<0.005$ (ANK); #### $p<0.0001$ (POS and NET ANK; POS and NET BIO)]

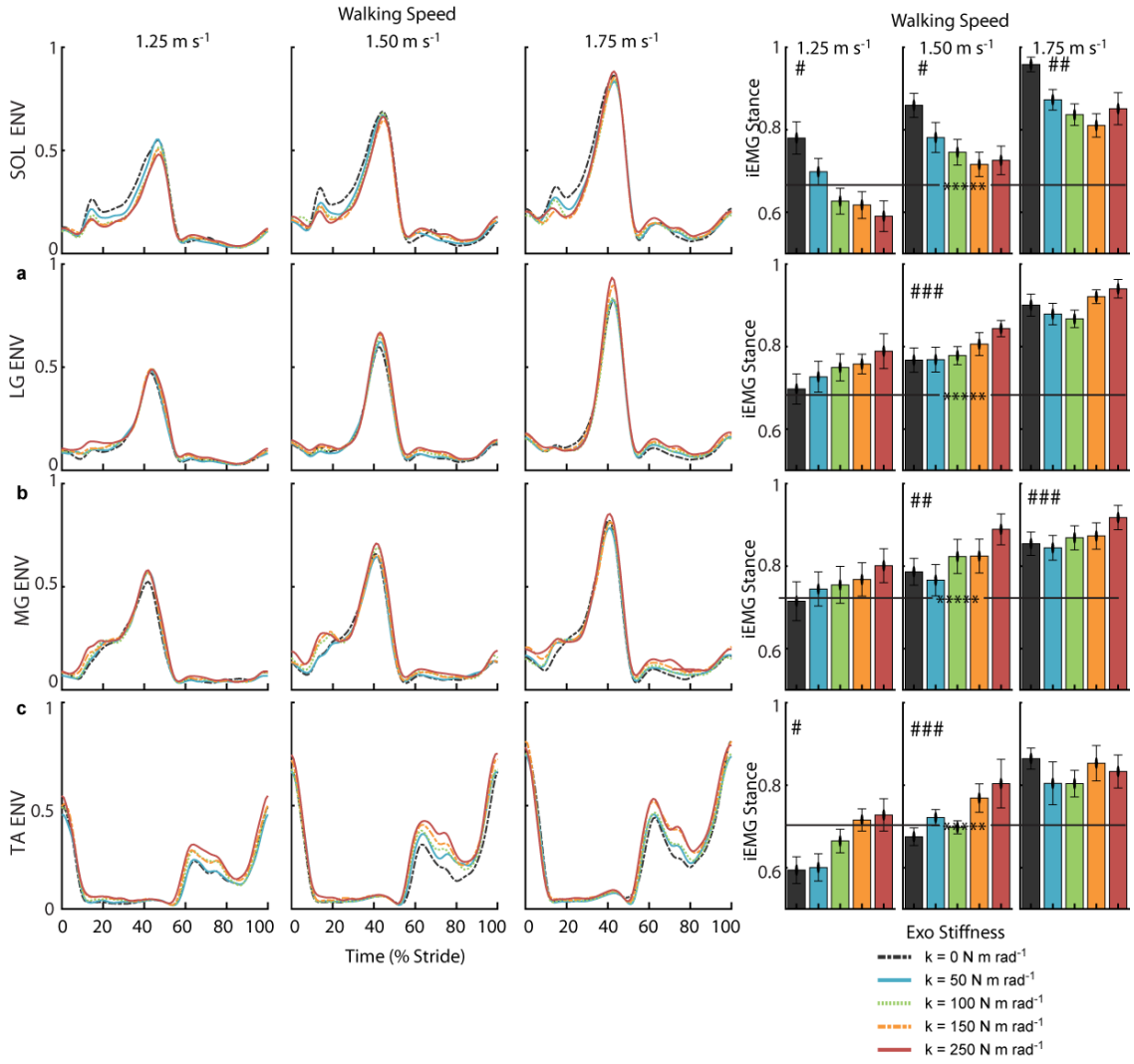

Figure 2.7: Muscle activity of triceps surae and tibialis anterior. For muscles other than the soleus, stiff assistance (red line) resulted in increased activation in early stance and at peak. Activation also increased as walking speed increased. Time series of EMG recordings. Amplitude normalized to the peak value across stiffness and speed for each subject. Bar charts show integrated EMG (iEMG) values as time integrals for the stance phase. Amplitude normalized to the peak value across stiffness and speed for each subject. [main effect: stiffness # p<0.0001; ## p<.005; ### p<.05; main effect: speed *****p<.0001]

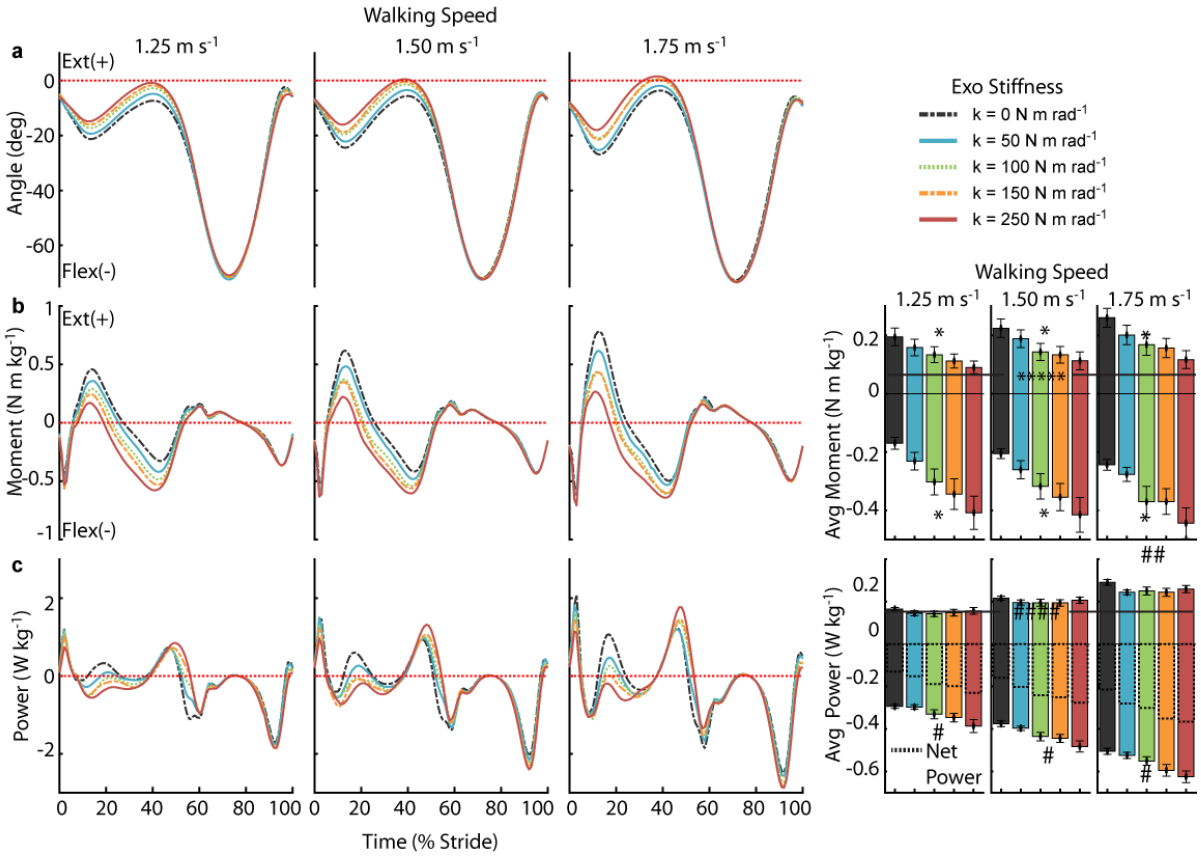

Figure 2.8: Knee joint mechanics across speeds. a, Knee angle became more extended with increased stiffness. Time series of knee joint angle for each stiffness and speed averaged across participants. **b**, With increased stiffness, knee moment generally became more flexive. Knee moment amplitude was larger at faster speed. Mass normalized moment for each stiffness and speed. Bar charts represent the average extension (+) and flexion (-) moment over the stride. **c**, Negative power increased with increasing stiffness and speed. Time series of 6DOF knee moment for each stiffness and speed. [main effect: stiffness * p<0.0001; # p<0.0001 (Negative and Net); ## p<.005; main effect: speed ***** p<.005 (Positive Only); #### p<.0001 (POS, NEG, NET)]

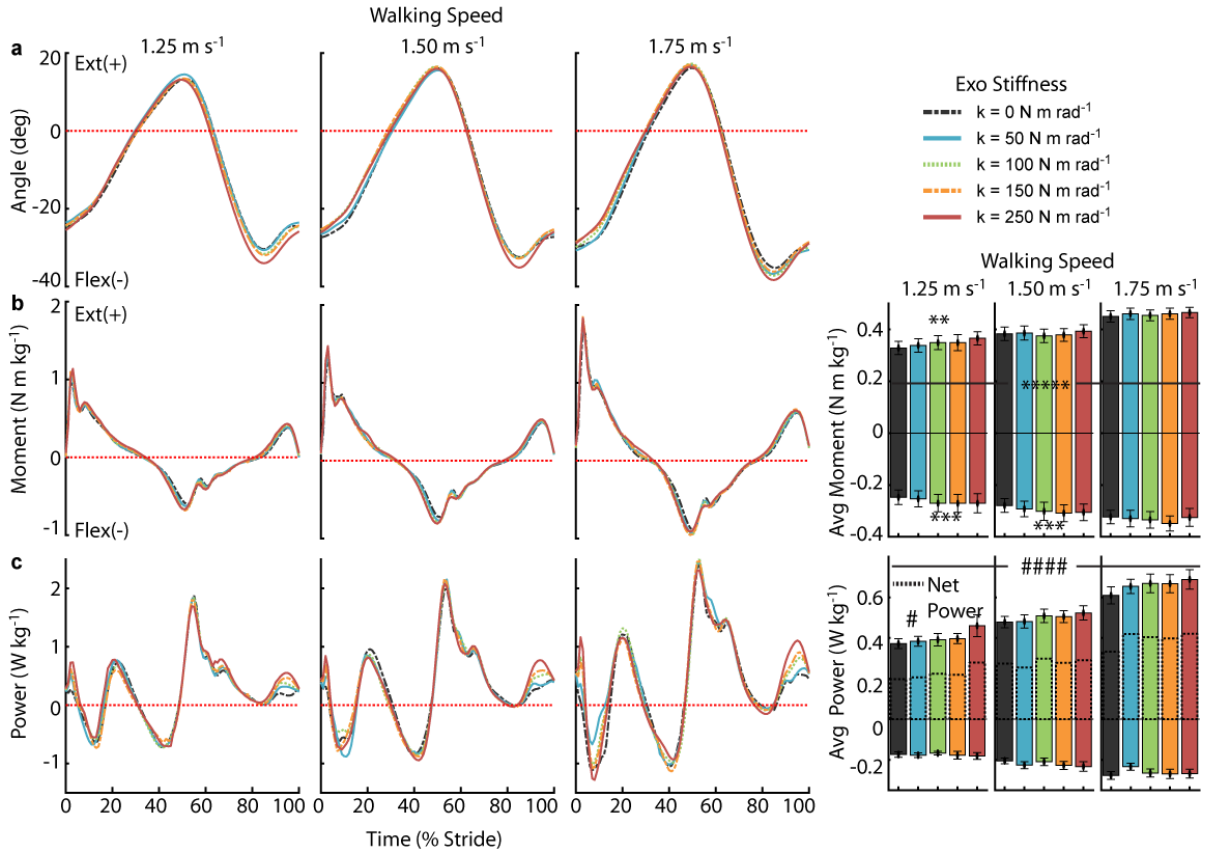

Figure 2.9: Hip joint mechanics across speeds. a, Hip angle was slightly more flexed prior to heel strike with higher stiffness. Time series of hip joint angle for each stiffness and speed averaged across participants. **b**, Hip moment is slightly greater at faster speeds. Mass normalized moment for each stiffness and speed. Bar charts represent the average extension (+) and flexion (-) moment over the stride. **c**, Hip positive power increases with speed. Time series of 6DOF knee moment for each stiffness and speed. [main effect: stiffness ** p<0.005; *** p<0.05; # p<.05 (Positive and Net); main effect: speed ***** p<.0001 (POS, NEG); #### p<.0001 (POS, NEG, NET)]

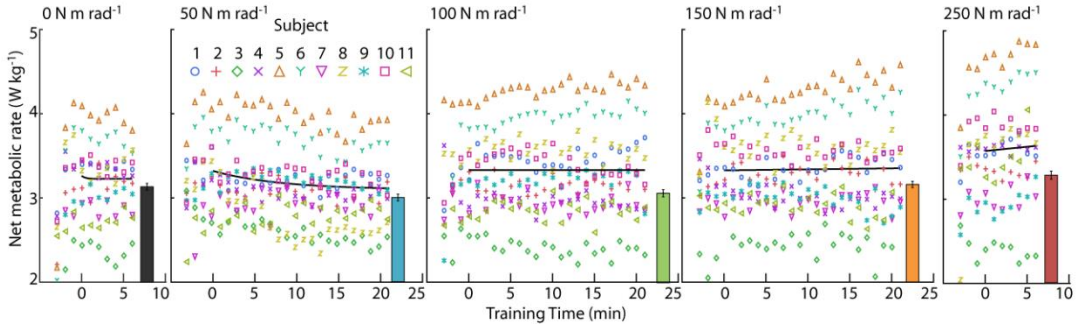

Figure 2.10: Net metabolic rate during exoskeleton training at 1.25 m s^{-1}. The only condition where subjects showed substantial improvement in metabolic rate from training was the 50 N m rad^{-1} stiffness. Each symbol represents the subject's average rate metabolic data for each minute of training. An exponential curve was fit to the data.

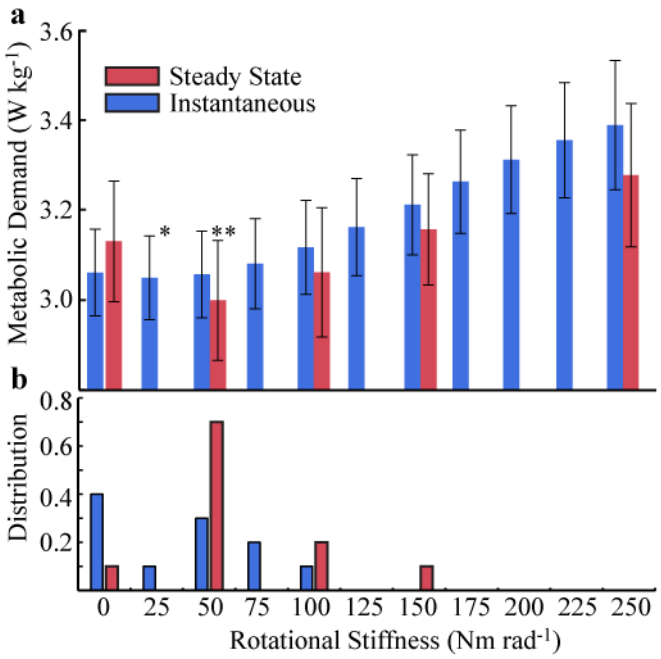

Figure 2.11: Comparison of metabolic demand using steady state and instantaneous approach at 1.25 m s^{-1}. a, Using the steady state approach, we found a minimum in metabolic demand at 50 N m rad^{-1}(**). The minimum using the instantaneous approach with a sweep of conditions was 25 N m rad^{-1}(*). When only comparing like conditions, the minimum in metabolic demand for both techniques was 50 N m rad^{-1}. **b**, Histogram showing distribution of stiffness condition for each subject where minimum metabolic demand was achieved.

Chapter 3 - Ultrasound Measurements of Soleus Fascicle Dynamics during Human Walking with Elastic Ankle Exoskeleton Assistance

In preparation for submission to Nature Communications

Introduction

Ankle plantarflexors serve an important mechanical role in walking by providing more than 50% of the positive power [23] and nearly the entirety of power for redirecting the center of mass in the push-off phase of stance (~50-60%) [24]. The critical role of ankle plantarflexors in locomotion is linked to their design. Muscle tendon units (MTU) with short pennate fibers and long compliant tendons are a characteristic of efficient locomotion across a range of animals [38, 63, 64]. During steady-state human walking, the interaction of the ankle plantarflexors and the Achilles tendon is highly tuned and allows for efficient energy storage and return and large positive power output in late stance. Studies suggest that fascicles of the plantarflexors operate on the ascending limb of their length-tension curve over a narrow operating range where force capacity is maximized [65]. The soleus, medial and lateral gastrocnemius also operate nearly isometric in early stance of walking [25, 66]. Because of this favorable operating point on the ascending limb of force-length curve as well as the advantageous low shortening velocity on the muscle's force-velocity curve, force production capacity of the muscle is maximized [41, 42, 67]. This isometric behavior occurs in the muscle despite the fact that the ankle and MTU undergoes changes in length and is accomplished through stretch and energy storage in the series Achilles tendon. This energy stored when the tendon stretches and is then returned in late stance at the time when the plantarflexors contract—this 'catapult mechanism' - provides a large burst of positive power [16, 25, 63]. Previous work has shown that recoil from the tendon provides up to 50% of the positive power in late stance

[16]. Therefore, any disruption in the catapult mechanism of the ankle may have consequences for the economical production of power at the ankle.

In recent years, researchers have demonstrated that ankle exoskeletons can reduce the metabolic cost of walking [2, 5, 6]. Collins, Wiggins, and Sawicki demonstrated that the metabolic cost of walking could be reduced by up to 7.2% below added mass using a portable passive elastic exoskeleton [6]. By applying an intermediate rotational stiffness, the human-machine interaction allowed for improved efficiency of walking upon what was already a highly tuned system. However, at stiffnesses below or above this value, metabolic demand was greater than during unassisted walking even though muscle force was reduced in all walking conditions. This bowl shape of the metabolic demand curve, where the metabolic minimum occurs at an intermediate stiffness, was in part attributed to compensations of other lower limb joints and increased contraction of the antagonist tibialis anterior muscle. In this work, we extended the previous work by identifying the optimal 'exo-tendon' stiffness that conveyed the largest metabolic benefit across a range of walking speeds in addition to adding ultrasound measurements of soleus fascicle dynamics. We theorize that changes in metabolic cost due to stiffness are directly linked to the underlying muscle-tendon dynamics and disruption of the tuned catapult mechanism.

This theory of muscle disruption due to exoskeleton assistance has been proposed in previous work [6] and has been demonstrated in experimentally in hopping and in models [36, 39, 68] . In human hopping, an exoskeleton providing parallel stiffness at the ankle reduced muscle force and metabolic demand. However, they showed that muscle fascicle excursion also increased resulting in no decrease in muscle work despite the decrease in force [36]. In a follow-up model, limits on the metabolic reduction from exoskeleton assistance in hopping was attributed to increased fascicle velocities and unfavorable fascicle operating lengths [68]. A modeling study of walking with an elastic exoskeleton showed that decreased force resulted in decreased length of the tendon and increased strain in muscle fascicles. These studies highlight that exoskeletons may disrupt

the normal catapult mechanism and reduce the ability for elastic tissues to efficiently store and return elastic energy during locomotion [39].

To our knowledge, no study has provided experimental evidence to directly show the effects of exoskeleton rotational stiffness on plantarflexor muscle dynamics during walking. In addition, here we aim to understand the coupled effects of exoskeleton rotational stiffness and walking speed on plantarflexor muscle dynamics during walking. Our goal was to directly measure the mechanics of the soleus muscle fascicles when a range of ankle exoskeleton stiffnesses (k_{exo} = 0, 50, 100, 150, 250 Nm rad^{-1}) were applied over a range of walking speeds (1.25, 1.5, and 1.75 m s^{-1}). We hypothesized that stiff ankle exoskeletons will detune the normal muscle force-length behavior. Specifically, we hypothesized that the reduction in soleus force requirements would result in an increase in soleus fascicle lengths and an increase in fascicle velocity. Finally, we hypothesized that these changes in muscle dynamics will offset benefits from decreased muscle force and lead to suboptimal improvements in metabolic cost.

Methods

Participants: Eleven healthy adults (n = 11, mass: 76.8 ± 8.2 kg, age: 27.7 ± 3.3 years, height: 1.75 ± 0.07 m, 4 female, 7 male) participated in the study. All participants gave written consent prior to participation in the study which was approved by the Institutional Review Board at University of North Carolina at Chapel Hill.

Exoskeleton testbed: The exoskeleton end effector was a lightweight carbon fiber ankle foot orthosis (AFO) that applies plantarflexor torque to the ankle. The device consisted of bilateral ankle exoskeletons driven by benchtop motors. The control system imposed a torque angle relationship to emulate an elastic device providing rotational stiffness in parallel with the ankle. We calculated desired torque based off a predefined rotational stiffness and the real-time ankle angle (Eq 3.1)

$$\tau_{exo} = k_{exo} \times (\theta_0 - \theta_{ankle}) \quad (3.1)$$

where k_{exo} was rotational stiffness of the exoskeleton, θ_0 was the onset angle, and θ_{ankle} was the real-time ankle angle. Extensive details were provided in Chapter 1 and 2.

Walking Trials: Participants completed testing over a three-session period in which they walked at three speeds (1.25, 1.5, and 1.75 m s^{-1}) at five ankle exoskeleton rotational stiffness conditions (k_{exo} = 0, 50, 100, 150, 250 Nm rad^{-1}) and one no exoskeleton condition (NE). The order of the three testing sessions was (1) exoskeleton training, (2) gait mechanics, (3) steady state metabolic demand. The imposed waiting period between testing session was 2-7 days to allow for learning and retention [27].

1. **Training:** Previous work has demonstrated the importance of training on the acceptance of mechanical assistance in exoskeletons [13, 28, 29]. Each participant walked in the exoskeleton at 1.25 m s^{-1} for a total of 95 minutes over 5 trials. The participants walked at each of intermediate stiffness conditions (k_{exo} = 50, 100 150 Nm rad^{-1}) for 25 minute trials and at the min and max condition (k_{exo} = 0, 250 Nm rad^{-1}) for 10 minutes. Indirect calorimetry data was collected for each of the trials.
2. **Gait Mechanics:** The participant walked for 2 minutes for each of the 11 trials. Five conditions at 1.25 m s^{-1}, and three at both 1.50 and 1.75 m s^{-1}. The order of the trials was pseudo-randomized where the order of the walking speed was randomized and within each speed the order of the stiffness was additionally randomized. The participant was instrumented with EMG on the left shank, ultrasound over the right soleus, and lower limb motion capture markers.
3. **Steady State Metabolic Demand:** To allow participants metabolic rate to reach steady state, each walking trial lasted 5 minutes. Similar to the gait mechanics session, the subjects walked for each of the 18 trials and order was pseudo-randomized. The testing order was not maintained between the gait mechanics

session and steady state metabolic demand session. Indirect calorimetry data was collected for each of the trials.

Biomechanics measurements: Lower limb kinematics was measured using reflective marker motion capture system (120 Hz, Vicon, Oxford, UK) and the subject was instrumented with 44 reflective markers to capture 6-DOF motion of the foot, shank, thigh, and pelvis. Joint angles were calculated from marker data and joint velocity was calculated as the first derivative of angle (Visual 3D, C-Motion Germantown, MD). Force ergometry was captured with a split-belt instrumented treadmill (980 Hz, Bertec). We performed inverse dynamic analysis to calculate the joint moment of the ankle, knee, and hip (Visual 3D). Analog data was filtered at 25Hz and marker positions were filtered at 6Hz. The biological contribution to ankle moment was calculated by subtracting the directly measured exoskeleton torque from the total ankle moment. Joint angles and moments were reported for the sagittal plane. Rigid foot, 6-DOF joint power was calculated using techniques similar to Zelik *et al* [30].

For a given subject, time-domain measurements for each of the 18 conditions were calculated by time normalizing each stride between heel-strike and heel-strike of the subsequent stride. Multiple strides (15.5 ± 1.1) were then averaged together to obtain a single normalized stride for the condition. Integrated and peak values were calculated prior to inter-stride averaging. Average stride joint moment and power were calculated by integrating the time-domain moment/power and dividing by stride time. Average data for particular phases were calculated as the time-integral over that phase divided by the time of the gait phase. Peak values for a given measurement and condition were the average of the peaks for each stride within that condition.

EMG measurements: Muscle activity of the ankle plantarflexors (medial and lateral gastrocnemius, soleus) and ankle dorsiflexor (tibialis anterior) were measured with

electromyography on the left leg (SX230, Biometrics, UK). To obtain EMG envelope, the raw EMG data was high-pass filtered at 20 Hz, rectified, and low-pass filtered at 10 Hz. Integrated EMG (iEMG) was calculated as the time-integral of the EMG envelope averaged across each stride for a condition. The amplitude of the EMG envelope and the integrated EMG for each muscle was normalized to the peak amplitude for the muscle across all conditions and speeds for each subject.

Energetic measurements: We calculated metabolic power (W kg^{-1}) using a portable indirect calorimetry system (OxyCon Mobile, Carefusion, USA) and applying standard calorimetry equations [31]. To obtain net metabolic power for each condition, we subtracted the averaged metabolic power collected during the pre/post standing trials from metabolic power for the walking conditions. For steady-state metabolic demand, we averaged the breath-by-breath data for the last minute of each five-minute trial.

Muscle-tendon dynamics: B-mode ultrasound images of the soleus muscle were captured using a linear ultrasound system (LV 7.5/60/96Z; Telemed, Lithuania). The probe was placed over the right soleus muscle below the contact point with the exoskeleton and secured with elastic adhesive wrap. In post-processing, images were digitized using automated tracking software to determine soleus fascicle length and pennation angle [69-71]. In brief, we digitized a region of interest (soleus) and the fascicle of interest in an initial frame. The algorithm then tracks the fascicle in sequential frames by implementing an affine flow model. The UltraTrack [71] program also incorporates a 'key-frame correction' algorithm that assists with removing temporal drift. The ultrasound data was synched with the motion capture data via a digital pulse from the ultrasound system that initiated the capture. The timing delay between systems was incorporated in the analysis.

Plantarflexor MTU length and force were calculated from biological ankle joint kinematics and dynamics [72] using methods similar to previous studies [73]. Fascicle velocity was calculated as the first derivative of length. Soleus muscle force contribution

was estimated as the ratio of the cross sectional area of the soleus to the total plantarflexor area (54%) [74]. For each subject, time-domain measurements for each condition were calculated by time normalizing each stride between heel-strike and heel-strike of the subsequent stride. A minimum of three normalized strides (6 ± 0.6 stride average) were then averaged together to obtain a single normalized stride for the condition. Integrated and peak values were calculated prior to inter-stride averaging. For each stride, integrated and peak values were calculated during early (0-40%) and late (40-60%) stance and averaged across strides for a condition.

We calculated fascicle length at peak dorsiflexion with the intention of observing changes in fascicle length due to MTU stretch. In many cases, peak dorsiflexion occurred just prior to peak force. To avoid temporal drift associated with the affine flow algorithm, we manually measured fascicle length in individual frames at the time of peak dorsiflexion. For each condition, we then averaged the length measured at dorsiflexion for 5 strides. The researchers were not blinded to the conditions during processing but conditions were processed in random order.

Dynamic ultrasound data was included for 10 or 11 subjects due to inability to track one subject's data. Ultrasound data for walking speeds greater than 1.25 m s^{-1} were collected on 9 of the 11 subjects. Biomechanics data for respective removed conditions were not used in comparative analysis.

Statistics: Statistical analysis was only performed on exoskeleton conditions to isolate the role of stiffness rather than the effect of the weight and other structural impacts of the device. For joint dynamics, muscle-tendon dynamics, EMG, and net metabolic demand, we report the means and standard errors calculated across subjects. Muscle fascicle dynamics was a primary outcome measure of this study. We performed a two-factor ANOVA (random effect: subject; main effect: k_{exo}) to test the effect of exoskeleton assistance on fascicle length and velocity ($\alpha = 0.05$; JMP Pro, SAS). For the speeds where we found a main effect, we ran a Tukey post-hoc test at each speed to compare the

exoskeleton conditions against the no assistance condition ($p < 0.05$). To test the effect of stiffness on other biomechanical metrics, we also performed a two-factor ANOVA (random effect: subject; main effect: k_{exo}) on muscle activation, and force metrics. A Shapiro-Wilk W test confirmed normality for affected tests.

Results

Metabolic Demand: Ankle exoskeletons providing a low level of rotational stiffness (50 N m rad^{-1}) resulted in the optimal decrease in metabolic demand at 1.25 m s^{-1} (Fig 2c). We found a significant relationship between metabolic demand and the square of exoskeleton stiffness (n=11, k^2_{exo} $p = 0.022$). The minimal stiffness condition of 50 Nm rad^{-1} resulted a significant decrease in metabolic demand of 4.2% (CI:<0.4%, 7.8%>; two tailed paired t-test $p = 0.032$). A similar result was observed for faster walking (1.75 m s^{-1}) where we found both a main effect of square of stiffness (k^2_{exo} $p = 0.009$) and a significant reduction in metabolic demand at 50 Nm rad^{-1} of 4.7% (CI:<1.4%, 7.1%>; two tailed paired t-test p =0.009). We did not find a significant relationship between net metabolic demand and stiffness at the intermediate speed of 1.5 m s^{-1} (k^2_{exo} p = 0.071), and the 50 Nm rad^{-1} stiffness resulted in an average increase of 0.5%.

Joint Dynamics: Increasing exoskeleton stiffness resulted in an increase in exoskeleton torque and a concomitant decrease in biological ankle moment (Fig 2a). Exoskeleton torque reached a peak of 0.441 Nm kg^{-1} in the stiffest condition. This resulted in a 0.464 Nm kg^{-1} (29%) reduction in biological moment. At the metabolically optimal stiffness (50 Nm rad^{-1}) the exoskeleton provided a peak torque of 0.198 Nm kg^{-1} resulting in a decrease in biological moment of 0.189 Nm kg^{-1} (12%). Similar results were observed at 1.5 m s^{-1} and 1.75 m s^{-1}. Peak biological moment increased with increasing speed while exoskeleton contribution decreased. For 50 Nm rad^{-1} condition, biological moment was 1.392, 1.552, 1.647 Nm kg^{-1} while the peak exoskeleton torque was 0.198, 0.184, and 0.169 Nm kg^{-1} for 1.25, 1.50, and 1.75 m s^{-1} respectively.

Biological power was reduced and exoskeleton power increased as increasing stiffness was applied (Fig. 2b). Biological average positive power decreased by 44% from the 0 to 250 Nm rad^{-1} conditions and exoskeleton positive power increased by 21%. This resulted in a 30% reduction in average net ankle positive power from the no assistance (0 Nm rad^{-1}) to highest stiffness (250 Nm rad^{-1}) condition. For 50 Nm rad^{-1} condition, from 1.25 m s^{-1} to 1.75 m s^{-1}, exoskeleton positive power increased by 16% although not in proportion to the increase in biological contribution (57%).

Ankle kinematics were affected by the amount of rotational stiffness applied (not shown). Ankle dorsiflexion decreased with increasing stiffness. Peak dorsiflexion ranged from 17.7 to 7.3 deg. for 0 and 250 Nm rad^{-1} stiffness reflecting a maximum reduction of 58%. Peak dorsiflexion was 14.7 deg. for 50 Nm rad^{-1} (metabolically optimal stiffness). Dorsiflexion also decreased with increasing speed. In the 0 Nm rad^{-1} condition, peak dorsiflexion was 17, 16.9, and 15.7 deg., for 1.25, 1.50, and 1.75 m s^{-1} speeds respectively and 14.7, 13.9, and 12.2 deg. for 50 Nm rad^{-1}.

Muscle-Tendon Dynamics at 1.25 m s^{-1}: Soleus force decreased with increased exoskeleton stiffness ($p < 0.0001$) (Fig 3a). Peak force for the five conditions were 1674±69, 1472±66, 1347±76, 1256±62, and 1168±70 N. Integrated soleus force decreased in both early and late stance but the percent reduction was greater in early stance (Fig 3b). Soleus EMG activation for 50, 100, 150, 250 Nm rad^{-1} decreased by 15, 28, 27, and 33% in early stance compared to no assistance ($p <0 .0001$). The maximum reduction in late stance was 14% for the 250 Nm rad^{-1} condition. Soleus force per activation increased with increased stiffness by up to 28% in early stance ($p = 0.0149$) and decreased in late stance by up to 24% compared to no assistance ($p = 0.0344$) (Fig 3d).

The length of the MTU decreased with increasing stiffness ($p< 0.0001$) (Fig 3c). Compared to the no assistance conditions, MTU peak length decreased by -2.8 mm (0.9%) and -7.1 mm (2.3%) for the 50 Nm rad^{-1} and 250 Nm rad^{-1} conditions.

Soleus fascicle lengths increased with exoskeleton stiffness (Fig 3e, Fig 5). Fascicle lengths at peak dorsiflexion were significantly longer at higher stiffness compared to no assistance ($p < 0.0001$, $R^2 = 0.97$) (Fig 5). Compared to the 0 Nm rad^{-1} condition, fascicle lengths changed by -0.16±0.70 mm (-0.6%), 1.76±0.31 mm (4.9%), 2.09±0.53 mm ($p = 0.0174$) (5.6%), and 4.5±0.83 mm ($p < 0.0001$) (11.8%) for 50, 100, 150, 250 Nm rad^{-1} respectively. Fascicle shortening velocities at peak force increased with assistance ($p = 0.027$) (Fig 3f). Fascicle shortening velocities at peak force were 0.47±2.5, 0.91±2.9, 2.6±2.6, 3.6±2.5, and 4.2±2.3 mm s^{-1} for 0, 50, 100, 150 and 250 Nm rad^{-1} respectively.

Muscle-Tendon Dynamics Across Speed: Soleus force increased with increasing walking speed ($p < 0.0001$) (Fig 4a). Peak force for the 50 Nm rad^{-1} condition was 1472, 1616, and 1670 N for 1.25, 1.50, and 1.75 m s^{-1} respectively. Integrated force in early stance remained constant and decreased in late stance as speed increased. Peak EMG increased significantly with speed by up to 38% while integrated EMG did not increase as substantially (Fig 4b). Soleus force per activation decreased in early ($p < 0.0001$) and late stance ($p = .0014$) with increased speed (Fig 4d). Decrease in force per activation was 12% and 35 % at 1.75 m s^{-1} in early stance and 2% and 14% in late stance for 1.5 and 1.75 m s^{-1} respectively compared to 1.25 m s^{-1}. The length of the MTU decreased with increasing stiffness (Fig 4c).

Soleus fascicle absolute lengths at peak dorsiflexion decreased with increase in walking speed ($p < 0.0001$) (Fig 4e). Fascicle lengths at peak dorsiflexion were on average 2.2 and 2.5 mm shorter at 1.5 and at 1.75 m s^{-1} compared to 1.25 m s^{-1}. Fascicle average shortening velocity ($p =0.004$) and shortening velocity at peak ($p < 0.0001$) increased with increasing speed (Fig 4f). At 1.5 and 1.75 m s^{-1}, fascicle velocity at peak force was 11.5 and 14.7 m s^{-1} compared to 0.47 at 1.25 m s^{-1}.

When low level stiffness (50 Nm rad^{-1}) was applied, fascicle lengths relative to no assistance (Δl_{fas}^{50}) were -0.17±0.69 mm (-0.7%), 2.42±1.31 mm (7.9%), and 1.05±0.72 mm (3.6%) at 1.25, 1.50, and 1.75 m s^{-1} respectively (Fig 5a). Although these results suggest

that the greatest increase in fascicle length is at the intermediate speed (1.50 m s^{-1}), no significant effect was found between fascicle length change and speed. There was no significant effect of speed on the change in fascicle velocity due to exoskeleton assistance compared to no assistance (Δv_{fas}^{50}).

Muscle Fascicle Dynamics and Metabolics Demand: We found a significant linear relationship between change in muscle fascicle length relative to no assistance (Δl_{fas}^{0}) and change in metabolic demand (ANOVA; random: subject; main effect: Δl_{fas}^{0}; $p = 0.0109$; R^2=0.34). (Fig 5c). We found no significant relationship between fascicle velocity at peak force and metabolic reduction.

Discussion

As hypothesized, application of ankle exoskeleton rotational stiffness resulted in altered muscle tendon dynamics. At a walking speed of 1.25 m s^{-1}, increasing rotational stiffness resulted in increased fascicle length at peak dorsiflexion and increased shortening velocity at peak force. These results are consistent with previous experimental hopping and modeling studies where exoskeleton parallel assistance resulted in increased fascicle excursions [36, 43, 68, 75]. A study assessing the effect of exoskeleton orthosis stiffness on gastrocnemius length of children with cerebral palsy showed that fascicle length could be increased but results were variable [76]. A more recent model of walking with exoskeleton assistance showed increased fascicle excursion, and increased velocity leading to decreased force generating capacity in the muscle [77]. In human walking, added stiffness to the foot has also been shown to alter fascicle dynamics where reduced velocity allowed for higher muscle force generation [73].

Muscle force production and economy: Muscle force production capacity is, in part, governed by intrinsic force-length (F-L) and force-velocity (F-V) properties [37, 41, 42, 67, 78, 79]. Disrupting the normal tuned muscle tendon interaction can have an impact of

muscle force production and muscle economy [39, 43] In human gait, the soleus fascicles normally operate on the ascending limb of the force-length curve [65]. We cannot be certain where the participants were operating on the F-L curve because we did not measure optimal operating length (L_0). However, the average length of the measured fascicles with no assistance was ~37 mm which was just slightly shorter than the L_0 of soleus reported in previous studies (38mm[65], 44mm[80]). When operating on the ascending limb, a shift to shorter fascicle would result in a decrease in force production capacity while a shift to longer lengths could potentially increase force capacity. In our results, the shift to longer fascicle lengths (~2-4 mm) resulting from exoskeleton stiffness could likely have shifted the fascicles to the plateau or potentially to the descending limb of the F-L curve where passive structures contributed to force. This shift could help explain why muscle economy (force per activation) increased in early stance when assistance was applied.

With respect to velocity, muscle force capacity is sensitive to velocity in the near isometric region of the F-V curve. Increased shortening velocities limit force capacity and increase metabolic power consumption [79, 81]. The soleus has been shown to be near isometric especially in early stance [25] and our measured average (~8 mm s^{-1}) and peak (~15 mm s^{-1}) shortening velocities were considerably less than reported v_{max} of the soleus (~400 m s^{-1}) [82]. Therefore, a relatively small increase in fascicle velocity due to increased stiffness and speed would likely have a large impact on muscle force capacity. With increasing exoskeleton assistance, we measured an increase in fascicle velocity at the time of peak force ranging from 0.47 to 4.2 mm s^{-1}. Using equations from Alexander 1997 [81] and a v_{max} of 400 mm s^{-1}, the small increase in velocity would result in a 5% reduction in force capacity and a 15% increase in metabolic power consumption of the muscle. At the same time of the gate cycle in late stance, muscle economy – measured force per activation - was significantly reduced with increasing stiffness. Our findings of reduced force capacity due to increased velocity were in line with predicted effects from musculoskeletal models of walking with exoskeleton assistance [77].

From an energetic standpoint, our data suggested that the effect from exoskeleton assistance on the muscle dynamics have whole body metabolic consequences. To reiterate, our results suggested that increased lengths beneficially allowed for enhanced force capacity. Increased velocity of shortening createed a disadvantage due to reduced force capacity. At the minimum exoskeleton stiffness (50 Nm rad^{-1}), we found the greatest metabolic reduction -4.2% while no significant change in fascicle length was observed. Additionally, we also saw no significant change in length at the 100 N m rad^{-1} stiffness and achieved a metabolic reduction of 2.2.%. The higher two stiffness conditions had significantly different fascicle lengths from the no assistance condition and we measured increased metabolic demand of 1.2% and 4.7% for 150 and 250 N m rad^{-1} respectively. Fascicle shortening velocity also increased with increased stiffness. Overall, the results suggest that the fascicle dynamics at higher stiffness are most disrupted. It could be that at higher stiffness conditions, the benefit to muscle economy from favorable fascicle lengths and large reductions in force may be swamped by increased velocities. At lower stiffness values (50 and 100 N m rad^{-1}), the favorable reduction in force was reduced and fascicles were shorter, but the fascicle economy was not hurt substantially by increased velocity. These findings are consistent with both experimental and modeling work from hopping with elastic assistance. Because of the less favorable fascicle velocity/length combinations when assistance is applied, metabolic energy consumption of the muscle was not reduced, despite the reduction in required force [36, 68]. The relationship between muscle dynamics and metabolic demand was further supported by the significant linear relationship between the length at peak dorsiflexion and metabolic reduction. The relationship suggested that when muscle fascicles were shorter, metabolic demand was reduced.

These results suggest that exoskeleton assistance had two-edged effects on muscle dynamics where the favorable contribution of increased length in early stance disrupts the higher velocity catapult mechanism in late stance. Increased length appeared to have a favorable contribution to muscle economy (force per activation) in early stance.

The metabolic cost of locomotion and the amount of energy a muscle consumes has been linked to the activation and force produced [35, 81, 83, 84]. EMG can be assumed to be proportional to the number of active muscle fibers [85]. The ratio of force produced to muscle economy (force per activation) therefore provides insight into how energy demand of the muscle changes with increased stiffness. In early stance, force decreased slightly and economy increased. This ratio would indicate that energetic demand of the muscle was reduced in early stance. However, we also saw diminishing returns and a plateau in the force per activation at higher stiffnesses suggesting that energy savings diminish at high stiffness conditions. In late stance, increased velocity likely limited force capacity and was detrimental to muscle economy. Decreased force from exoskeleton assistance was offset by decreased muscle economy (force per activation) in late stance and potentially resulted in increased energy demand from the muscle. Together these findings suggest that a balance in exoskeleton stiffness between too stiff and too compliant (*i.e.* finding the 'sweet spot' in stiffness) allowed us to optimally balance the competing dynamics between early/mid stance and late stance.

The recent modeling study of walking with ankle exoskeleton assistance by Jackson *et al.* gives support to our findings and conclusions [77]. In this study, they found that muscle operated at longer lengths closer to their optimal length resulting in increased force generation. However, this resulted in increased shortening velocities in late stance and a decline in force production capacity. The model was especially insightful in terms of muscle heat rates and energy usage. Due to trade-off between decreased force (decline in activation/maintenance heat rate), increased fascicle excursion and shortening (increase in lengthen/shortening heat rate), and increased fascicle work, they found no significant change in muscle metabolic rate. These findings support our suggestion of the tradeoff between improved efficiency and decreased force in early/mid stance and decreased force / poor efficiency in late stance. In contrast with our study, they found no reduction in metabolic rate for the muscle [77] or whole body [12]. One important difference between the two studies could be the torque assistance profiles. In

their profile, a linear torque ramp was prescribed from early to late stance. In this study, exoskeleton torque increased early before starting to plateau in mid stance. Importantly, the subjects in our study had full control over the applied torque through their ankle position. During this mid stance phase we measured the best force per activation ratios and potentially prolonging the time in this range allowed us to make the metabolic improvement. These findings support remarks on mechanisms in our previous exoskeleton work that the passive device promotes metabolic improvements by supporting force in mid stance [6].

In our results, the shift to shorter fascicles and higher shortening velocity was also a likely explanation for the increase in activation and decrease in force per activation at higher walking speeds. Increased lengths has been shown in previous data [86] and this decline in force production capacity has been explained as a likely determinant of the walk to run transition [87].

Muscle-level compensations to exoskeleton assistance: When not considering the muscle level dynamics, in theory the subject should be able to maximize the benefits of the exoskeleton by minimizing biological power and maximizing exoskeleton power. The participants should be able to fully utilize the maximum stiffness of the exoskeleton. Our data and other studies suggest however that humans do not do this and instead compensations arise. As discussed in Chapter 2, we saw compensations at the ankle and knee in addition to a plateau in exoskeleton torque at high stiffness values. As discussed previously in this chapter, one potential reason for compensations were to maximize the economy of the muscle. Another could be to reduce incident of injury as studies have shown that the biological system may be resistant to increased strain on the muscles as a stability mechanism and to prevent muscle injury [44-46, 88]. Therefore, because of increased fascicle lengths resulting from stiff exoskeleton assistance, compensations may be limiting range of motion to prevent the muscle from operating on the descending limb of the F-L curve may arise. Our maximum observed increase in fascicle length compared

to no assistance was 13% in the 250 Nm rad^{-1} conditions. This was still below the 25% reported as damaging levels of strain [88], but we also observed reduced dorsiflexion in ankle angle. Without the compensation of MTU length (7.1 mm), the fascicle strain at 250 Nm rad^{-1} would have been approximately 29%. These compensation patterns observed in this study (*e.g.* increased plantarflexion) were consistent to what has been observed in hopping with springy assistance [36].

Another potential explanation for the user not being able to maximize the assistance was due to their inability to 'turn down' their muscle activation in proportion to the level of assistance provided. Research has shown that joints (and limbs) maintain constant stiffness during a given locomotion condition [37]. It is believed that this is accomplished through a combination of stretch reflexes (spindle organs) and force sensors (Golgi tendon organs) that are responsible for maintaining a nearly constant ratio of force to length [37]. Because exoskeleton assistance resulted in decreased soleus force and increased fascicle length, the apparent stiffness of the biological components was reduced. Therefore, a sensory feedback Golgi tendon / muscle spindle mismatch could be a possibility and the reflex system could be attempting to increase force or reduce length. This control is further regulated through higher neural centers. Much of walking is automatic and unconsciously controlled though spinal level CPGs, reflexes, cerebellar regulation, and the brainstem [40]. For this reason, users of the exoskeleton may not be able to turn off their plantarflexors as would be required to obtain maximal benefit or coordination with the exoskeleton. Further work in humans and animals into the role of feedforward/feedback mechanisms and the effect of disrupted dynamics in walking would be insightful.

Finally, humans prefer to maintain constant ankle kinetics when wearing assistive devices at a fixed speed on a treadmill [5, 6, 47, 89]. Participants may have reduced biological contribution to force to maintain total moment and increased fascicle length and increased velocity are, in part, a by-product of the desire to maintain joint moment.

Reduction in soleus force due to exoskeleton assistance should not be attributed solely to reduction in force production capacity.

Why no metabolic reduction at 1.50 m s^{-1}? These data provided some insight into why we did not measure an average decline in metabolic cost for the intermediate stiffness. Although the change was not significant, the average increase in length of the fascicles due to exoskeleton assistance Δl_{fas}^{50} were higher at 1.50 m s^{-1} than the other two speeds. We found a positive relationship between change in length and change in metabolic demand thus we suspect that the lack of reduction in metabolic demand at 1.50 m s^{-1} was driven in part by changes in fascicle length.

The decrease in fascicle velocity for the 50 N m rad^{-1} / 1.75 m s^{-1} could potentially explain why we see a reduction in metabolic cost for that condition compared to no assistance. Alternatively, we measured a large increase in fascicle velocity for the 1.5 m s^{-1} / 50 Nm rad^{-1} conditions and a small increase in metabolic demand. These large changes in fascicle velocity could be set up by the fascicle length changes observed.

Coupling of ankle moment, ankle dorsiflexion, and fascicle length. In our results, the observed changes in muscle fascicle length resulting from exoskeleton assistance were influenced by counterbalancing effects from a decrease in ankle dorsiflexion and a decrease in ankle moment. The dynamics of the soleus muscle, tendon, and ankle joint were invariably coupled. When the MTU is modeled for simplicity as two series elements (muscle and tendon) attached to a lever (ankle), we can more easily decipher the effects of exoskeleton stiffness on kinematic compensation at the ankle and force unloading from the MTU. This set up is in fact the Hill-model that is used in many musculoskeletal models [68, 77]. The summed length of the muscle and the tendon was the length of the overall MTU, and the MTU force was equivalent through the muscle and the tendon (accounting for pennation angle). We found a decrease in ankle range of motion with increased

rotational stiffness. This decrease in ankle range of motion would result in a decrease in overall MTU length change, and when assuming no change in force or moment arm, the length change of the muscle (or fascicle) would also be lessened. For example, the length of the MTU at peak dorsiflexion was 7.1 mm shorter in the stiffest condition compared to no assistance. If force was equivalent (thus tendon strain is constant), the relative length of the muscle in the stiffest condition was also 7.1 mm shorter. The decrease in soleus force resulting from exoskeleton assistance has the opposite effect on fascicle length. Given that we find a decrease in soleus force, it was likely that tendon strain decreased due to its elastic properties. Assuming no change in MTU length, the length of the soleus muscle would increase as tendon length decreases. Using the same example as before, soleus fascicle force was 400 N smaller at peak dorsiflexion in the stiffest condition relative to no assistance. For a tendon stiffness of 200 N mm^{-1} [39], the tendon length was 2.2 mm shorter in the stiff condition. Therefore, assuming no change in MTU length, fascicle length was 2.2 mm longer in the stiffest condition. When considering both effects, the net effect for the stiffest condition compared to no assistance was a fascicle 4.8 mm shorter. Similar analysis for the other conditions predicted fascicles that were shorter by 1.9, 2.9, and 3.6 mm for 50, 100, and 150 N m rad^{-1} compared to no assistance at peak dorsiflexion. Interestingly, we find that the measured length changes were -0.16, 1.7, 2.1, and 4.5 mm where positive numbers indicate increased length. This calculation predicted overall fascicle shortening (swamped by change in ankle angle) however we measured overall lengthening of the muscle fascicles.

One potential explanation was that we are overestimating the stiffness of the tendon at short MTU lengths. Humans tendons have a toe region of stress-strain relationship at short lengths where stiffness is reduced [90, 91]. We did not measure tendon length or tendon rest length so we cannot be definite in this explanation. If the tendon was approaching slack length however, then the force unloading effects on increased muscle lengths would be exasperated. The mismatch between the prediction and observed data could be related to oversimplification of how force was distributed

among the muscles of the triceps surae and the Achilles tendon [92]. New evidence suggest that Achilles moment arm is load dependent in addition to being angle dependent [93]. It was also possible that we are underestimating ankle dorsiflexion in stiff conditions due to deformation of the exoskeleton.

We acknowledge that there are other limitations within the study. The causal relationship between the soleus force and muscle fascicle length and velocity can be difficult to decipher. Whether the participant decided to reduce force to maintain torque or rather force was reduced due muscle dynamics cannot definitively ascertained by this dataset. The assumption that soleus force was proportional to cross-sectional area and all triceps surae muscles were activated similarly was an oversimplification. Our analysis of soleus force also assumed no antagonist muscle was contributing to net ankle moment. In our results and in our previous work [6], we saw an increase in TA activity with increasing stiffness. Therefore, we may be underestimating soleus force in high stiffness conditions. Due to the difficulty of the procedure, we did not measure subject specific optimal fiber length (L_0) of the fascicles. We compared the measured lengths to literature values. We did not report changes with respect no exoskeleton. Instead our goal was to assess the effects of stiffness and reduced muscle force on the soleus fascicle dynamics. Added mass cost of the system reported in Chapter 2 was 19%. We have previously shown that a portable elastic ankle exoskeleton can reduce metabolic demand below added mass [6].

Ultimately, an overall goal of our exoskeleton research was to develop assistive devices that can reduce the metabolic cost of walking. Central to this goal was the understanding of how the exoskeleton can elicit changes to the user. We have shown that application of ankle exoskeleton assistance in walking disrupts normal muscle dynamics by increasing fascicle length and shortening velocity. Metabolic improvements were obtained when we balance the benefit of reduced muscle force with the cost of altered fascicle dynamics. These findings may provide insight into the development of future exoskeleton designs and the importance of muscle level analysis in the design

consideration. More generally when viewed as a perturbation experiment, it can provide insight into the mechanics and energetics of the soleus muscle in human walking. Finally, this work has shown that we can augment the mechanics of the soleus MTU by applying elastic parallel assistance. While these changes can be detrimental to the normally tuned MTU of young adults when too much assistance was provided, the changes measured could present an opportunity for restoring the morphology of the MTU in individuals where muscle tendon dynamics were already altered or disrupted as in what happens in aging adults[62].

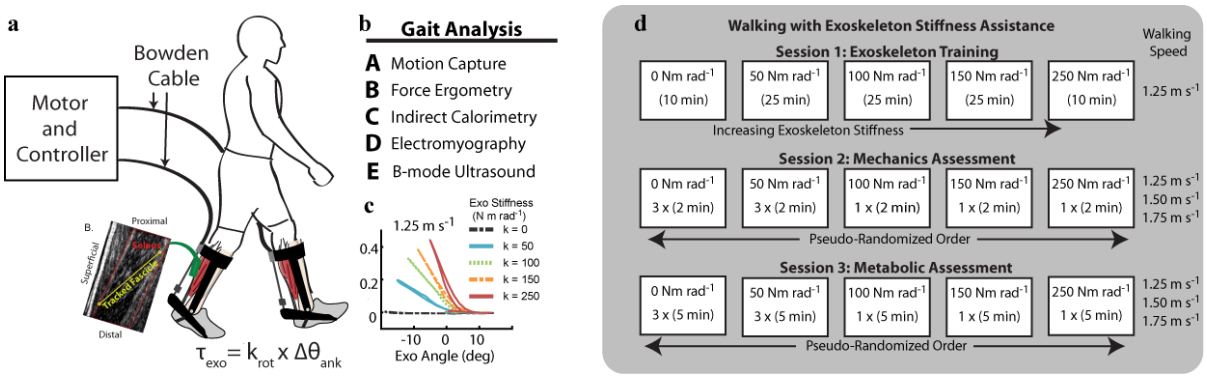

Figure 3.1: Exoskeleton testbed and test protocol. a, Representative setup of the exoskeleton testing platform for evaluating rotational stiffness plantarflexion assistance. The exoskeleton provided plantarflexion torque to the bilateral ankle exoskeletons through off-board motors. The controller emulated elastic rotational stiffness by imposing a torque angle relationship control law ($\tau_{exo} = k_{rot} * \Delta\theta_{ank}$). **b**, In addition to traditional gait analysis tools, we used B-mode ultrasound to track soleus fascicle length changes while exoskeleton assistance was applied. **c,** Stiffness could be changed in software and representative work loop data is shown. **d,** Protocol for the three testing sessions. Subjects were trained in the first session on all stiffnesses at 1.25 m s^{-1}. During the second session, we recorded joint mechanics, EMG, and ultrasound data for 6 exoskeleton conditions (No Exo, k_{rot} = 0, 50, 100, 150, 250 N m rad^{-1}) at walking speeds of 1.25, 1.5, and 1.75 m s^{-1}. In the third session, we recorded steady state metabolic demand for the same conditions. Here we report data for all stiffness conditions at 1.25 m s^{-1} and the 0 and 50 N m rad^{-1} conditions for 1.5 and 1.75 m s^{-1}.

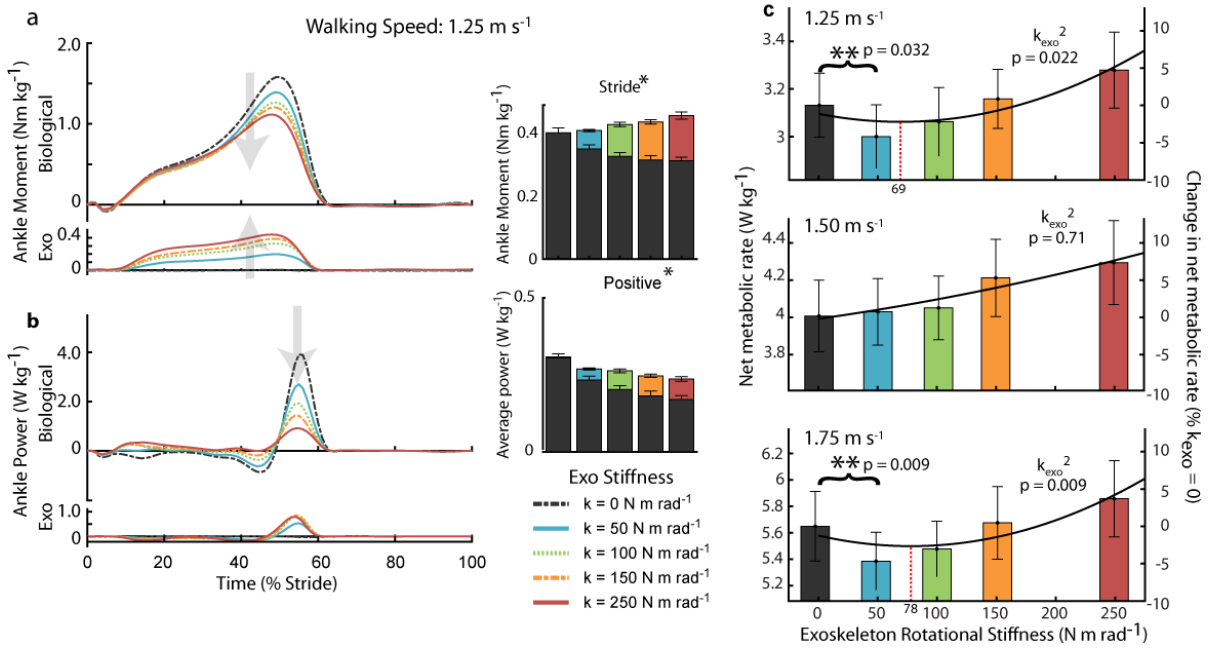

Figure 3.2: Effect of ankle exoskeleton on ankle joint mechanics and whole body metabolic demand. **a**, Increasing exoskeleton stiffness resulted in increased exoskeleton torque and decreased biological moment. Mass normalized biological moment and exoskeleton torque for each stiffness averaged over participants. Stacked bar charts represent the average biological (black-lower) and exoskeleton (colors-upper) contribution to total ankle moment for the stride. **b**, Exoskeleton power remained fairly constant at high stiffnesses and biological power decreased with increased stiffness. Biological positive power decreased while exoskeleton power was fairly constant. Time series of 6DOF biological power and exoskeleton torque for each stiffness. Stacked charts represent biological and exoskeleton contribution to ankle power. **c,** We saw a significant reduction in metabolic demand at both 1.25 and 1.75 m s^{-1} at the 50 N m rad^{-1} stiffness condition. Net metabolic demand for each condition and speed on bar charts. Vertical red line indicates the minimum of the regression line representing optimal stiffness for reducing metabolic demand. We report the metabolic demand for high stiffness exoskeleton conditions at fast speeds (100-250 N m rad^{-1}) although muscle mechanics data is not reported for those conditions. [main effect: stiffness * $p<0.0001$ (BIO, EXO, and ANK)]

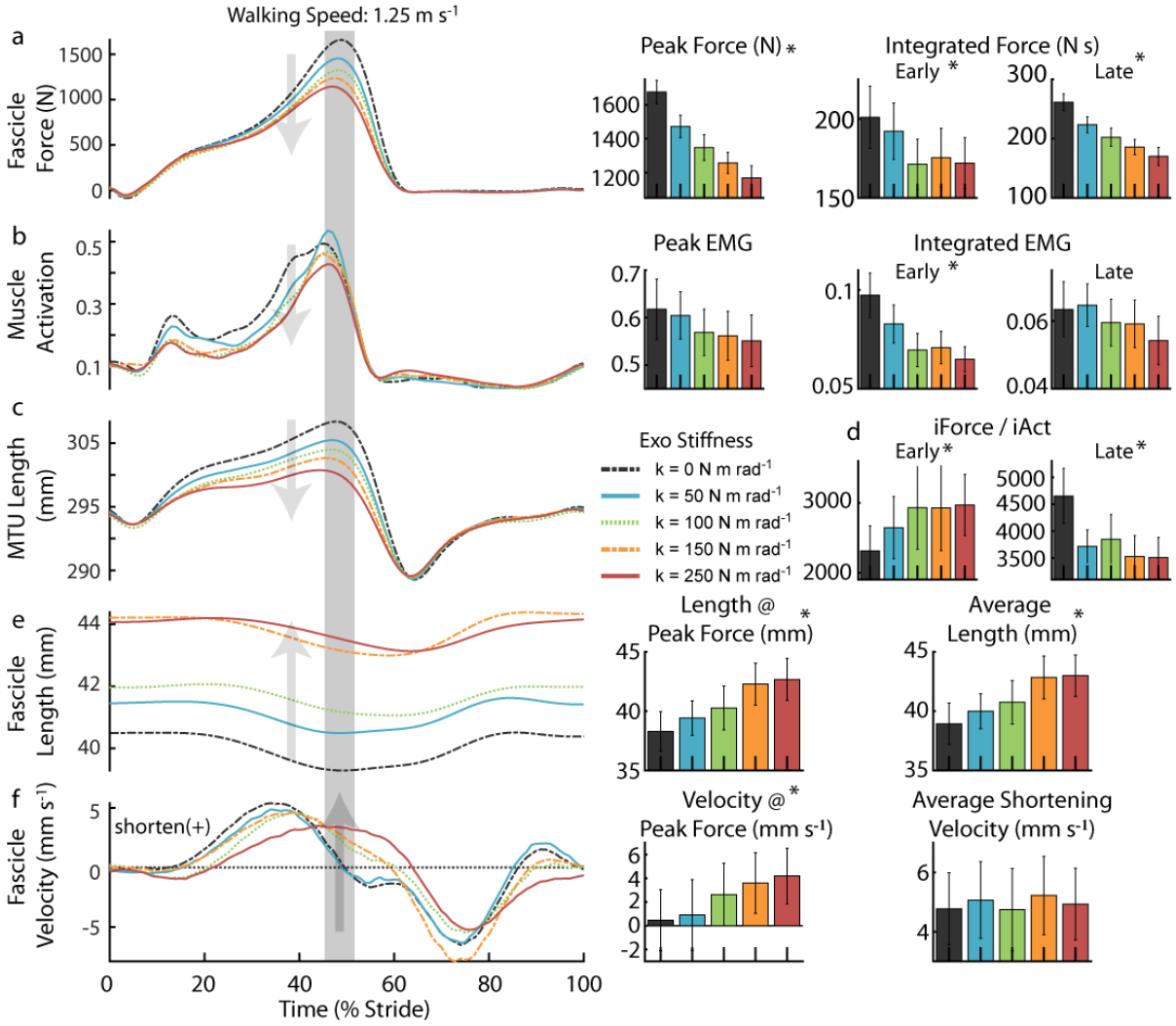

Figure 3.3: Soleus muscle mechanics and muscle activity during walking at 1.25 m s^{-1}. a, Increasing exoskeleton stiffness resulted in decreased force generation from the soleus. Soleus force for each stiffness averaged over participants. Bar charts represent the soleus peak and integrated force contribution for the stance phase of gait. Region of peak force highlighted in time series data. Early stance is 0-40% of stride and late stance is 40-60% of stride. **b**, Soleus EMG decreased with increasing exoskeleton assistance in early stance. Time series of soleus muscle activation where amplitude is normalized to the peak activation across all conditions (speed and stiffness) for each participant. Integrated muscle activation decreased with increasing stiffness particularly in early stance. **c**, Peak length decreased with increasing stiffness ($p < 0.05$). Time series of muscle-tendon unit length. **d,** Muscle force per unit activation increased with increasing stiffness in early stance and decreased with stiffness in late stance. **e,** Fascicle length increased with increasing exoskeleton stiffness. **f,** Fascicle shortening velocity at peak increases with stiffness and and muscle lengthening appears to be delayed with increased stiffness. [main effect: stiffness * $p<0.05$]

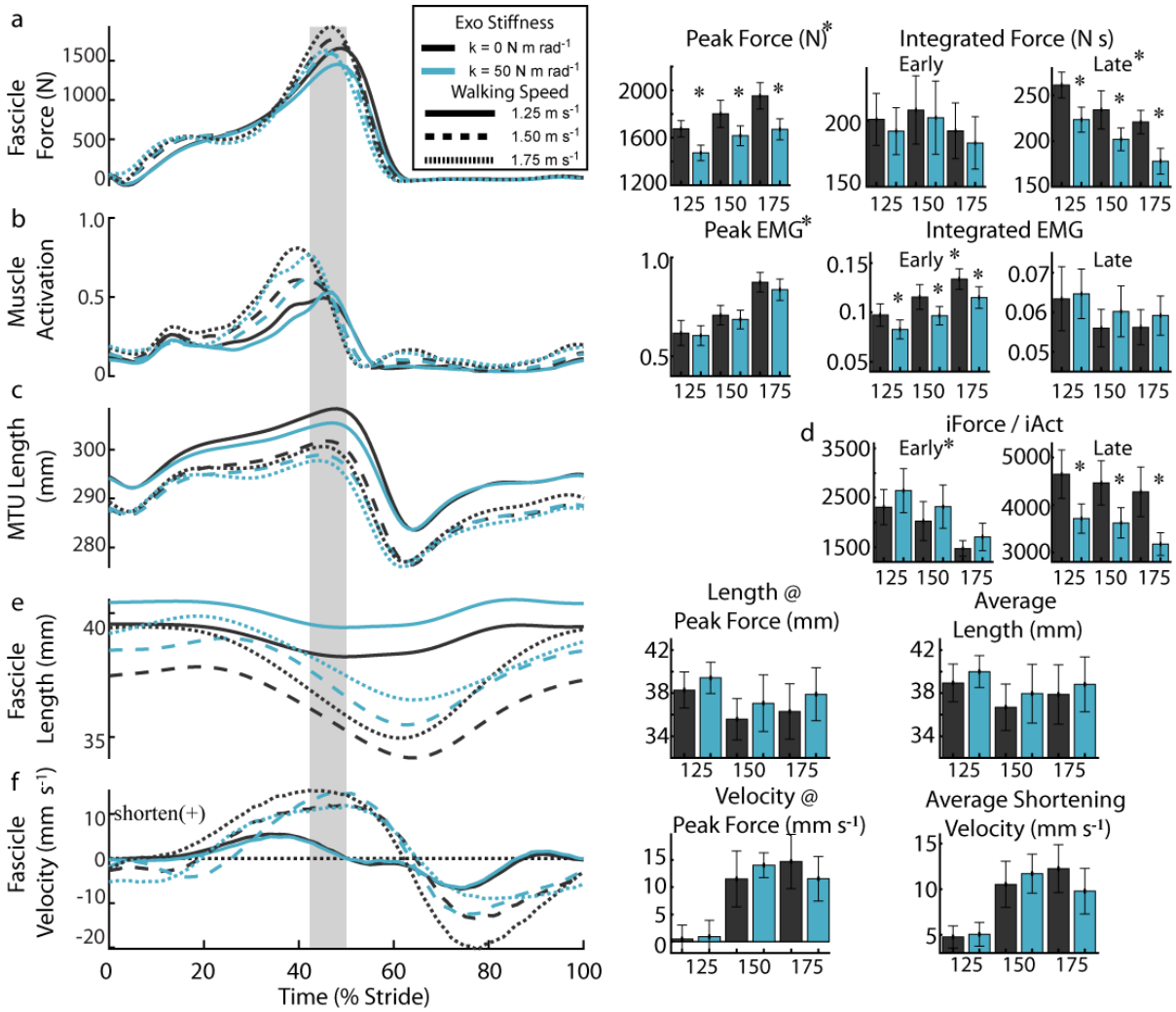

Figure 3.4: Soleus muscle mechanics and muscle activity during walking at 1.25, 1.50, and 1.75 m s^{-1}. **a,** Increasing walking speed resulted in increased soleus force ($p < 0.05$) and exoskeleton stiffness resulted in decreased force generation from the soleus. No assistance (0 N m rad^{-1}) (black) and 50 N m rad^{-1} (blue) stiffness for walking at 1.25 (solid), 1.50 (dash), and 1.75 (dot) m s^{-1} averaged over participants. Bar charts represent the soleus peak and integrated force contribution for the stance phase of gait in early (0-40%) and late (40-60%) of stride. Region of peak force highlighted in time series data. **b**, Muscle activation increased with increasing walking speed ($p < 0.05$). iEMG decreased in late stance across speed likely due to shift in peak EMG timing. In early stance, iEMG decreased with assistance and in late stance iEMG increased with assistance. Time series of soleus muscle activation where amplitude is normalized to the peak activation across all conditions (speed and stiffness) for each subject. **c**, Muscle-tendon unit length decreased with speed and application of assistance. Time series of muscle-tendon unit length. **d**, Muscle force per unit activation decreased with increasing speed ($p < 0.05$). Muscle force per unit activation increased with increasing stiffness in early stance ($p < 0.05$) and decreased with stiffness in late stance ($p < 0.05$). Time series of muscle-tendon unit length. Muscle force per activation is the integrated force divided by integrated activation. **e**, Fascicle length is shorter at faster walking speed. **f,** Fascicle average shortening velocity and velocity at peak increased with increasing walking speed ($p < 0.05$). Significant effect of stiffness on metrics are indicated by symbols on the graph. [main effect: stiffness * $p<0.05$]

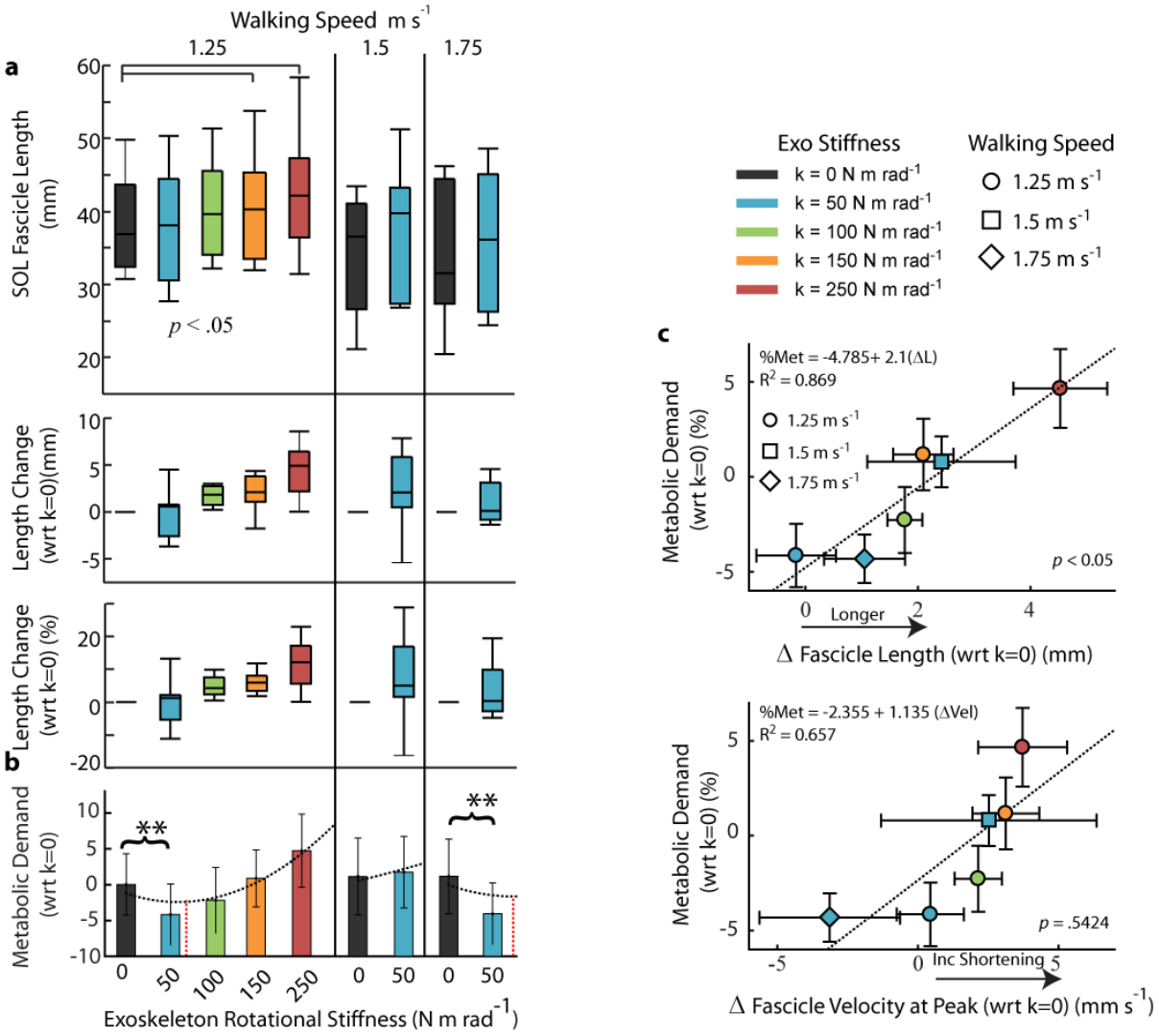

Figure 3.5: Soleus muscle mechanics and whole-body energetics at 1.25, 1.50, and 1.75 m s^{-1}. a, Soleus fascicle length increased with increasing exoskeleton stiffness ($p < 0.05$). The two high stiffness conditions (orange and red) were significantly longer than 0 N m rad^{-1} (Tukey $p < 0.05$). No significant difference was observed between no assistance and 50 N m rad^{-1} at faster walking speeds although the increase in length appears to be larger at the intermediate speed. **b,** Percent reduction in metabolic demand when walking with assistance. Significant reductions were observed at 50 N m rad^{-1} for 1.25 and 1.75 m s^{-1} **c,** A significant relationship between fascicle length and metabolic reductions was observed. Metabolic demand was lower on average when fascicle length at peak dorsiflexion were shorter. Percent metabolic reduction plotted against change in fascicle length and velocity with respect to no assistance (k = 0 Nm rad^{-1}).

Chapter 4 - Elastic Mechanisms in Wearable Robotics: A Framework for Biologically Inspired Passive Exoskeletons to Augment Human Performance

In preparation for submission to Exercise and Sport Sciences Reviews

Introduction: Active vs Passive Exoskeletons.

Lower-limb exoskeletons can be used to restore, preserve, or enhance locomotor performance by applying torque in parallel with biological muscle-tendons at a given joint. Most exoskeleton devices are powered which allows them to deliver net mechanical energy to lower-limb joints that are known to generate large amounts of mechanical energy. Not surprisingly, most of these devices have focused on delivering power to the ankle [2, 5, 12-14, 22, 94] and the hip [95-97] joints - two major sources of mechanical energy during human walking [23]. However, the maximum metabolic benefits of portable powered devices (i.e., ~8% [2] and 13% [97] at the ankle and hip, respectively) are significantly attenuated by the metabolic cost of carrying the actuators that power the device. While promising, powered devices do have a central limitation - delivering power fundamentally requires added mass with diminishing metabolic returns. Moreover, powered devices have only recently been applied outside research labs in the clinical or real world environments and are expensive, can be unwieldly, and require careful maintenance. These issues will continue to limit their acceptance by end users and health care providers [94, 98]. Powered devices aim to displace biological power or enhance net power done at the joint. Metabolic reduction in powered devices have been shown to be proportional to net work (Fig 1a).

Passive systems on the other hand can provide no positive net work. The mechanism of passive/elastic devices on the user is fundamentally different from that of powered/active devices (Fig 1b). Rather, passive devices work by improving efficiency of

the user or augmenting the underlying structural deficits which we contend may be at the core of mobility impairment in clinical and aging populations. As an alternative to powered devices, our research lab has been developing and evaluating novel, bio-inspired alternatives to powered assistive technology - passive elastic ankle exoskeletons [6, 99]. Inspired by advances in understanding triceps surae neuromechanical function [16, 25, 56, 66, 86, 92, 100-106], these portable, lightweight passive devices are equipped with a clutch and an "exo-tendon" attached in parallel with biological muscle-tendon units spanning the ankle [107]. In our previous work, we demonstrated that young adults using elastic assistance at the ankle improved their walking economy by up to 7% rivaling results from powered counterparts [2]. In this work, we have demonstrated that an exoskeleton testbed emulating an elastic passive device can achieve similar results. We extended the previous work by identifying the optimal 'exo-tendon' stiffness that resulted in the largest metabolic benefit across a range of walking speeds and directly measured the underlying soleus fascicle dynamics using B-mode ultrasound. In both studies, when parallel assistance that was either too compliant or stiff, we observed increases in metabolic demand. Therefore, there appears a 'Goldilocks Zone' in the amount of parallel stiffness supplied by the passive ankle exoskeleton where the human-machine interaction is just right.

Elastic devices work by improving the efficiency of the system. Based on this idea, we propose a hypothesis that by adding parallel exoskeleton stiffness at the ankle, we can alter the morphology of the calf plantarflexors to restore or augment performance in human walking.

Elastic Mechanisms in Locomotion.

Through our work in exoskeletons, as well as results from modeling and animal studies performed by our lab and other research groups, we have developed an understanding of the central role that elastic mechanisms play in human walking. Elastic mechanisms serve a diverse and vital role in effective locomotion [64]. Across a range of

animals, the interaction of elastic tissue in series with muscles has been shown to be critical in energy conservation (*e.g.* walking), energy amplification tasks (*e.g.* jumping), as well as energy absorption tasks (*e.g.* landing from a fall) (Fig 2) [64]. Due to our focus on human walking, the work in our lab has been primarily focused on the energy conservation role of elastic tissue, and to a smaller extent, power amplification. The critical role of ankle plantarflexors in locomotion is linked to their design. Muscle tendon units (MTU) with short pennate fibers and long compliant tendons are a characteristic of efficient locomotion across a range of animals [38, 63, 64]. The Achilles tendon facilitates efficient energy storage and impulsive ankle power output during walking. Ultrasound imaging during dynamic tasks [16, 25, 56, 66, 86, 92, 100-102, 106] and recent advances in musculoskeletal modeling and simulation [103, 105, 108-112] have elucidated the underlying mechanisms driving the highly efficient operation that is capable of high peak ankle power output during walking. In normal human walking, it is the tuned interaction of the ankle plantarflexors and Achilles tendon which allow for this highly efficient and powerful operation. Cumulatively, these studies reveal that the large burst of ankle power during 'push-off' is not directly driven by muscles. Instead, the complex interaction of the series elastic Achilles tendon with the triceps surae muscles (i.e., soleus and gastrocnemii) enables power amplification by way of a 'catapult mechanism'. During early stance, the triceps surae muscles are highly active but relatively isometric, acting like stiff struts or biological clutches that enable significant elastic energy storage via stretch of the Achilles tendon (i.e., the 'catapult' cocking phase) [16, 25, 56, 66, 86, 92, 100-102, 106]. Later, that elastic energy is quickly released and allows for rapidly shortening muscle fascicles to power ankle push-off [16].

The passive properties of the Achilles tendon alone do not guarantee efficient and powerful operation of the ankle plantarflexors. An effective ankle 'catapult' requires an optimally tuned interaction between the timing of activation of the triceps surae muscles and series elastic tendon. When activation of the triceps surae muscles is well-matched to the fixed passive stiffness of the Achilles tendon, a neuromechanical resonance arises

[104, 113, 114], whereby the activation of the muscle is 'tuned' to drive ankle push-off through a transmission (tendon) with effective energy transfer [55, 56, 100]. Modeling studies [26, 105] also strongly suggest that for a given walking speed, there is an 'optimal' muscle-tendon stiffness that yields an effective ankle 'catapult' and simultaneously minimizes metabolic cost. Complementary studies indicate that this stiffness can be 'dynamically tuned' via activation-dependent changes[8, 115, 116].

Findings suggest that alterations on effective muscle-tendon stiffness, through assistive exoskeletons [6] or through age-related reductions in Achilles tendon stiffness (k_T) [61, 117-123], could disrupt the optimally tuned neuromechanical interaction between active muscles and the passive elastic Achilles tendon. A model-based on an isolated muscle experiment of the plantarflexors acting like a simple harmonic oscillator helped demonstrate the energetic relationship between activation timing and elastic properties in the muscle [104]. The resonant frequency, w_0, of a system acting over a levered system such as the ankle can be described by the equation 4.1.

$$w_0 = \sqrt{k_{tot} / m} \frac{l_{in}}{l_{out}} \quad (4.1)$$

where k_{tot} is passive stiffness of the system, m is mass, and l_{in} is the moment arm of the spring element (*i.e.* tendon) and l_{out} is the moment arm of the load. By matching the drive frequency of activation with the natural frequency of the passive system, force was maximized while maximum power was delivered from the elastic element. These trends have also been shown in human hopping where maximum power from the series elastic element is delivered and metabolic demand minimized at a preferred hopping frequency [104].

Effects of Exoskeleton Assistance.

In our recent work, we have successfully implemented a high-fidelity impedance controller programmed to exhibit torque-angle behavior (*i.e.,* rotational stiffness).

Exoskeleton plantarflexion torque emulated an elastic element (*i.e.,* exo-tendon) of given stiffness (k_{exo}) in parallel with the biological triceps surae muscle-tendons (Fig 3).

With low exoskeleton stiffness (k_{exo} = 50 N m rad^{-1}), younger adults walked with preserved ankle moment while lowering soleus muscle activations, reducing soleus force, and improving walking economy. These results were shown for both slow (1.25 m s^{-1}) and fast (1.75 m s^{-1}) walking speeds. These findings also match our previous whole-body and joint-level results from a portable, unpowered elastic exoskeleton at 1.25 m s^{-1}[6]. Additionally, we collected ultrasound measurements of soleus fascicle dynamics which confirmed our previous musculoskeletal simulation predictions that increasing k_{exo} elicits a shift towards longer fascicle operating lengths [39] (Fig. 3). Conceptually, this translates to a downward, rightward shift in force-length-activation space, yielding lower muscle stiffness (Fig 4a). Given the right circumstances (*i.e.* intermediate stiffness), exoskeleton structural stiffness can effectively augment muscle-tendon neuromechanics governing the 'ankle catapult', yielding lower muscle activations at longer lengths with a significant metabolic benefit. Our previous studies have also demonstrated that high stiffness can disrupt the highly tuned dynamics by substantially increasing the length of the muscle fascicles leading to increased shortening velocities and higher metabolic demand in young adults.

The changes we observe in young adults provide evidence that we can alter the morphology of the muscle-tendon unit and shift the operating point of the muscle on the force-length curve through application of elastic exoskeletons. In young adults, the increase in length of muscle fascicles due to high exoskeleton stiffness often acts to disrupt the normal tuned dynamics. However, these measured changes in fascicle dynamics shown in young adults could be used to counteract or restore function in populations that have altered muscle-tendon compliance. In particular, we are interested testing whether elastic exoskeleton assistance could be applied to alter the morphology of aging adults. In ageing, the Achilles tendon compliance increases. In this population, the measured effects of parallel exo-tendons (k_{exo}) potentially act to reverse the effects of

age-related reduction in Achilles tendon stiffness, on muscle activation, and fascicle length change dynamics (Fig 4c).

Effects of Aging on the Elastic Structure of the Triceps Surae.

Advancing age offers a translationally important test of the functional significance of the tight coupling between active muscle and passive tendon properties within the triceps surae. *In vivo* studies of humans during isolated ankle contractions strongly suggest that age-related changes in the microstructure of the Achilles tendon reduces k_T by as much as 40% as compared to young adults [61, 117-123]. These age-related changes in k_T may be linked to impaired mechanics and energetics of walking in older adults. Our conceptual (Fig 4b) and preliminary computational models suggest that even small reductions in k_T cause a 'structural bottleneck' that disrupts the (normally tuned) muscle-tendon interaction during walking with severe metabolic penalties [124].

Age-related reductions in k_T would elicit more stretch for a given load. The task demands of walking (*i.e.,* body weight/inertia) are met with identical ankle joint kinematics, and thus muscle-tendon unit lengths, between young and older adults [125-127]. This implies that muscle fascicles in older adults must operate at shorter lengths for a given MTU length (Fig 4b) Simulations of walking at 1.25 m s^{-1} show that to maintain the same ankle power output (*i.e.,* via tuned muscle-tendon interaction), reduced Achilles tendon stiffness (*i.e.,* lower k_T) causes muscle fascicles to operate at shorter (*i.e.,* further from optimal) lengths with higher excitations [124].

Preliminary Effects of Passive Elastic Ankle Exoskeleton on Older Adults.

We have also completed preliminary efficacy and proof-of-concept testing in one older adult female participant (age: 68 years) who walked for 5 min in the exoskeleton simulator without assistance (k_{exo} =0 Nm rad^{-1}) and with simulated exo-tendons at two levels (k_{exo} = 100 and 150 Nm rad^{-1}– only 150 Nm rad^{-1} shown) (Fig 5a). Compared to

walking with no assistance, the stiffest exo-tendon (150 Nm rad^{-1}) reduced soleus muscle activity by 12% and increased average soleus fascicle operating length by 8.5% (Fig 5b). Using k_{exo} to augment structural stiffness of the triceps surae muscle-tendon also conveyed a significant metabolic benefit; reducing net metabolic rate by 5% compared to walking with no assistance. This provides preliminary evidence that indicates our results from younger adults can be extended to aging populations. These data also reflect the likelihood that this older user had an underlying deficit in Achilles tendon stiffness k_T, as the k_{exo} required to convey benefit here (150 Nm rad^{-1}) was 2 to 3 times the optimal k_{exo} identified for young adults (~50-80 Nm rad^{-1}).

Future Directions: Augmenting the Structure of the Triceps Surae to Improve Performance.

We have provided preliminary results that demonstrate that elastic exoskeletons can offset structural deficits of the ankle triceps surae by stiffening the joint. Specifically, our results of longer muscle fascicles permit reduced muscle activation and increased muscle economy. We propose that a similar technique can be applied to other populations affected by structural deficits and where push-off may be reduced (e.g. stroke, cerebral palsy).

Another future opportunity for elastic exoskeletons is in re-tuning of activation dependent neuromechanical interaction between muscle and tendon. If we again revisit the equation for the plantarflexor acting as a series-elastic oscillator , ($w_0 = \sqrt{k_{tot}/m}\,\frac{l_{in}}{l_{out}}$), this equation provides insight into how changes to the morphology may disrupt the optimal natural tuning of the MTU. In a follow up study to the muscle prep model where parallel elastic assistance was modeled, increased parallel stiffness $k_{tot} = k_{bio} + k_{exo}$ resulted in misalignment of activation frequency with resonant frequency [128]. Next, the knowledge that we can shift the optimal frequency should provide opportunities for

fixing inefficiencies. Exoskeleton assistance could be used in combination to offset changes in mass, moment arm ratio of the foot, or decreases in biological stiffness while maintaining resonant frequency. For example, a recent study showed that adding stiffness to the foot decreased soleus contraction velocity in walking [73]. The addition of stiffness to the foot effectively increases l_{out}. Potentially an exoskeleton offering increased stiffness to k_{tot} could counteract the effect of l_{out}, restore the tuned dynamics of the muscle-tendon complex, and improve user performance.

In a 'tuned' efficient system such as what we see in young adults, the optimal prescription of elastic assistance may be limited due to disruption of the muscle-tendon interaction. However, as we have shown in our preliminary data, passive elastic exoskeletons offer opportunities to beneficially augment the efficiency of biological systems that may be already disrupted. Although these data we present focus almost solely on the ankle due to the long elastic Achilles tendon, possibilities for optimization of various tasks are likely.

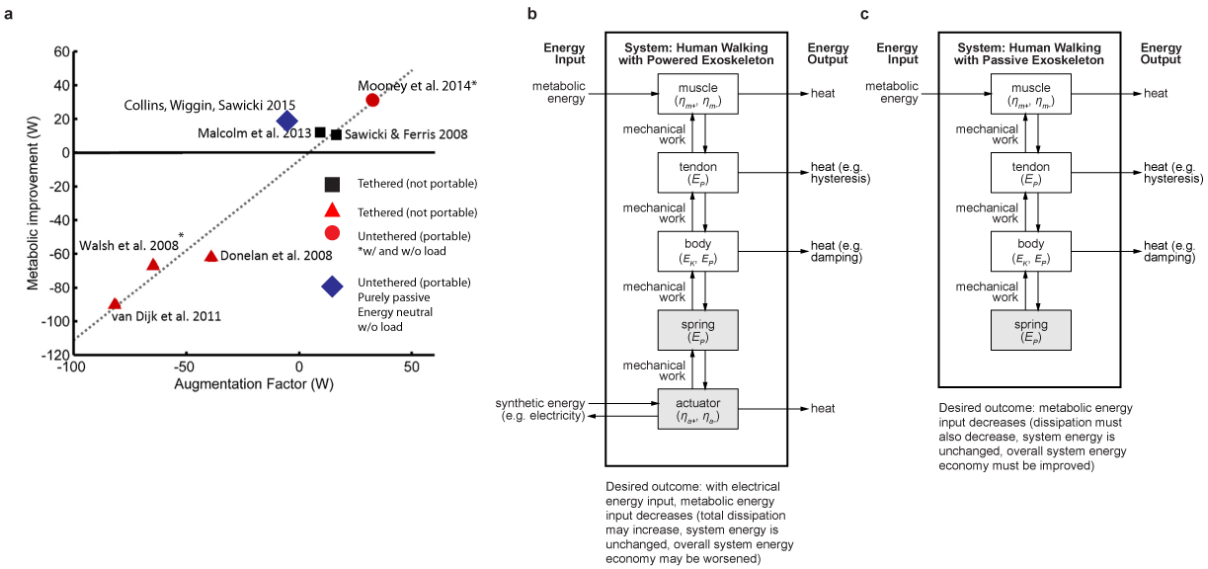

Figure 4.1: Augmentation factor for lower limb exoskeletons and energy exchange in active and passive exoskeletons. a, A comparison of exoskeleton augmentation factor to metabolic improvement. Augmentation factor is based on how much power is provided to or removed from the user by the exoskeleton. The linear relationship indicates that net positive power provided should be provided to the user [Modified from Mooney et al 2014]. However, metabolic improvement can be achieved when energy is dissipated [Collins, Wiggin, Sawicki 2015] **b,** Energy flow in a powered exoskeleton incorporating human and device system. **c,** Energy flow in a passive exoskeleton incorporating human and device system. System energy efficiency must be improved. [Modified from Collins, Wiggin, Sawicki 2015].

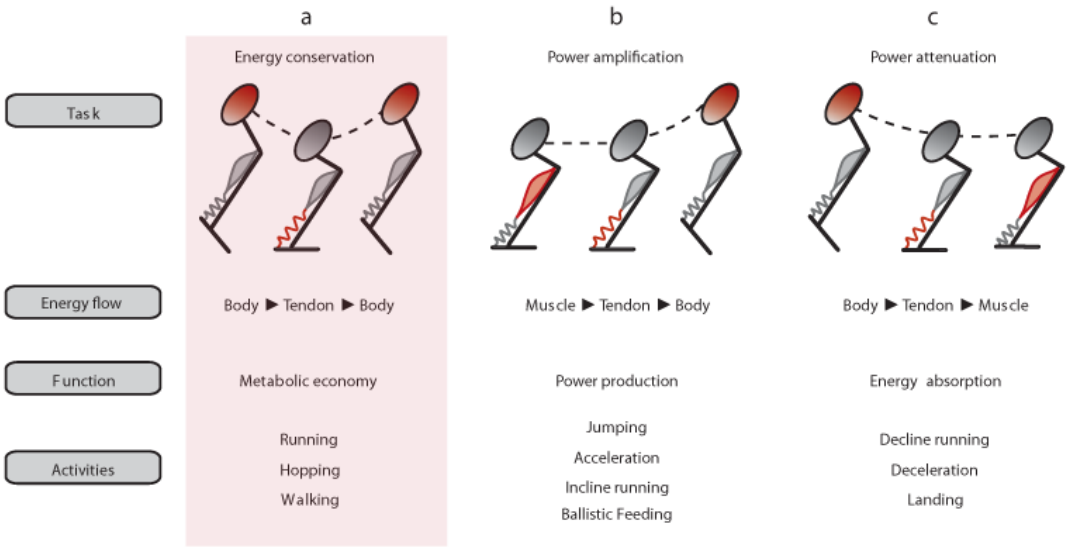

Figure 4.2: Energy flow in muscle-tendon systems. a, Energy can be conserved by elastic structures storing and returning energy. **b,** Muscles can contract to store energy in tendons which can be quickly released for high power movements. **c,** Muscles can dissipate energy stored in tendon by lengthening against a force (negative work). [Modified from Roberts and Azizi, 2011].

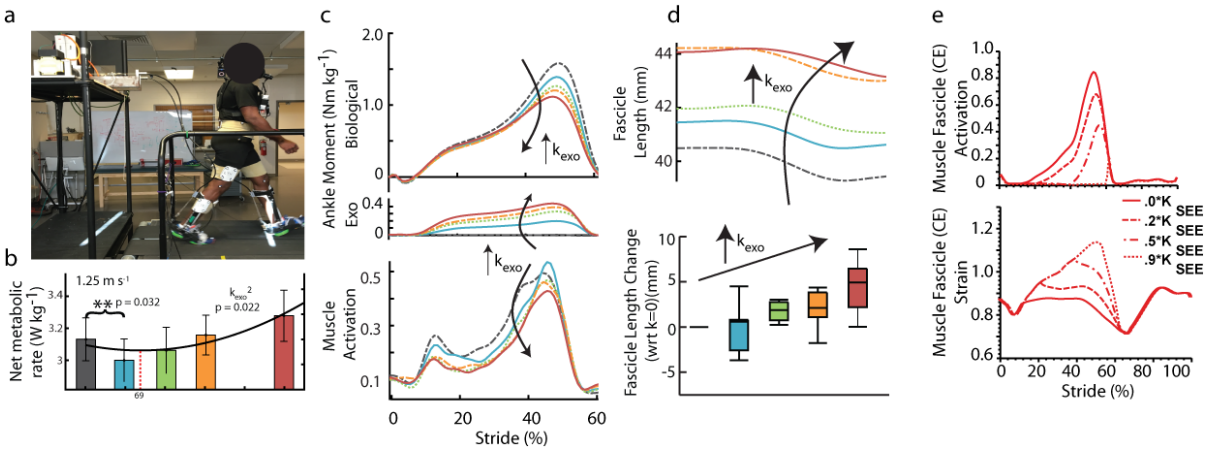

Figure 4.3: Experimental and modeling results of elastic exoskeleton assistance on joint and muscle neuromechanics. a, The subject walked in the exoskeleton emulator which provided plantarflexion rotational stiffness at the ankle. **b,** Exoskeleton assistance reduced metabolic demand at an intermediate stiffness by 4.2%. **c**, Increasing exoskeleton stiffness resulted in increased exoskeleton torque and decreased biological moment. Soleus muscle activation decreased with assistance. **d,** Increased stiffness yielded longer fascicle length across the stance and at peak dorsiflexion. **e,** Our data is supported by mechanistic simulation which demonstrates longer fascicles at high rotational stiffness [Modified from Sawicki et al 2016].

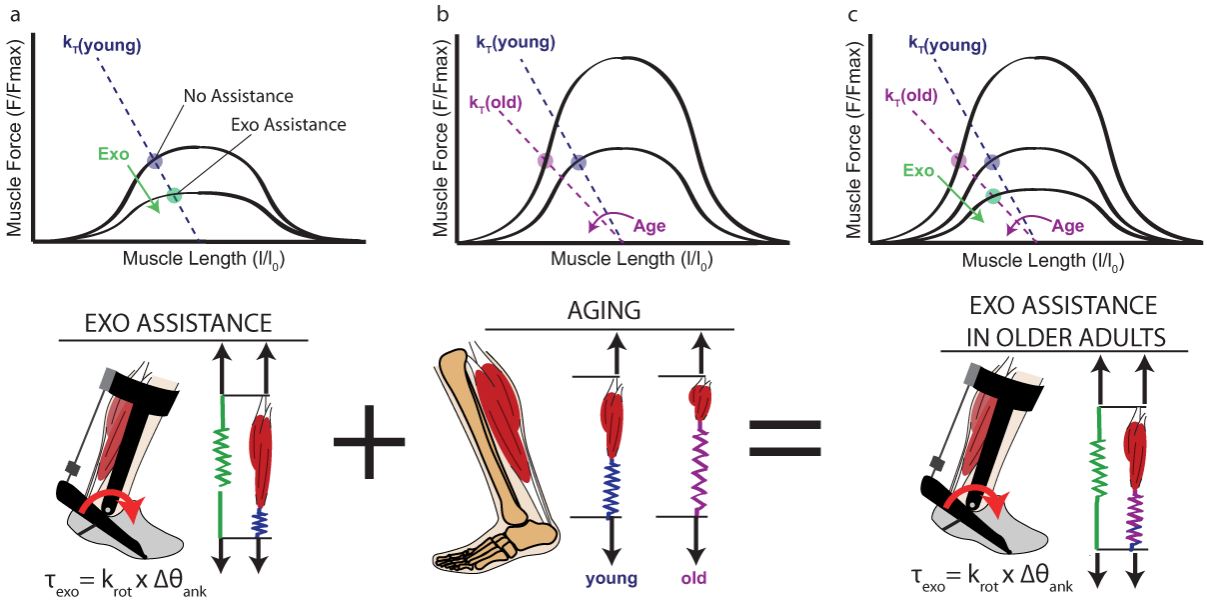

Figure 4.4: Conceptual schematic for the effect of parallel elastic assistance on the muscle fascicle operating point. a, Exoskeleton assistance offloads force from the parallel muscle tendon unit. As a result the tendon shortens and the fascicle lengthens. This shifts the operating point of the fascicle down and to the right on the F-L curve. **b,** Older adults have more compliant tendons. To maintain the same force, the muscle fascicle length is shorter and muscle activation increases. **c,** We propose that application of exoskeleton assistance in an older adults will restore the muscle to a more favorable operating point on the F-L curve.

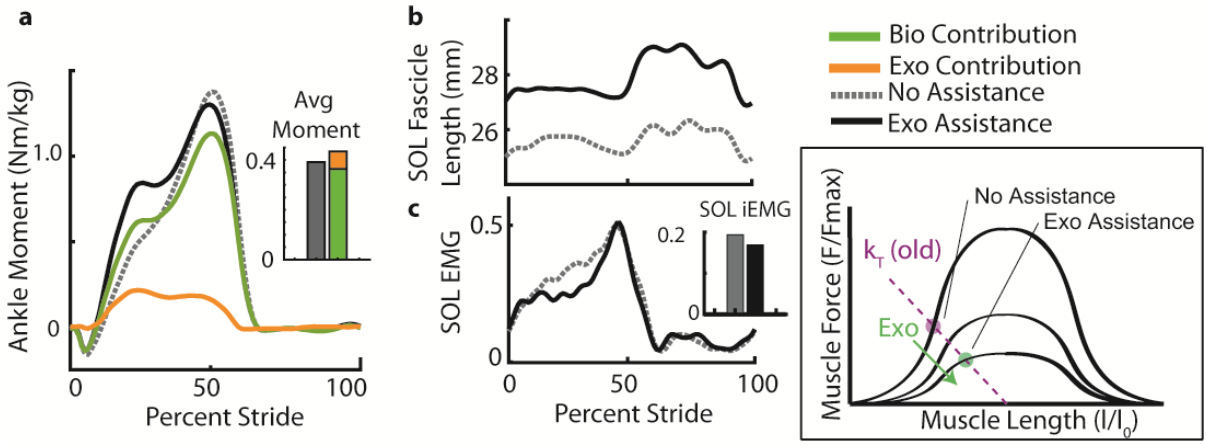

Figure 4.5: Exoskeleton assistance in an older adult to offset reduced tendon stiffness. a, At the ankle joint, exoskeleton assistance (yellow) results in decrease in biological moment (green) compared to the no assistance condition (dashed -grey). **b,** Exoskeleton parallel stiffness resulted in decreased muscle activations (black), **c,** increased SOL fascicle operating lengths, and a decreased in metabolic demand by 5%. **Insert:** Exoskeleton assistance potentially shifted SOL fascicle operating point to a more favorable operating point on the F-L curve.

REFERENCES

1. Takahashi, K.Z., M.D. Lewek, and G.S. Sawicki, *A neuromechanics-based powered ankle exoskeleton to assist walking post-stroke: a feasibility study.* Journal of neuroengineering and rehabilitation, 2015. **12**(1): p. 23.

2. Mooney, L.M., E.J. Rouse, and H.M. Herr, *Autonomous exoskeleton reduces metabolic cost of human walking during load carriage.* Journal of neuroengineering and rehabilitation, 2014. **11**: p. 80-0003-11-80.

3. Krishnan, C., et al., *Active robotic training improves locomotor function in a stroke survivor.* Journal of neuroengineering and rehabilitation, 2012. **9**: p. 57-0003-9-57.

4. Hidler, J., et al., *Multicenter randomized clinical trial evaluating the effectiveness of the Lokomat in subacute stroke.* Neurorehabilitation and neural repair, 2009. **23**(1): p. 5-13.

5. Malcolm, P., et al., *A simple exoskeleton that assists plantarflexion can reduce the metabolic cost of human walking.* PloS one, 2013. **8**(2): p. e56137.

6. Collins, S.H., M.B. Wiggin, and G.S. Sawicki, *Reducing the energy cost of human walking using an unpowered exoskeleton.* Nature, 2015.

7. Kuo, A.D., *Energetics of actively powered locomotion using the simplest walking model.* Journal of Biomechanical Engineering, 2002. **124**(1): p. 113-120.

8. Shamaei, K., G.S. Sawicki, and A.M. Dollar, *Estimation of quasi-stiffness and propulsive work of the human ankle in the stance phase of walking.* PloS one, 2013. **8**(3): p. e59935.

9. Jiménez-Fabián, R. and O. Verlinden, *Review of control algorithms for robotic ankle systems in lower-limb orthoses, prostheses, and exoskeletons.* Medical engineering & physics, 2012. **34**(4): p. 397-408.

10. Caputo, J.M. and S.H. Collins, *A universal ankle-foot prosthesis emulator for human locomotion experiments.* Journal of Biomechanical Engineering, 2014. **136**(3): p. 035002.

11. Zhang, J., C.C. Cheah, and S.H. Collins. *Experimental comparison of torque control methods on an ankle exoskeleton during human walking.* in *Robotics and Automation (ICRA), 2015 IEEE International Conference on.* 2015. IEEE.

12. Jackson, R.W. and S.H. Collins, *An experimental comparison of the relative benefits of work and torque assistance in ankle exoskeletons.* Journal of applied physiology (Bethesda, Md.: 1985), 2015. **119**(5): p. 541-557.

13. Sawicki, G.S. and D.P. Ferris, *Mechanics and energetics of level walking with powered ankle exoskeletons.* The Journal of experimental biology, 2008. **211**(Pt 9): p. 1402-1413.

14. Koller, J.R., et al., *Learning to walk with an adaptive gain proportional myoelectric controller for a robotic ankle exoskeleton.* Journal of neuroengineering and rehabilitation, 2015. **12**(1): p. 97-015-0086-5.

15. Eilenberg, M.F., H. Geyer, and H. Herr, *Control of a powered ankle–foot prosthesis based on a neuromuscular model.* Neural Systems and Rehabilitation Engineering, IEEE Transactions on, 2010. **18**(2): p. 164-173.

16. Farris, D.J. and G.S. Sawicki, *Human medial gastrocnemius force-velocity behavior shifts with locomotion speed and gait.* Proceedings of the National Academy of Sciences of the United States of America, 2012. **109**(3): p. 977-982.

17. Shadwick, R.E., *Elastic energy storage in tendons: mechanical differences related to function and age.* Journal of applied physiology (Bethesda, Md.: 1985), 1990. **68**(3): p. 1033-1040.

18. Giest TN, N.R., Sawicki GS. *"Speed-dependent, proportional myoelectric exoskeleton controller with adaptive gains".* in *40th Annual Meeting of American Society of Biomechanics.* 2016. Raleigh, NC.

19. Nuckols, R.G., TN; Philius, S; Sawicki, GS. *"Embodying human plantarflexor muscle-tendon physiology for neuromuscular model-based control of a powered ankle exoskeleton".* in *40th Annual Meeting of American Society of Biomechanics*. 2016. Raleigh, NC.

20. Quinlivan, B., et al., *Assistance magnitude versus metabolic cost reductions for a tethered multiarticular soft exosuit.* Science Robotics, 2017. **2**(2): p. eaah4416.

21. Galle, S., et al., *Enhancing performance during inclined loaded walking with a powered ankle-foot exoskeleton.* European journal of applied physiology, 2014.

22. Sawicki, G.S. and D.P. Ferris, *Mechanics and energetics of incline walking with robotic ankle exoskeletons.* The Journal of experimental biology, 2009. **212**(Pt 1): p. 32-41.

23. Farris, D.J. and G.S. Sawicki, *The mechanics and energetics of human walking and running: a joint level perspective.* Journal of the Royal Society, Interface / the Royal Society, 2012. **9**(66): p. 110-118.

24. Kuo, A.D., J.M. Donelan, and A. Ruina, *Energetic consequences of walking like an inverted pendulum: step-to-step transitions.* Exercise and sport sciences reviews, 2005. **33**(2): p. 88-97.

25. Ishikawa, M., et al., *Muscle-tendon interaction and elastic energy usage in human walking.* Journal of applied physiology (Bethesda, Md.: 1985), 2005. **99**(2): p. 603-608.

26. Bregman, D.J., et al., *The effect of ankle foot orthosis stiffness on the energy cost of walking: a simulation study.* Clinical biomechanics (Bristol, Avon), 2011. **26**(9): p. 955-961.

27. Schmidt, R.A. and T. Lee, *Motor control and learning.* 1988: Human kinetics.

28. Gordon, K.E. and D.P. Ferris, *Learning to walk with a robotic ankle exoskeleton.* Journal of Biomechanics, 2007. **40**(12): p. 2636-2644.

29. Galle, S., et al., *Adaptation to walking with an exoskeleton that assists ankle extension.* Gait & posture, 2013. **38**(3): p. 495-499.

30. Zelik, K.E., K.Z. Takahashi, and G.S. Sawicki, *Six degree-of-freedom analysis of hip, knee, ankle and foot provides updated understanding of biomechanical work during human walking.* J Exp Biol, 2015. **218**(Pt 6): p. 876-86.

31. Brockway, J.M., *Derivation of formulae used to calculate energy expenditure in man.* Human nutrition.Clinical nutrition, 1987. **41**(6): p. 463-471.

32. Felt, W., et al., *"Body-In-The-Loop": Optimizing Device Parameters Using Measures of Instantaneous Energetic Cost.* PloS one, 2015. **10**(8): p. e0135342.

33. Selinger, J.C. and J.M. Donelan, *Estimating instantaneous energetic cost during non-steady-state gait.* Journal of applied physiology (Bethesda, Md.: 1985), 2014. **117**(11): p. 1406-1415.

34. Koller, J.R., et al., *Confidence in the curve: Establishing instantaneous cost mapping techniques using bilateral ankle exoskeletons.* Journal of Applied Physiology, 2017. **122**(2): p. 242-252.

35. Holt, N.C., T.J. Roberts, and G.N. Askew, *The energetic benefits of tendon springs in running: is the reduction of muscle work important?* The Journal of experimental biology, 2014. **217**(Pt 24): p. 4365-4371.

36. Farris, D.J., B.D. Robertson, and G.S. Sawicki, *Elastic ankle exoskeletons reduce soleus muscle force but not work in human hopping.* Journal of applied physiology (Bethesda, Md.: 1985), 2013. **115**(5): p. 579-585.

37. McMahon, T.A., *Muscles, reflexes, and locomotion.* Princeton, Princeton, 1984.

38. Roberts, T.J., *The integrated function of muscles and tendons during locomotion.* Comparative biochemistry and physiology.Part A, Molecular & integrative physiology, 2002. **133**(4): p. 1087-1099.

39. Sawicki, G. and N. Khan, *A simple model to estimate plantarflexor muscle-tendon mechanics and energetics during walking with elastic ankle exoskeletons.* IEEE transactions on bio-medical engineering, 2015.

40. Enoka, R.M., *Neuromechanics of human movement*. 2008: Human kinetics.

41. Hill, A., *Length of muscle, and the heat and tension developed in an isometric contraction.* The Journal of physiology, 1925. **60**(4): p. 237-263.

42. Hill, A.V., *The Heat of Shortening and the Dynamic Constants of Muscle.* Proceedings of the Royal Society of London. Series B - Biological Sciences, 1938. **126**(843): p. 136-195.

43. Robertson, B.D., D.J. Farris, and G.S. Sawicki, *More is not always better: modeling the effects of elastic exoskeleton compliance on underlying ankle muscle–tendon dynamics.* Bioinspiration & biomimetics, 2014. **9**(4): p. 046018.

44. Morgan, D.L., *New insights into the behavior of muscle during active lengthening.* Biophys J, 1990. **57**(2): p. 209-21.

45. Morgan, D.L. and D.G. Allen, *Early events in stretch-induced muscle damage.* Journal of applied physiology (Bethesda, Md.: 1985), 1999. **87**(6): p. 2007-2015.

46. Allinger, T.L., M. Epstein, and W. Herzog, *Stability of muscle fibers on the descending limb of the force-length relation. A theoretical consideration.* J Biomech, 1996. **29**(5): p. 627-33.

47. Kao, P.C., C.L. Lewis, and D.P. Ferris, *Invariant ankle moment patterns when walking with and without a robotic ankle exoskeleton.* Journal of Biomechanics, 2010. **43**(2): p. 203-209.

48. Zajac, F.E., R.R. Neptune, and S.A. Kautz, *Biomechanics and muscle coordination of human walking: Part I: Introduction to concepts, power transfer, dynamics and simulations.* Gait & posture, 2002. **16**(3): p. 215-232.

49. Visser, J., et al., *Length and moment arm of human leg muscles as a function of knee and hip-joint angles.* European journal of applied physiology and occupational physiology, 1990. **61**(5): p. 453-460.

50. Winter, D.A., *Kinematic and kinetic patterns in human gait: variability and compensating effects.* Human Movement Science, 1984. **3**(1): p. 51-76.

51. Lelas, J.L., et al., *Predicting peak kinematic and kinetic parameters from gait speed.* Gait & posture, 2003. **17**(2): p. 106-112.

52. Browning, R.C., et al., *Effects of obesity and sex on the energetic cost and preferred speed of walking.* Journal of Applied Physiology, 2006. **100**(2): p. 390-398.

53. Selinger, J.C., et al., *Humans Can Continuously Optimize Energetic Cost during Walking.* Current biology : CB, 2015. **25**(18): p. 2452-2456.

54. Minetti, A.E., et al., *Effects of stride frequency on mechanical power and energy expenditure of walking.* Medicine and Science in Sports and Exercise, 1995. **27**(8): p. 1194-1202.

55. Lichtwark, G.A. and A.M. Wilson, *Optimal muscle fascicle length and tendon stiffness for maximising gastrocnemius efficiency during human walking and running.* Journal of theoretical biology, 2008. **252**(4): p. 662-673.

56. Lichtwark, G.A. and A.M. Wilson, *Is Achilles tendon compliance optimised for maximum muscle efficiency during locomotion?* Journal of Biomechanics, 2007. **40**(8): p. 1768-1775.

57. Zelik, K.E., et al., *The role of series ankle elasticity in bipedal walking.* Journal of theoretical biology, 2014. **346**: p. 75-85.

58. Zhang, J., et al., *Human-in-the-loop optimization of exoskeleton assistance during walking.* Science, 2017. **356**(6344): p. 1280-1284.

59. Lichtwark, G.A., et al., *Commentaries on Viewpoint: On the hysteresis in the human Achilles tendonINFERRING TENDON MECHANICAL PROPERTIES USING ULTRASOUND IMAGINGTHE HYSTERESIS OF TENDON, IN VITRO AND IN VIVOCOMMON PROBLEMS IN THE MEASUREMENT OF HUMAN TENDON HYSTERESIS IN VIVOVIEWPOINT: ON THE HYSTERESIS IN THE HUMAN ACHILLES TENDONON THE HYSTERESIS IN THE HUMAN ACHILLES TENDON: INFLUENCE OF THE LOADING RATE AND MUSCLE COORDINATIONCOMMENTARY ON VIEWPOINTSTIFFNESS AND HYSTERESIS OF HUMAN TENDONS.* Journal of Applied Physiology, 2013. **114**(4): p. 518-520.

60. Morrison, S.M., T.J. Dick, and J.M. Wakeling, *Structural and mechanical properties of the human Achilles tendon: Sex and strength effects.* J Biomech, 2015. **48**(12): p. 3530-3.

61. Onambele, G.L., M.V. Narici, and C.N. Maganaris, *Calf muscle-tendon properties and postural balance in old age.* Journal of Applied Physiology, 2006. **100**(6): p. 2048-2056.

62. Franz, J.R., *The Age-Associated Reduction in Propulsive Power Generation in Walking.* Exerc Sport Sci Rev, 2016. **44**(4): p. 129-36.

63. Biewener, A.A. and T.J. Roberts, *Muscle and tendon contributions to force, work, and elastic energy savings: a comparative perspective.* Exerc Sport Sci Rev, 2000. **28**.

64. Roberts, T.J. and E. Azizi, *Flexible mechanisms: the diverse roles of biological springs in vertebrate movement.* Journal of Experimental Biology, 2011. **214**(3): p. 353-361.

65. Rubenson, J., et al., *On the ascent: the soleus operating length is conserved to the ascending limb of the force-length curve across gait mechanics in humans.* The Journal of experimental biology, 2012. **215**(Pt 20): p. 3539-3551.

66. Lichtwark, G.A. and A.M. Wilson, *Interactions between the human gastrocnemius muscle and the Achilles tendon during incline, level and decline locomotion.* Journal of Experimental Biology, 2006. **209**(21): p. 4379-4388.

67. Gordon, A.M., A.F. Huxley, and F.J. Julian, *The variation in isometric tension with sarcomere length in vertebrate muscle fibres.* J Physiol, 1966. **184**(1): p. 170-92.

68. Farris, D.J., et al., *Musculoskeletal modelling deconstructs the paradoxical effects of elastic ankle exoskeletons on plantar-flexor mechanics and energetics during hopping.* The Journal of experimental biology, 2014. **217**(Pt 22): p. 4018-4028.

69. Cronin, N.J., et al., *Automatic tracking of medial gastrocnemius fascicle length during human locomotion.* Journal of applied physiology, 2011. **111**(5): p. 1491-1496.

70. Gillett, J.G., R.S. Barrett, and G.A. Lichtwark, *Reliability and accuracy of an automated tracking algorithm to measure controlled passive and active muscle fascicle length changes from ultrasound.* Computer methods in biomechanics and biomedical engineering, 2013. **16**(6): p. 678-687.

71. Farris, D.J. and G.A. Lichtwark, *UltraTrack: Software for semi-automated tracking of muscle fascicles in sequences of B-mode ultrasound images.* Computer methods and programs in biomedicine, 2016. **128**: p. 111-118.

72. Hawkins, D. and M.L. Hull, *A method for determining lower extremity muscle-tendon lengths during flexion/extension movements.* J Biomech, 1990. **23**(5): p. 487-94.

73. Takahashi, K.Z., et al., *Adding Stiffness to the Foot Modulates Soleus Force-Velocity Behaviour during Human Walking.* Sci Rep, 2016. **6**: p. 29870.

74. Fukunaga, T., et al., *Physiological cross-sectional area of human leg muscles based on magnetic resonance imaging.* Journal of orthopaedic research, 1992. **10**(6): p. 926-934.

75. Gunther, M. and R. Blickhan, *Joint stiffness of the ankle and the knee in running.* Journal of Biomechanics, 2002. **35**(11): p. 1459-1474.

76. Choi, H., T.A.L. Wren, and K.M. Steele, *Gastrocnemius operating length with ankle foot orthoses in cerebral palsy.* Prosthetics and orthotics international, 2017. **41**(3): p. 274-285.

77. Jackson, R.W., et al., *Muscle-tendon mechanics explain unexpected effects of exoskeleton assistance on metabolic rate during walking.* The Journal of Experimental Biology, 2017.

78. Zajac, F.E., *Muscle and tendon: properties, models, scaling, and application to biomechanics and motor control.* Critical Reviews in Biomedical Engineering, 1989. **17**(4): p. 359-411.

79. Fenn, W. and B. Marsh, *Muscular force at different speeds of shortening.* The Journal of Physiology, 1935. **85**(3): p. 277.

80. Ward, S.R., et al., *Are current measurements of lower extremity muscle architecture accurate?* Clinical orthopaedics and related research, 2009. **467**(4): p. 1074-1082.

81. Alexander, R.M., *Optimum muscle design for oscillatory movements.* Journal of theoretical Biology, 1997. **184**(3): p. 253-259.

82. Zajac, F.E. and M.E. Gordon, *Determining muscle's force and action in multi-articular movement.* Exercise and sport sciences reviews, 1989. **17**(1): p. 187-230.

83. Kram, R., C.J. Arellano, and J.R. Franz, *The metabolic cost of locomotion; muscle by muscle.* Exercise and sport sciences reviews, 2011. **39**(2): p. 57-58.

84. Griffin, T.M., T.J. Roberts, and R. Kram, *Metabolic cost of generating muscular force in human walking: insights from load-carrying and speed experiments.* Journal of Applied Physiology, 2003. **95**(1): p. 172-183.

85. Roberts, T.J., et al., *Muscular force in running turkeys: the economy of minimizing work.* Science (New York, N.Y.), 1997. **275**(5303): p. 1113-1115.

86. Lai, A., et al., *In vivo behavior of the human soleus muscle with increasing walking and running speeds.* Journal of applied physiology (Bethesda, Md.: 1985), 2015. **118**(10): p. 1266-1275.

87. Neptune, R.R. and K. Sasaki, *Ankle plantar flexor force production is an important determinant of the preferred walk-to-run transition speed.* Journal of Experimental Biology, 2005. **208**(5): p. 799-808.

88. Lieber, R.L. and J. Friden, *Muscle damage is not a function of muscle force but active muscle strain.* Journal of applied physiology (Bethesda, Md.: 1985), 1993. **74**(2): p. 520-526.

89. Bregman, D.J., et al., *Spring-like Ankle Foot Orthoses reduce the energy cost of walking by taking over ankle work.* Gait & posture, 2012. **35**(1): p. 148-153.

90. Alexander, R.M., *Elastic mechanisms in animal movement.* 1988: Cambridge University Press.

91. Magnusson, S.P., et al., *Load-displacement properties of the human triceps surae aponeurosis in vivo.* The Journal of physiology, 2001. **531**(1): p. 277-288.

92. Franz, J.R., et al., *Non-uniform in vivo deformations of the human Achilles tendon during walking.* Gait & posture, 2015. **41**(1): p. 192-197.

93. Rasske, K., D.G. Thelen, and J.R. Franz, *Variation in the human Achilles tendon moment arm during walking.* Computer methods in biomechanics and biomedical engineering, 2017. **20**(2): p. 201-205.

94. Galle, S., et al., *Exoskeleton plantarflexion assistance for elderly.* Gait Posture, 2017. **52**: p. 183-188.

95. Young, A.J., et al., *Influence of Power Delivery Timing on the Energetics and Biomechanics of Humans Wearing a Hip Exoskeleton.* Front Bioeng Biotechnol, 2017. **5**: p. 4.

96. Ryder, M.C. and F. Sup, *Leveraging gait dynamics to improve efficiency and performance of powered hip exoskeletons.* IEEE Int Conf Rehabil Robot, 2013. **2013**: p. 6650440.

97. Seo, K., et al. *Fully autonomous hip exoskeleton saves metabolic cost of walking*. in *2016 IEEE International Conference on Robotics and Automation (ICRA)*. 2016. Stockholm, Sweden.

98. Lee, H.J., et al., *A Wearable Hip Assist Robot Can Improve Gait Function and Cardiopulmonary Metabolic Efficiency in Elderly Adults*. IEEE Transactions on Neural Systems and Rehabilitation Engineering, 2017. **PP**(99): p. 1-1.

99. Wiggin, M.B., G.S. Sawicki, and S.H. Collins, *An exoskeleton using controlled energy storage and release to aid ankle propulsion*. IEEE Int Conf Rehabil Robot, 2011. **2011**: p. 5975342.

100. Lichtwark, G.A. and A.M. Wilson, *Effects of series elasticity and activation conditions on muscle power output and efficiency*. J Exp Biol, 2005. **208**(Pt 15): p. 2845-53.

101. Cronin, N.J. and G. Lichtwark, *The use of ultrasound to study muscle-tendon function in human posture and locomotion*. Gait & Posture, 2013. **37**(3): p. 305-312.

102. Lichtwark, G.A., K. Bougoulias, and A.M. Wilson, *Muscle fascicle and series elastic element length changes along the length of the human gastrocnemius during walking and running*. Journal of Biomechanics, 2007. **40**(1): p. 157-164.

103. Endo, K. and H. Herr, *A model of muscle-tendon function in human walking at self-selected speed*. IEEE Trans Neural Syst Rehabil Eng, 2014. **22**(2): p. 352-62.

104. Robertson, B.D. and G.S. Sawicki, *Unconstrained muscle-tendon workloops indicate resonance tuning as a mechanism for elastic limb behavior during terrestrial locomotion*. Proc Natl Acad Sci U S A, 2015. **112**(43): p. E5891-8.

105. Zelik, K.E., et al., *The role of series ankle elasticity in bipedal walking*. J Theor Biol, 2014. **346**: p. 75-85.

106. Hansen, A.H., et al., *The human ankle during walking: implications for design of biomimetic ankle prostheses*. J Biomech, 2004. **37**(10): p. 1467-74.

107. Wiggin, M.B., G.S. Sawicki, and S.H. Collins, *Apparatus and clutch for using controlled storage and release of mechanical energy to aid locomotion. US patent 0046218.*, 2013: U.S.

108. Neptune, R.R., C.P. McGowan, and S.A. Kautz, *Forward dynamics simulations provide insight into muscle mechanical work during human locomotion.* Exerc Sport Sci Rev, 2009. **37**(4): p. 203-10.

109. Delp, S.L., et al., *OpenSim: open-source software to create and analyze dynamic simulations of movement.* IEEE Trans Biomed Eng, 2007. **54**(11): p. 1940-50.

110. Arnold, E.M., et al., *How muscle fiber lengths and velocities affect muscle force generation as humans walk and run at different speeds.* J Exp Biol, 2013. **216**(Pt 11): p. 2150-60.

111. Arnold, E.M., et al., *A model of the lower limb for analysis of human movement.* Ann Biomed Eng, 2010. **38**(2): p. 269-79.

112. Lai, A., et al., *Tendon elastic strain energy in the human ankle plantar-flexors and its role with increased running speed.* J Exp Biol, 2014. **217**(Pt 17): p. 3159-68.

113. Dean, J.C. and A.D. Kuo, *Energetic costs of producing muscle work and force in a cyclical human bouncing task.* J Appl Physiol (1985), 2011. **110**(4): p. 873-80.

114. Robertson, B.D. and G.S. Sawicki, *Exploiting elasticity: Modeling the influence of neural control on mechanics and energetics of ankle muscle-tendons during human hopping.* J Theor Biol, 2014. **353**: p. 121-32.

115. Sartori, M., et al., *Modeling and simulating the neuromuscular mechanisms regulating ankle and knee joint stiffness during human locomotion.* Journal of neurophysiology, 2015. **114**(4): p. 2509-2527.

116. Rouse, E.J., et al., *Estimation of human ankle impedance during the stance phase of walking.* IEEE Trans Neural Syst Rehabil Eng, 2014. **22**(4): p. 870-8.

117. Stenroth, L., et al., *Age-related differences in Achilles tendon properties and triceps surae muscle architecture in vivo.* Journal of Applied Physiology, 2012. **113**(10): p. 1537-44.

118. Narici, M.V., C. Maganaris, and N. Reeves, *Myotendinous alterations and effects of resistive loading in old age.* Scandinavian journal of medicine & science in sports, 2005. **15**(6): p. 392-401.

119. Csapo, R., et al., *Age-related greater Achilles tendon compliance is not associated with larger plantar flexor muscle fascicle strains in senior women.* Journal of Applied Physiology, 2014. **116**(8): p. 961-9.

120. Mian, O.S., et al., *Gastrocnemius muscle-tendon behaviour during walking in young and older adults.* Acta Physiol (Oxf), 2007. **189**(1): p. 57-65.

121. Panizzolo, F.A., et al., *Soleus fascicle length changes are conserved between young and old adults at their preferred walking speed.* Gait Posture, 2013. **38**(4): p. 764-9.

122. Franz, J.R. and D.G. Thelen, *Depth-dependent variations in Achilles tendon deformations with age are associated with reduced plantarflexor performance during walking.* J Appl Physiol, 2015. **119**(3): p. 242-9.

123. Franz, J.R. and D.G. Thelen, *Imaging and simulation of Achilles tendon dynamics: implications for walking performance in the elderly.* J Biomech, 2016. **In Press**.

124. Orselli, M., J.R. Franz, and D.G. Thelen, *The effects of Achilles tendon compliance on triceps surae mechanics and energetics in walking.* Journal of Biomechanics, In Revision.

125. Franz, J.R. and R. Kram, *Advanced age and the mechanics of uphill walking: a joint-level, inverse dynamic analysis.* Gait & posture, 2014. **39**(1): p. 135-140.

126. Kerrigan, D.C., et al., *Kinetic alterations independent of walking speed in elderly fallers.* Arch Phys Med Rehabil, 2000. **81**(6): p. 730-5.

127. Kerrigan, D.C., et al., *Biomechanical gait alterations independent of speed in the healthy elderly: evidence for specific limiting impairments.* Arch Phys Med Rehabil, 1998. **79**: p. 317-22.

128. Robertson, B.D., S. Vadakkeveedu, and G.S. Sawicki, *A benchtop biorobotic platform for in vitro observation of muscle-tendon dynamics with parallel mechanical assistance from an elastic exoskeleton.* Journal of Biomechanics, 2017. **57**: p. 8-17.